CERN 93-01
28 April 1993

ORGANISATION EUROPÉENNE POUR LA RECHERCHE NUCLÉAIRE
CERN EUROPEAN ORGANIZATION FOR NUCLEAR RESEARCH

CERN HEAVY-ION FACILITY DESIGN REPORT

N. Angert (GSI), M.P. Bourgarel (GANIL), E. Brouzet, R. Cappi, D. Dekkers, J. Evans, G. Gelato, H. Haseroth, C.E. Hill, G. Hutter (GSI), J. Knott, H. Kugler, A. Lombardi (INFN, Legnaro), H. Lustig, E. Malwitz (GSI), F. Nitsch, G. Parisi (INFN, Legnaro), A. Pisent (INFN, Legnaro), U. Raich, U. Ratzinger (GSI), L. Riccati (INFN, Torino), A. Schempp (IAP, Frankfurt), K. Schindl, H. Schönauer, P. Tètu, H.H. Umstätter, M. van Rooij, D. Warner, M. Weiss.

Editor: D. Warner

GENEVA
1993

ISBN 92-9083-050-6

CERN 93–01
28 April 1993

ORGANISATION EUROPÉENNE POUR LA RECHERCHE NUCLÉAIRE
CERN EUROPEAN ORGANIZATION FOR NUCLEAR RESEARCH

CERN HEAVY-ION FACILITY DESIGN REPORT

N. Angert (GSI), M.P. Bourgarel (GANIL), E. Brouzet, R. Cappi, D. Dekkers, J. Evans, G. Gelato, H. Haseroth, C.E. Hill, G. Hutter (GSI), J. Knott, H. Kugler, A. Lombardi (INFN, Legnaro), H. Lustig, E. Malwitz (GSI), F. Nitsch, G. Parisi (INFN, Legnaro), A. Pisent (INFN, Legnaro), U. Raich, U. Ratzinger (GSI), L. Riccati (INFN, Torino), A. Schempp (IAP, Frankfurt), K. Schindl, H. Schönauer, P. Têtu, H.H. Umstätter, M. van Rooij, D. Warner, M. Weiss.

Editor: D. Warner

GENEVA
1993

CERN–Service d'information scientifique–RD/905–2000–mai 1993

ABSTRACT

The design of the CERN Heavy-Ion Facility is described. This facility will be based on a new ion linear accelerator (Linac 3), together with improvements to the other accelerators of the CERN complex to allow them to cope with heavy ions, i.e. to the Proton Synchrotron Booster (PSB), the Proton Synchrotron (PS) and the Super Proton Synchrotron (SPS). For this reference design, the pure isotope of lead, ^{208}Pb, is considered. The bulk of the report describes Linac 3, a purpose-built heavy-ion linac mainly designed and constructed in collaboration with several CERN member state laboratories, but also with contributions from non-member states. Modifications and improvements to existing CERN accelerators essentially concern the RF acceleration, beam control and beam monitoring (all machines), beam kickers and septa at the input and output of the PSB, and major vacuum improvements, aiming to reduce the pressure by factors of at least seven and three in the PSB and PS respectively. After injection from the Electron Cyclotron Resonance source at 2.5 keV/u the partially stripped heavy-ion beam is accelerated successively by a Radio Frequency Quadrupole and an Interdigital-H linac to 4.2 MeV/u. After stripping to $^{208}Pb^{53+}$, the beam is again accelerated, firstly in the PSB (to 98.5 MeV/u), then in the PS (to 4.25 GeV/u). The final stage of acceleration in the SPS takes the fully stripped $^{208}Pb^{82+}$ ions to 177 GeV/u, delivering a beam of $4 \cdot 10^8$ ions per SPS supercycle (15.2 s) to the experiments. The first physics run with lead ions is scheduled for the end of 1994. Finally, some requirements for carrying out heavy-ion physics at the Large Hadron Collider are mentioned.

PREFACE

This design report is in a way a continuation of the CERN yellow report 90-01 'Concept for a Lead-Ion Accelerating Facility at CERN' [1] . Whereas the former described a concept, or even several concepts, this report is a complete description of the facility as it will be built.

On March 9, 1990, there was a meeting, called by CERN's Director General, Prof. Carlo Rubbia, to start a collaboration between different laboratories and CERN. Delegates from most member states, a US-observer and spokesmen from the different heavy ion experiments were present. It was agreed that most of the major components and subsystems would be built by laboratories outside CERN with additional financial contributions covering general items.

It was clear from the outset that the collaborating laboratories would influence strongly the design philosophy and would make choices based on their particular experience and local manufacturing facilities e.g. the choice of the Interdigital-H structure for the linac.

As did the previous report, the present report has profited from the strong and efficient cooperation of many people outside CERN, mainly in the collaborating institutes but also consultants from other institutions. To all of them go our sincere thanks for their efforts and important contributions.

Helmut Haseroth
Project leader for the CERN
Heavy Ion Accelerating Facility

CONTENTS

EDITOR'S PREAMBLE

The aims of this report should be self-evident from its contents but nevertheless it was clear from a study of the draft version that some additional explanations would help the understanding.

The wide range of CERN accelerators implicated in the heavy ion project, and the many outside institutions collaborating with CERN, have brought with them a heterogeneous and polyglot set of abbreviations and acronyms. These are often explained in the text but for completeness they are collected in a separate list at the beginning of this report.

There is another type of abbreviation occuring in the text concerning the nomenclature used for accelerator components. Again a comprehensive list is given; the context should resolve possible confusion between the two lists. Neither list includes controls abbreviations.

This report is intended as a reference for the design and as such includes much tabular data concerning detailed component characteristics. In order not to overload the main text, only a limited number of summary tables is given there, with a complete set of tables collected in an appendix. The longer term aim was to have a reference set of data which could be updated and reissued at a later date, so there is both unavoidably and purposely some duplication between the appendix and the text body.

ACRONYMS AND ABBREVIATIONS FOR ACCELERATORS AND INSTITUTES

AAC	Antiproton Accumulator and Collector rings in the CERN accelerator complex
BARC	Bhabha Atomic Research Centre, Bombay
CAPRICE	Acronym for a particular series of Electron Cyclotron Resonance sources (ECR) used at GANIL
CAT	Centre of Advanced Technology, Indore
ECR	Electron Cyclotron Resonance source, generally used for production of ions in highly charged states
EPA	Electron Positron Accumulator in the CERN accelerator complex
FISC	Filament scintillation counters used in the beam lines after the Super Proton Synchrotron (SPS)
GANIL	Grand Accelerateur National des Ions Lourds, Large National Accelerator for Heavy Ions, situated at Caen, France
GSI	Gesellschaft für Schwerionenforschung mbH, Public Limited Company for Heavy Ion Research near Darmstadt, initially based on a heavy ion linac, the UNILAC
HLI	Hoch-Ladungs-Injektor (high charge state injector situated at GSI)
IAP	Institute of Applied Physics - University of Frankfurt
IN2P3	Institut National de Physique Nucléaire et de Physique des Particules, National Institute for Nuclear Physics and Particle Physics in France
INFN	Istituto Nazionale di Fisica Nucleare - the Italian National Nuclear Physics Institute
ISR	Intersecting Storage Rings used for hadron-hadron collision experiments at CERN between 1971 and 1985
LEAR	Low Energy Antiproton Ring in the CERN accelerator complex
LBL	Lawrence Berkeley Laboratory, California
LHC	Large Hadron Collider, CERN's next major project
Linac	Common name for any RF linear accelerator
Linac 1	CERN's first Linac, used until 1979 as 50 MeV proton injector and later as a light ion injector
Linac 2	High current 50 MeV proton linac, used as main injector to the CERN accelerator complex since 1971
Linac 3	The Heavy Ion Linac treated in this report, replacing Linac 1 in building 351.
LNL	Laboratori Nazionali di Legnaro, Legnaro National Laboratories - constituent laboratories of INFN
MAFIOS	Acronym for an earlier design of the ECR source
PPM	Pulse-to-pulse Modulation, as applied to accelerators in the proton synchrotron complex which allows acceleration of different particle types to different energies on different cycles of the same super-cycle
PS	Proton Synchrotron. Abbreviation used for the CERN 28 GeV Proton Synchrotron
PSB	Proton Synchrotron Booster, commonly called the Booster, which accelerates protons from 50 MeV to 1 GeV, or heavier ions (lead for the present project) from 4.2 MeV/u to 95.4 MeV/u
PSCC	Proton Synchrotron and Synchro Cyclotron Committee
SPS	Super Proton Synchrotron - CERN's largest proton synchrotron
TIFR	Tata Institute for Fundamental Research, Bombay
TT20, TT60	Identifying code for beam transfer channels
VECC	Variable Energy Cyclotron Centre, Calcutta

CONVENTIONAL AND PS DIVISION NAMES AND ABBREVIATIONS FOR ACCELERATOR ELEMENTS

The naming scheme used in PS Division follows the so-called 'Barbalat' system where the abbreviations have a strict format. Essentially they consist of a single letter denoting the accelerator, 'I' in the case of Linac 3, followed immediately by up to three letters or figures denoting the system, e.g. A1 denotes the first accelerating cavity of the Interdigital-H structure used on Linac 3. The second part of the name (or 'nomenclature') follows a full stop (the 'delimiter') and consists of a standard abbreviation identifying the type of component and qualifying information, e.g. location. The following list applies to many of the components mentioned in the body of the text, including some in the booster synchrotron (PSB). For completeness the 'conventional' abbreviations of larger components are also given and identified by a superscript asterisk.

BE.	Booster extraction region
BI.	Booster injection region
BHZ	Magnet which bends the beam in the horizontal plane
BT.	Beam transport after the booster
CRF	General RF cavity, e.g. for beam bunching
DHZ	Dipole steering magnet giving horizontal deflection
DVT	Dipole steering magnet giving vertical deflection
ECR*	Electron Cyclotron Resonance source, as used for producing highly charged lead ions in the present project
HEBT*	High Energy Beam Transport after a linac (includes ITF and LTB on Linac 3)
IA1.	First (1) of three accelerating cavities (A) on Linac 3 (I)
IAQ.	Radio-frequency quadrupole on Linac 3
IH*	Interdigital-H, structure used on Linac 3 (see IA1. above)
IP.	Pre-injector region (P) of Linac 3 (I), including the ECR source
ITF.	Beam transport (T) in the filter (F) region after Linac 3
ITL.	Beam transport at low (L) energy, i.e. 2.5 keV/u, between pre-injector (IP) and radio-frequency quadrupole in Linac 3
ITM.	Beam transport at medium (M) energy, i.e. 250 keV/u, in Linac 3
KFA.	'Fast' beam kickers
KSW.	'Slow' beam kickers
LBE.	Emittance measuring line branching from the LTB. transfer line
LEBT*	Low Energy Beam Transport–conventional name for ITL.
LTB.	Beam transfer line between the filter region of Linac 3 (ITF) and the booster synchrotron
MEBT*	Medium Energy Beam Transport–conventional name for ITM.
MSG	Beam measuring secondary emission grid, e.g. MSGHV will measure in both horizontal and vertical planes
QDN	Quadrupole lens, defocusing in the horizontal plane
QFN	Quadrupole lens, focusing in the horizontal plane
RFQ*	Radio-Frequency Quadrupole (IAQ. is the assigned name for Linac 3)
SOL	Solenoid lens

* Conventional abbreviation, not generally conforming to rules and format of PS names.

1 INTRODUCTION

1.1 HISTORY OF THE PRESENT PROJECT

Particles accelerated at CERN in the early days were uniquely protons but since 1964 more possibilities have been opened up, in particular the acceleration of deuterons and alpha particles, and more recently antiprotons and leptons. The acceleration of the light ions, like deuterons and alpha particles, followed in 1986 and until 1992 by oxygen and sulphur ions, gradually developed into the strong coherent programme of heavy ion physics which forms the basis of the project for a heavy ion facility.

First machine experiments to accelerate deuterons with the CERN 50 MeV proton linac (later called Linac 1) were already carried out in 1964 using the so-called 2 $\beta\lambda$ mode for acceleration [2]. Further successful operation of Linac 1 with deuterons prompted requests from the ISR user community first for deuterons and later for alpha particles [3,4].

It was quite clear, from then onwards, that Linac 1 was able to accelerate any fully stripped ions (up to about calcium) as long as they could be provided at the input and neglecting recombination losses due to the imperfect vacuum. The subsequent machines had no major difficulties, except for some RF gymnastics (like change of the harmonic number) and the lower intensity of the beams. A detailed study [5,6], which was launched following a letter of intent addressed to the Proton Synchrotron and Synchro-Cyclotron Committee (PSCC) at CERN [7], showed that it would be possible, with moderate investments, to accelerate considerably heavier ions than in the past, with the existing CERN machines. To implement the required changes to the CERN accelerators, a collaboration was created between GSI (Darmstadt, Germany), LBL (Berkeley, USA) and CERN.

The plan was to use an electron cyclotron resonance source (ECR) capable of producing some 100 μAe beam of O^{6+} ions, to accelerate this beam with a DC potential of 15 kV and to build an RFQ for further acceleration. Linac 1 needed a 33 % increase in the RF accelerating fields as well as in the magnetic focusing fields. Some drastic improvements were required for the beam monitoring equipment in all the CERN machines to cope with this extremely low intensity. GSI provided the 10 GHz ion source (built by R. Geller, Grenoble) the RF amplifier (built by CERN), and beam transport elements in the low energy area. LBL built the RFQ and CERN supplied matching cavities between the RFQ and the first Alvarez tank of Linac 1. CERN also dealt with the necessary upgrade of Linac 1 and with the instrumentation of the different accelerators [8,9,10]. The ion source and the RFQ were delivered to GSI, together with the CERN-built RF power amplifier, and tested there [11]. One of the major problems proved to be the RF voltage holding capability, especially of tank 1 where an increase of 33% above the normal accelerating fields was required. Special cleaning and bake-out procedures together with additional cryopumping and the use of a computer controlled RF-conditioning program were needed to achieve the goal. The beam intensity at the end of the linac was in the range of 30 μA, the emittance was similar to that of the usual proton beams. Stripping by means of a carbon foil was done yielding a fairly pure beam of O^{8+}.

Apart from the intensity this beam was similar to deuteron or alpha particle beams for the downstream machines. Beam measurements after the linac were carried out by using secondary emission monitors, capable of measuring emittance and energy spread of beams with intensities well below 1 μA. Part of the time the PS complex operated with higher intensity deuteron beams supplied by Linac 2, interlaced between oxygen ion pulses to allow the setting-up of the SPS. The intensities in the SPS were usually well above 10^{10} charges per pulse. A new 14 GHz 'Geller' ion source (provided by GSI) resulted (1987) in a somewhat increased intensity for the oxygen beam with a large amount of S^{12+} ions. The majority of these ions was converted with the stripper foil at the end of the linac to a S^{16+} beam and accelerated in the PSB together with the oxygen beam. The PS also accelerated both beams up to transition energy and was then able to continue selectively with the sulphur beam [12].

With the fields increased by 33%, Linac 1 was really at the technological limit of its possibilities. Ions heavier than oxygen or sulphur, with the same charge to mass ratio are,

with present day sources, only available at much lower intensities which would be insufficient for SPS operation and for most physics experiments. To achieve the intensities required implies accepting lower charge states and hence proceeding to a complete replacement of Linac 1 [13]. Heavy ions with considerably lower charge-to-mass ratios will then be accelerated, so that full stripping will not be possible at the end of the linac, and the following machines will have to deal with partially stripped ions at lower velocities than at present.

This report describes the CERN heavy ion facility which ensued from this basic logic and is now under construction.

1.2 ORGANIZATION OF THE PROJECT

Offers to participate in this project had been made by some laboratories so that the discussions taking place on March 9, 1990 at a meeting, called by CERN's Director General, Prof. Carlo Rubbia, could launch the collaborations between different laboratories and CERN. With the presence of delegates from most member states, a US observer and spokesmen from the different heavy ion experiments it was possible to establish collaborations of several laboratories with CERN.

So far, the agreement is that IN2P3 will contribute an ECR-ion source via GANIL (Caen); INFN will supply the low energy beam transport between source and linac, including a radio frequency quadrupole, to be built by the Laboratori Nazionali di Legnaro; Germany will deliver the linac, including RF amplifiers, constructed by GSI (Darmstadt); Torino (INFN) will supply the high energy transport and filter lines as well as beam measuring equipment for the Super Proton Synchrotron. Financial contributions have been received from Sweden and Switzerland. Software effort for the controls of the lead ion linac has been obtained from BARC (Bombay) and VECC (Calcutta). A debuncher cavity will be built by IAP (Frankfurt). Some other contributions have been accepted, such as fabrication of certain components in non member state laboratories, e.g. from CAT (Indore), or are still under discussion.

CERN's contribution consists, apart from the effort of coordination, in supplying the necessary infrastructure and the substantial upgrades needed to cope with the ions in the transfer lines and in the circular machines. A schematic layout of the sequence of accelerators in the heavy ion facility is given in Fig. 1.1 with special emphasis on the tasks of the main collaborating institutions.

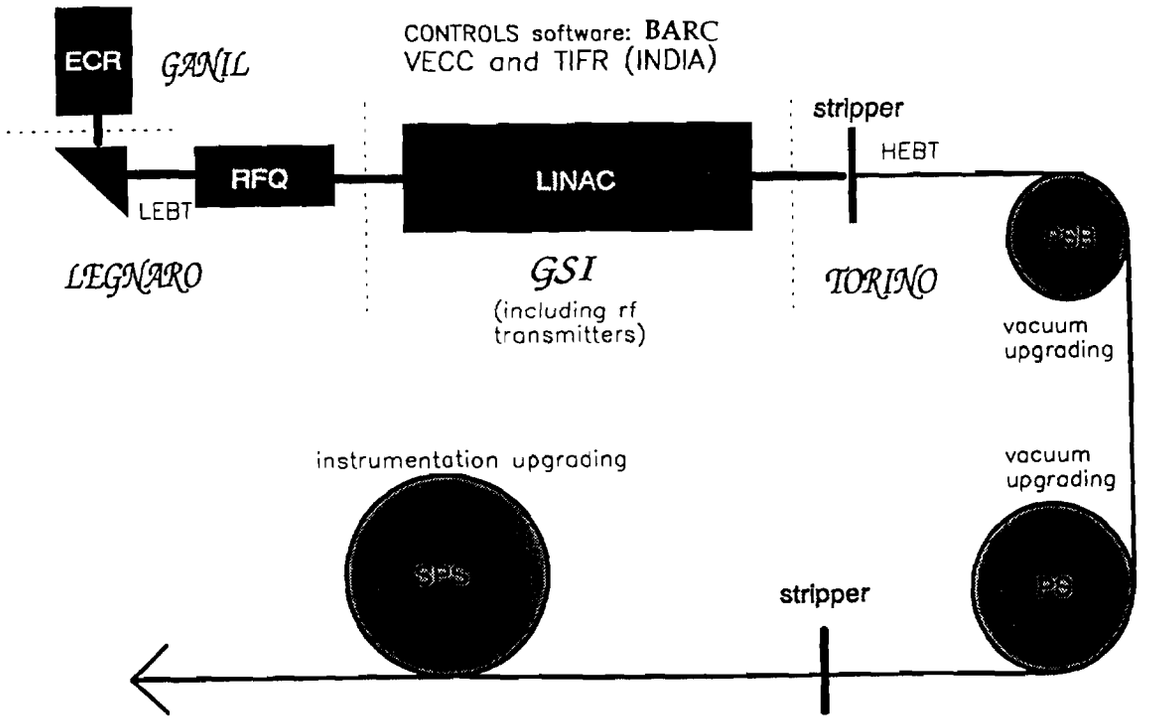

Fig. 1.1 Collaborations Involving Laboratories from France, Italy, Germany and India

1.3 LEAD ION ACCELERATION SCHEME: NOMINAL INTENSITIES AND EFFICIENCIES

Table 1.3.1 below summarizes the sequence of accelerators involved in lead ion acceleration and the nominal ion intensity and efficiency of each stage. The 'nominal' efficiencies are meant to be realistic estimates, based on the experience gained with the light ion (Oxygen/Sulphur) acceleration scheme. For heavy ions, two additional loss mechanisms have to be reckoned with.

1.3.1 Stripping at the Linac Exit

At the linac exit, Pb^{28+} ions are stripped by a carbon foil at 4.2 MeV/u. This energy is determined by the allowable rigidity of the beam in the booster injection line corresponding to the most probable charge state after stripping. The magnetic elements and the pulsed distributor must have a rigidity no more than 15% above that for 50 MeV protons. For the particular case of ^{208}Pb ions the non-relativistic approximation is used:

$$B\rho = 30W^{0.5}/Q$$

with W the lead ion energy in MeV/u, Bρ in Tm and Q the charge state. For lead ions between 2 and 8 MeV/u the most probable charge state Q produced after a carbon foil, is derived from an empirical formula due to E. Baron [14]

$$Q = 82\ (1 - \exp\ (-0.51W^{0.5})).$$

Solving the two expressions above for Bρ = 1.16 Tm, gives the linac energy of 4.2 MeV/u and Q = 53+. Experiments have shown that a carbon foil of the correct thickness will give a range of charge states around the chosen one, Pb^{53+}, which itself will correspond to about 16% of the input beam flux.

The second stripping stage in the scheme occurs between the PS and SPS at 4.25 GeV/u; in the GeV range, all electrons are stripped away, and the efficiency approaches 100%.

Table 1.3.1: Nominal intensities and efficiencies

Accelerator (or element)	Output β	Output T	Effic. η	Pb ions per PS cycle[1]	Pb ions per SPS cycle[1]	Comments
ECR Source	0.0023	2.5 keV/u		7.13 10^9	2.85 10^{10}	80μAe, 400μs Pb^{28+}
RFQ	0.023	250 keV/u	0.9			
IH Linac	0.094	4.2 MeV/u	0.9	5.78 10^9	2.31 10^{10}	65μAe Pb^{28+}
Stripper foil			0.16	9.25 10^8	3.70 10^9	Pb^{28+} => Pb^{53+} (20μAe) stripping loss
PSB injection			0.4			Multiturn injection, 4 * 18 turns
Acceler. (h=10)	0.421	95.4 MeV/u	0.6	2.22 10^8	8.88 10^8	RF capture, vacuum
PS injection			0.95			Including PSB-PS transfer (2 bunches => 1 bucket)
Acceler.(h=20)	0.984	4.25 GeV/u	0.7	1.48 10^8	5.91 10^8	Vacuum
Stripping			1.0			Pb^{53+}=> Pb^{82+}
SPS injection			0.95			Including PS-SPS transfer
Acceleration	~1	177 GeV/u	0.7		3.93 10^8	

[1]Source, RFQ, IH Linac , PSB: all one cycle per PS cycle. Four PS cycles per SPS cycle.

Overall ion acceleration efficiency between ion source and SPS extraction: η = 0.014

1.3.2 Introduction to Vacuum Losses in PSB and PS

Amongst the losses specific to heavy ions the dominant mechanism is charge exchange between molecules of the residual gas and the circulating ion, which loses or captures one or even more electrons. Any of these events causes an immediate loss of the ion in a circular accelerator. In order to evaluate the probability of loss during the acceleration cycle one needs to know the cross-sections for these processes as a function of the energies in the range of interest. Although there are numerous theoretical calculations there are only a few experimental points to verify the cross-sections. We have used an empirical formula fitted to GSI data [15] combined with calculations from LBL [16], and always used the more pessimistic one. Measurements at 4.66 MeV/u made at LBL [17] add some confidence to our assumptions in the region of the early acceleration in the PSB where most of these losses occur. Comparing LBL and GSI formulae for total cross-sections [18] one notices that LBL gives larger ones for energies <12 MeV/u and vice versa above 12 MeV/u. The experimental point at 4.66 MeV/u seems to fall right in between the two. Within the frame of this model one can compute the probability of survival for a given acceleration cycle as a function of vacuum pressure. The result is shown in Fig. 1.2. Note that pressure is defined as a partial pressure of non-hydrogen gas components, mainly H_2O, N_2 and CO which account for the quasi-totality of the loss effect compared with hydrogen, whose charge-exchange cross-sections are an order of magnitude lower. One can clearly see that beam loss dependence against gas pressure exhibits threshold character around a cross-over at about 5 10^{-9} Torr in the PS and 10^{-9} Torr in the PSB, in particular for the PSB power supply with $\dot{V}$>100 kV/s. For pressures less than 10^{-10} Torr the machines are practically transparent while above 5 10^{-9} Torr the beam losses due to residual gas are more than 90% in the PSB.

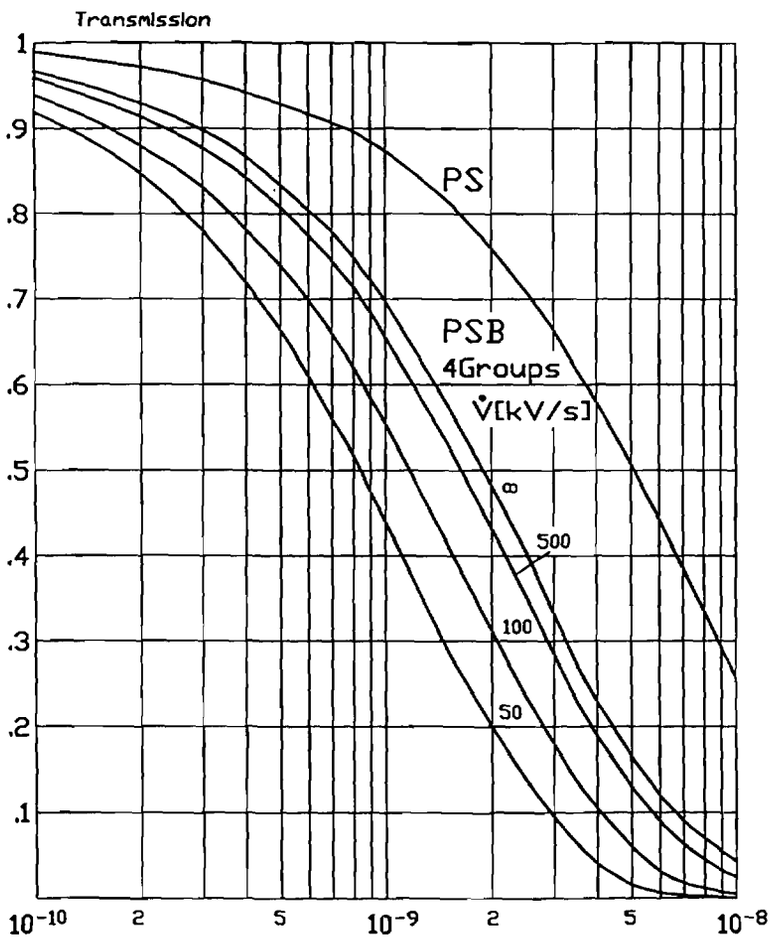

PSB parameters 50, 100, 500 and ∞ are initial rates of voltage rise (kV/s) of main power supply. Target value, to achieve an appreciable increase in dI/dt, is 150kV/s

Fig. 1.2 Ion Transmission in PSB and PS as Function of N_2 Pressure

2 LINAC 3 FROM ECR SOURCE TO INPUT OF BOOSTER

2.1 INTRODUCTION

As mentioned in Section 1.2, this linac (now called Linac 3) is being designed, constructed and largely financed by the collaborating institutions from CERN member states. The division of this chapter into sections naturally follows this division of responsibilities along the linac from source to booster input. An overall presentation of the beam characteristics as they evolve along the linac and filter stripper line is given in the table of parameters, 2.9.1.

There is a standard nomenclature for CERN accelerator components which, at the time this report was being prepared, was being applied wherever possible to this new Linac 3. The first identifier is 'I' so the prefixes used for the main linac systems are IP (ion preinjector including the source), ITL (low-energy beam transport), IAQ (radio-frequency quadrupole), ITM (medium-energy beam transport) and IA1, IA2, IA3 (the interdigital-H accelerator tanks). In Fig. 2.1, this PS nomenclature is illustrated for Linac 3, between source and measurement lines at 4.2 MeV/u. This nomenclature is used here to denote elements, especially in the tables where for simplicity the prefix Ixx. is often omitted. Examples of the application of these abbreviations to selected elements in Linac 3 and other accelerators of the PS complex are given in a foreword to this report.

It is worthwhile noting that the design and performance of the linac can logically be described for three charge states of the pure isotope ^{208}Pb, i.e. Pb^{25+}, Pb^{27+} and Pb^{28+}; the lowest charge state has been used for all the calculations in order to provide a reasonable (10%) margin over the operating parameters (e.g. RF level and magnetic focusing fields) required for the nominal operation at the highest charge state. In the mode of operation chosen for the ECR source the charge states Pb^{27+} and Pb^{28+} are produced with about the same currents so either could be chosen depending on the overall requirements of the machine, with a preference for Pb^{28+} if operating fields are to be minimised.

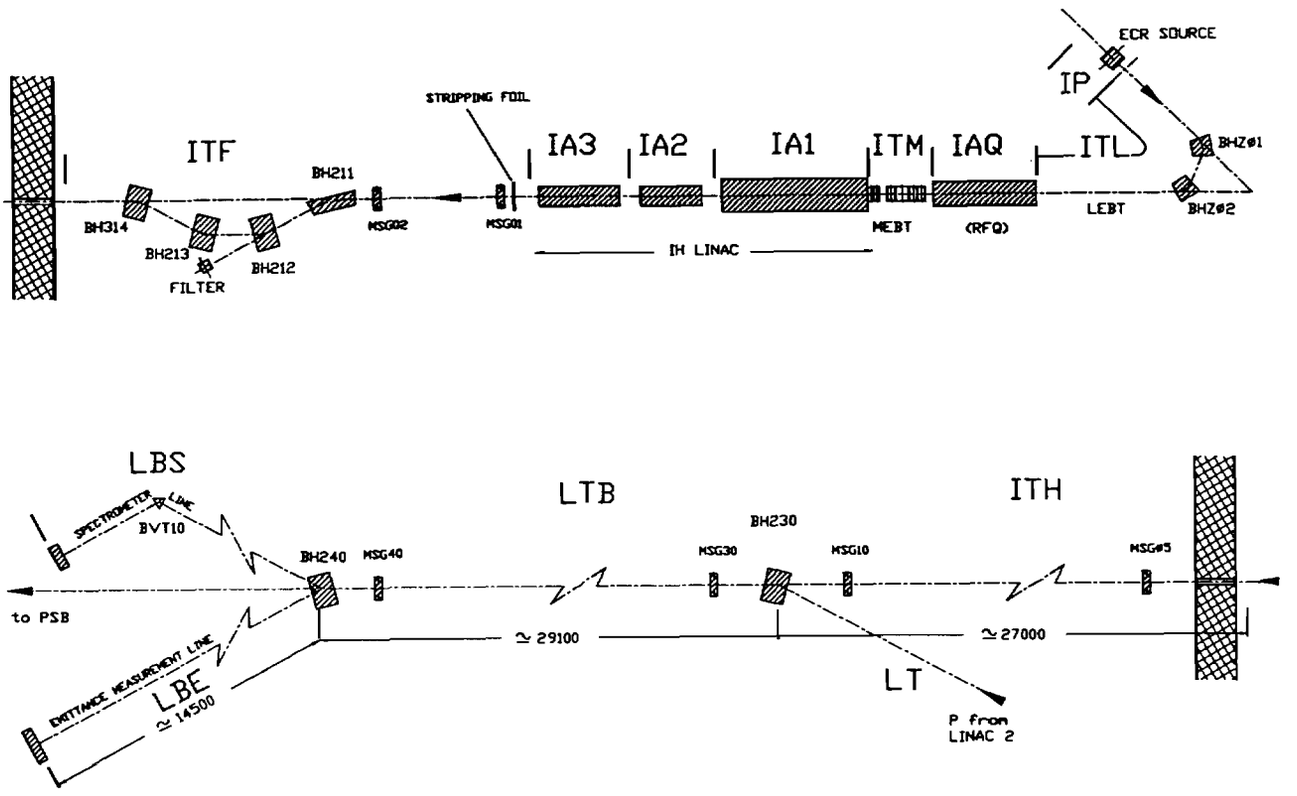

Fig. 2.1 Schematic Layout of Transport Lines Between Linac 3 and PSB

2.2 THE INJECTION SYSTEM

Although other types of sources for highly charged heavy ions exist, a 14.5 GHz Electron Cyclotron Resonance (ECR) ion source was chosen for lead ion production. This choice was based on the experience acquired at CERN during the light ion runs and the ready availability of such sources. The source, as described below, successfully completed its tests at GANIL and was delivered to CERN in November 1992.

2.2.1 The Ion Source (IP)

With the increased use of ECR sources in the accelerator and industrial fields, the ECR source has evolved away from the mini-MAFIOS design [19]. The source chosen for the project is a new version of the CAPRICE design [20,21] known as ECR4 which is shown schematically in Fig. 2.2.

Basically the source is a plasma generator with the plasma confined longitudinally in a magnetic bottle produced by a set of two solenoids. Radial confinement is achieved by superimposing on the axial field a strong radial field created by a Fe-Nd-B permanent magnet sextupole. The plasma is created by microwave RF ionisation. As within the plasma volume there is a small zone with magnetic field surfaces (0.52 T at 14.5 GHz) where the electron cyclotron resonance frequency corresponds to that of the injected RF power, plasma electrons crossing these surfaces will in general be heated to higher energies. These hot electrons can, by successive electron impact ionisation, increase the charge state of ions in the plasma. Ions escaping longitudinally from the plasma can be extracted by classical electrostatic means.

Lead ions are produced by evaporation of the metal from a 'micro oven' which is introduced into the plasma chamber through the inner conductor of the microwave waveguide to coaxial transition whose main function is to introduce the 14.5 GHz power. Oxygen is also added via this route to act as a plasma-generating support gas.

The main feature of this source is the rapid local variation of magnetic field gradient in the radial direction, i.e. strong sextupole component, to improve the plasma confinement. Along the radius of the cylindrical plasma chamber, the field varies between 0.4 and 1 T.

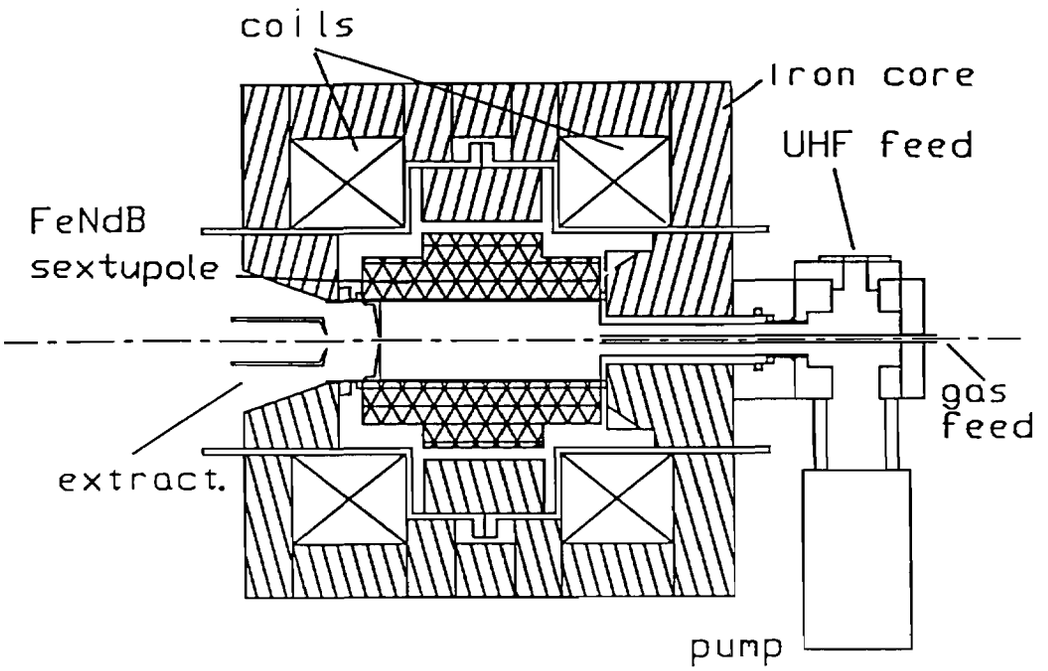

Fig. 2.2 Schematic Layout of the Central Region of the ECR Source

2.2.2 Design Characteristics

The following tables summarize the important parameters of the source and its ancilliary equipment. Further details of all the components are given in table A2.2.1 in the appendix.

Table 2.2.1: Main parameters of the ECR source

Peak Axial Field	1.1	T
Solenoid Magnet Power	≈60	kW
Typical Solenoid Current	1100	A
Mirror Ratio	2.2	
Sextupole Magnet Material	Fe-Nd-B	
Pole Tip Field	1.2	T
RF Frequency	14.5	GHz
RF Power Input (max)	2	kW
Plasma Chamber Bore Dia.	66	mm
Anode Aperture	16	mm
Extraction Aperture	13	mm
Total Length	600	mm
Total Outer Diameter	400	mm
Total Weight	≈500	kg

The sextupole is made of 3 slices of Fe-Nd-B alloy (VACODYN 370HR). Two sections of a smaller radius constitute the end cells so as to have smaller diameter solenoid coils where the axial field must be maximum. A larger centre section has a field gradient around the resonance region.

The solenoids are fully enclosed in an iron yoke terminated near the sextupole by two pole pieces acting as flux concentrators. Their main parameters along with those of their power supplies are given below.

Table 2.2.2: ECR source solenoids

Number of Coils	2	
Nominal Resistance/coil	27	mΩ
Nominal Voltage/coil	30	V
Nominal Current	1100	A
Voltage Stability (drift + ripple)	<50	mV
Current Stability at 1100A	$\pm 10^{-4}$	
Time constant	≈70	ms
Water Flow	35	l/min
Temperature Rise (approx.)	20	°C
Water pressure input	15	bar

The water-cooled plasma chamber is made up from two concentric stainless steel tubes for effective cooling. This double wall also acts as a heat shield for the permanent magnets and avoids any corrosion problems with the magnets if they should be in contact with water. The RF power is transported by a waveguide from the transmitter to the cooled copper waveguide-to-coaxial transition with a ceramic window in the guide acting as a vacuum seal.

A copper extension tube acts as the outer conductor of the coaxial line used for the injection of RF power into the plasma. Important parameters of the RF transmitter are given in table 2.2.3

Table 2.2.3: RF transmitter characteristics

Frequency (fixed)	14.5	GHz
Power Modulation	External	
Output Power Range	0–2.2	kW
Power slew rate	<1	ms
Power stability	±10-3	
Rise/Fall time	1	μs

Typically operational conditions require 10 Hz, 40 to 50% duty cycle.

To avoid the need of a high voltage platform, only the RF cavity and plasma chamber are at the extraction voltage of about 25 kV. The remaining components of the source are insulated from the above live parts and maintained at ground potential.

With regard to vacuum, two pumping systems are used. The first, using two TMP520M turbomolecular pumps, is used in the extraction chamber to obtain a pressure of $\approx 5\times10^{-7}$ Torr depending on the source operating conditions. A second system, using a small TPH60 turbo-pump, is used to pump the RF transition near the auxiliary gas injection to obtain an operational pressure of $\approx 2\times10^{-5}$ Torr. An air lock, also pumped by a TPH60 pump is used to enable the sample oven to be removed for maintenance and replacement of the lead sample, without affecting the source vacuum. Figure 2.3 shows the overall layout.

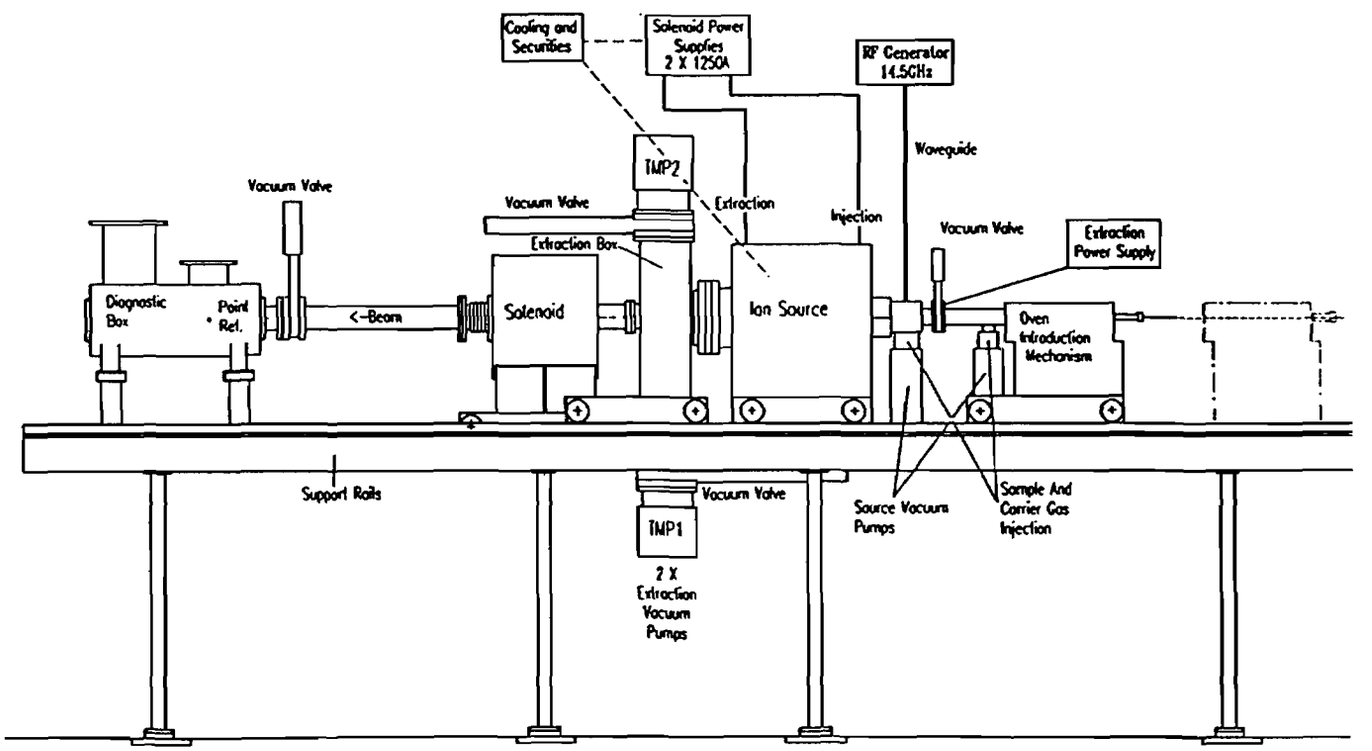

Fig. 2.3 Schematic Assembly of Complete ECR Source

2.2.3 Source Operation

An ECR has three useful modes of operation; continuous, pulsed or pulsed afterglow. As the project specification called for a 400μs pulse of 100μAe for ion species between Pb^{25+} and Pb^{28+}, the pulsed afterglow mode of operation is particularly convenient. The afterglow effect manifests itself by a sudden but brief increase in beam intensity occurring just after the end of the microwave power pulse. Experiments made at GANIL [22] showed that this mode of operation was possible with a 14.5 GHz pulsed source if it was tuned in such a way as to enhance this effect. Figure 2.4 shows the charge state distribution where one notes the strong perturbing spectral line from O^{2+} at the Pb^{26+} position. Figure 2.5 shows the Pb^{28+} current in the afterglow mode.

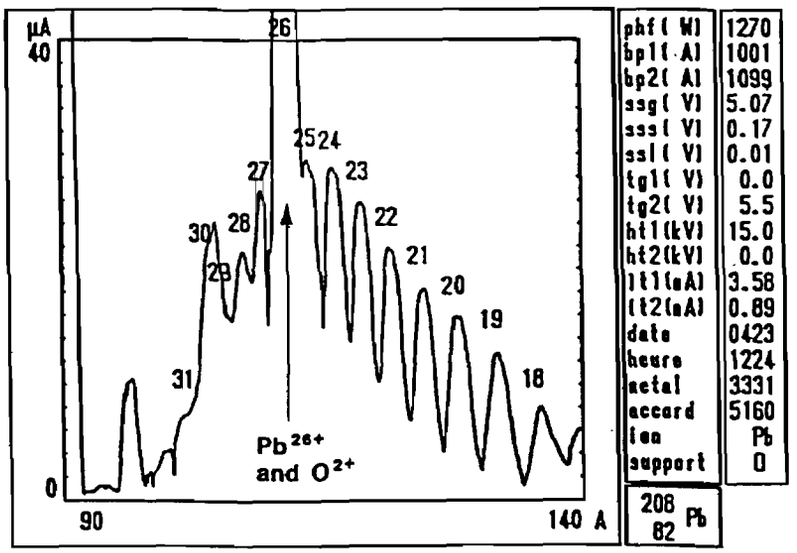

Fig. 2.4 Ion Spectrum Optimised for Pb^{28+} (about 20μAe) in Continuous Mode

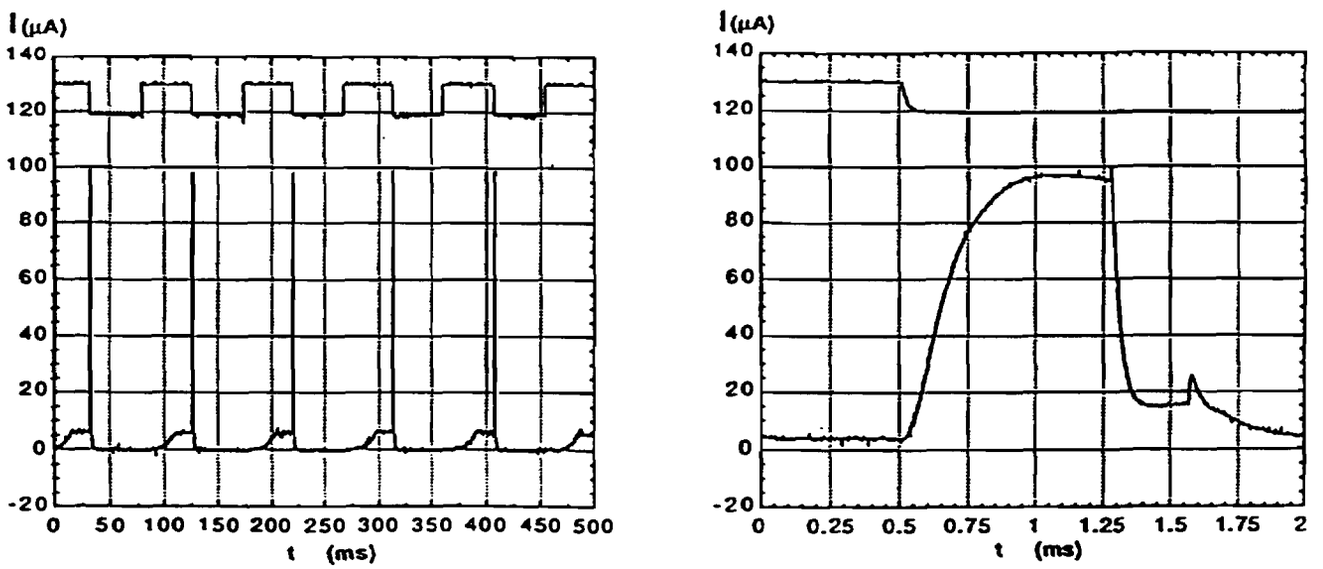

Fig. 2.5 Afterglow Pulsed Current of Pb^{28+}: Upper Traces RF Power, Lower Traces Beam Current

2.2.4 Beam Characteristics

The beam extracted from the source is transported to the entrance of the analysing section by a solenoid, SOL01, which focuses it onto an 'object' slit which also performs an initial charge state selection. The low energy beam transport between the object point and the RFQ is the subject of chapter 2.3.

Characteristics at the Object Waist.

It is important to know the beam properties at the waist to obtain maximum transmission in the LEBT. Measurements on the test bench which give the main characteristics of the source and the desired properties of the beam line to the waist, are given in table 2.2.4.

Table 2.2.4: Beam properties as measured on the test bench.

Horizontal emittance at 18kV: 100%	<120	π mm.mrad
80%	<100	π mm.mrad
70%	<60	π mm.mrad
Beam radius at waist	2.7	mm
Maximum divergence at waist	33	mrad
Extractor to SOL01 drift	480	mm
Solenoid effective length	300	mm
Nominal field	0.485	T
SOL01 to waist drift	0.818	m
Current through slit, corresponding to 80μAe of Pb^{28+}	≈480	μAe

The horizontal emittance measured on the test bench showed that due to the small beam size and the presence of a high density core, space charge needs to be taken into account in the analysing section [23]. The addition of a quadrupole after the analysing magnet has been tested as a means of maintaining the waist position and its dimensions. It would also be possible to move the source and solenoid backwards to give a larger waist and minimise the effect.

2.2.5 Beam Diagnostics

A measuring box which includes both horizontal and vertical slits, a Faraday cup and a profile monitor (47 wires, 1 mm step) will be located after the solenoid SOL01 to allow emittance measurements at the waist.

2.3 LOW ENERGY BEAM TRANSPORT (LEBT, ITL)

2.3.1 Functional Description

The LEBT connects the ECR ion source to the RFQ structure and it is shown in Fig. 2.6. It can be divided into three logical sections: from the output of the ECR source to the object focus of the spectrometer; the spectrometer itself; the matching section from the image point of the spectrometer to the input of the RFQ.

2.3.2 Source to the Object Focus of the Spectrometer

This section prepares the beam for the proper injection into the analysing system. It consists of a solenoid (SOL01) followed by a diagnostic box containing defining slits, a Faraday cup and a beam profile monitor. The object point of the spectrometer is the waist produced by the solenoid; the solenoid and the source can be longitudinally shifted to obtain the desired spot size at the object point and the desired resolution for a certain range of initial source operating conditions. This gives some flexibility in the choice of the parameters, that will be fixed according to commissioning experience. The technical characteristics of the solenoid, that focuses the beam into the diagnostic box, are described in table 2.2.4.

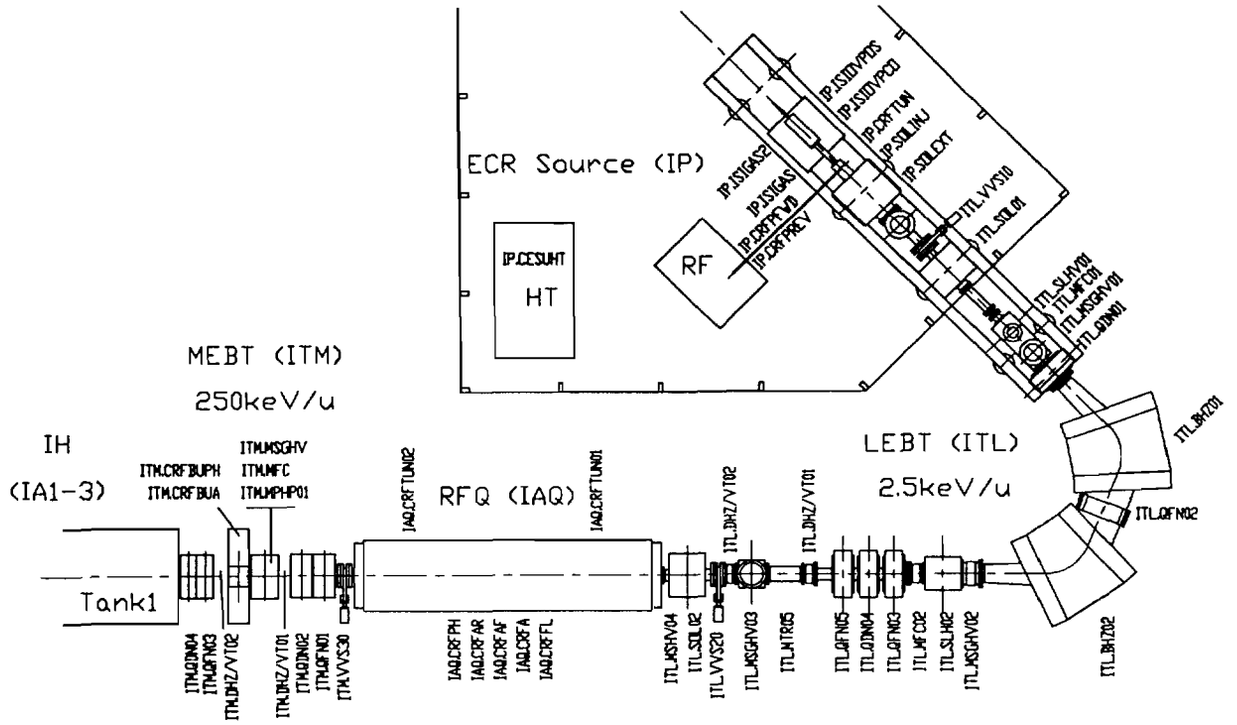

Fig. 2.6 Schematic Layout of LEBT, RFQ and MEBT Region

2.3.3 Waist to High Resolution Waist After 135^{0} Spectrometer

The central part of the LEBT is a compact spectrometer with a resolution of 3/1000. The choice of a bending radius = 0.4 m and a dipole field of 0.15 T is convenient for the engineering of the magnets and it has been selected from different configurations, taking into account the non-linear analysis which includes the magnetic aberrations in the dipole magnet, in order to accommodate a beam with a horizontal extension comparable with the bending radius. The spectrometer design used for the LEBT of the new high charge state injector (HLI) at GSI [24], has been selected. This has two separated 67.5^{0} magnets with the angles of all pole faces inclined by 25^{0}, to provide focusing in the vertical plane. The gap height is 90 mm and the pole width 480 mm (Fig. 2.7).

The advantage of this configuration (two magnets) is the possibility of shimming the internal faces of the magnets so as to introduce a sextupole correction; with a curvature of radius 2.7 m of these faces, the second order aberrations of the magnets can be corrected.

2.3.4 Waist to Input of RFQ

After the spectrometer, a quadrupole triplet restores the cylindrical symmetry of the beam, and the solenoid SOL02 focuses the beam to match the initial RFQ conditions. Two pairs of steering magnets (horizontal, DHZ and vertical, DVT) are located between the triplet and SOL02, to have the possibility of a position and angle correction at the entrance of the RFQ (Fig. 2.6).

2.3.5 Summary of Beam Dynamics Including Space Charge

In table 2.3.1 are listed the main matrix elements between the object and the image after correction; x_i is the horizontal beam dimension at the image point. For this particular matrix, involving imaging, the term $\partial x_i/\partial x'$ is ideally zero.

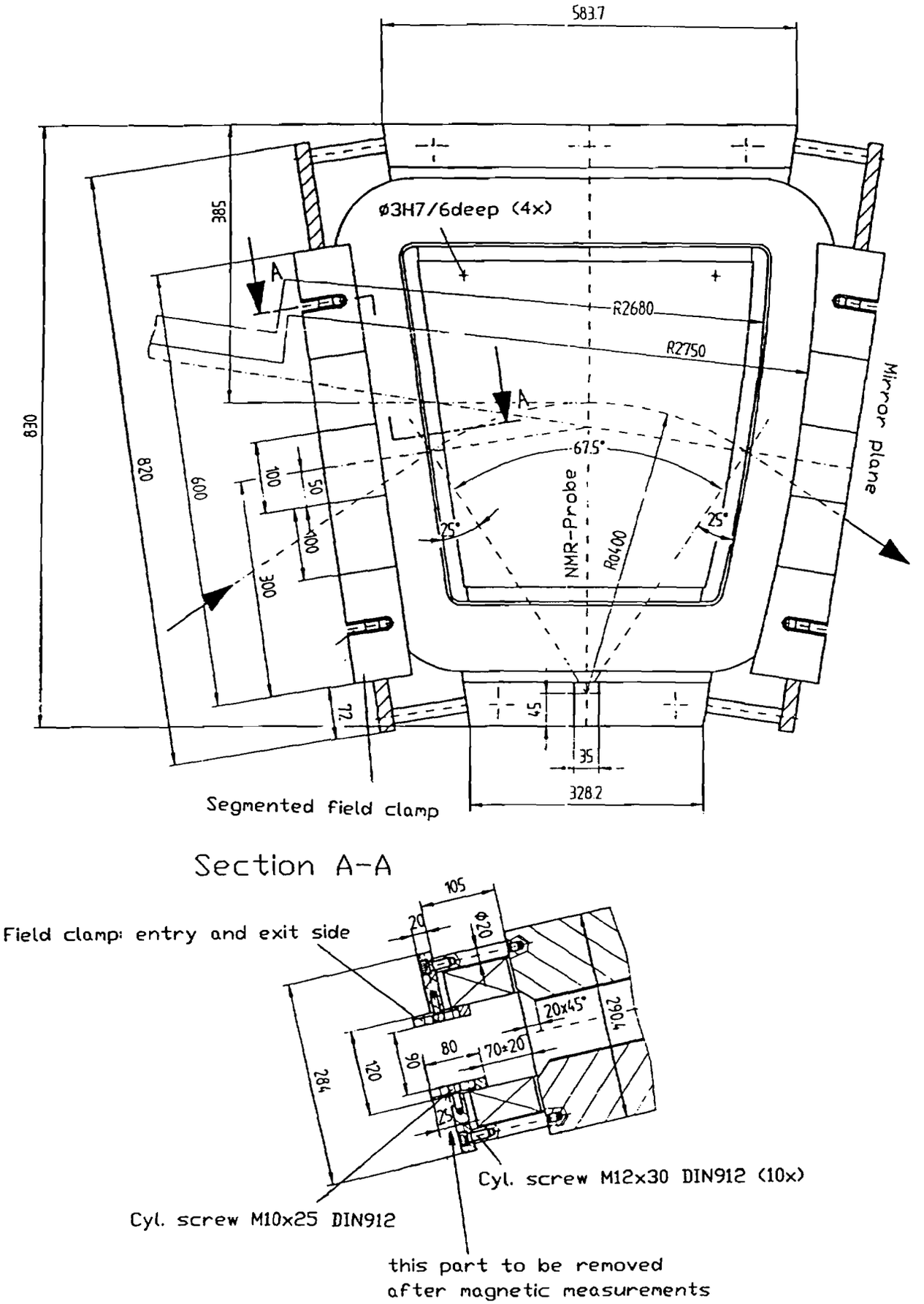

Fig. 2.7 Details of One of The Two Spectrometer Magnets (67.5 ° Bend)

Table 2.3.1: Matrix elements

Magnification	$\partial x_i/\partial x$	–0.44
Dispersion	$\partial x_i/\partial(\Delta m/m)$	+1.3 m
Aberrations	$\partial x_i/\partial x'$	$+7 \times 10^{-5}$ m
	$\partial^2 x_i/\partial(x'^2)$	-3×10^{-3} m
	$\partial^2 x_i/\partial(x^2)$	-9×10^{-2} m^{-1}
	$\partial^2 x_i/\partial(xx')$	-3×10^{-2}

Since the Twiss parameters, β, at the object and image points are much smaller than the distance between these points, one can consider the beam waist and the image point locations as coincident (independent of the object spot size).

The resolution, defined as:

$$R = \frac{\partial(\Delta m/m)}{\partial x_i} 2x_i = \frac{\partial(\Delta m/m)}{\partial x_i}\frac{\partial x_i}{\partial x} 2x \qquad (1)$$

depends on the beam dimensions at the object point or, for a given emittance, on the divergence. As BHZ01 and BHZ02 are the only bending magnets in the low energy part, the dispersion vector (D,D') will keep oscillating in the RFQ and in the IH preserving the invariant:

$$\varepsilon_D = \left[D^2 + (\alpha(z)D + \beta(z)D')^2\right]/\beta(z) \qquad (2)$$

where α(z) and β(z) are the Twiss functions and ε_D is analogous to the error invariant in the standard Courant and Snyder treatment [25]. This means that, if δ is the energy spread before the dipoles, $\varepsilon_D\,\delta^2$ is the corresponding contribution to the transverse emittance. Note that errors in some beam optics elements behave, in their action on the beam, like an energy spread, δ. It is easy to see that ε_D depends upon the square of the resolution; indeed at the object point:

$$\varepsilon_D \approx \frac{D^2}{\beta} = 4\varepsilon\frac{D^2}{4\varepsilon\beta} = \frac{4\varepsilon}{R^2} \qquad (3)$$

For this reason the system (with a high resolution and an intrinsically low acceptance in the accelerators) needs a high stability in the power supplies of the source and of the magnets to reduce the effective value of δ. In fact the power supply of BHZ01 and BHZ02 has been specified with 10^{-5} stability.

The preliminary operations of the source at GANIL have shown some space charge effects on beam optics. When the source works in afterglow mode, the image point is displaced forward by some cm; the effect is greater than is calculated by considering the current as uniformly distributed in a 150 π mm mrad emittance. According to first emittance measurements, this discrepancy could be explained by the inhomogeneous distribution of the beam in the horizontal phase plane. More data will be taken during the first operations of the source at CERN with the high resolution spectrometer.

For the correction of space charge the insertion of a quadrupole between the two bending magnets is foreseen. TRACE2D [26] computations indicate that a quadrupole strength of the order 0.0028 T is needed but a design value 5 times higher is adopted. Because of the limited space (only 0.14 m iron length) and the large aperture requirements of 0.40 m × 0.09 m it will be a window frame, 'Panofsky type', quadrupole.

2.3.6 Computational Results

In Fig. 2.8 are shown the beam envelopes in the LEBT (corresponding to 4 ε_{rms} as TRACE 2D is used) for a typical set of source output parameters.

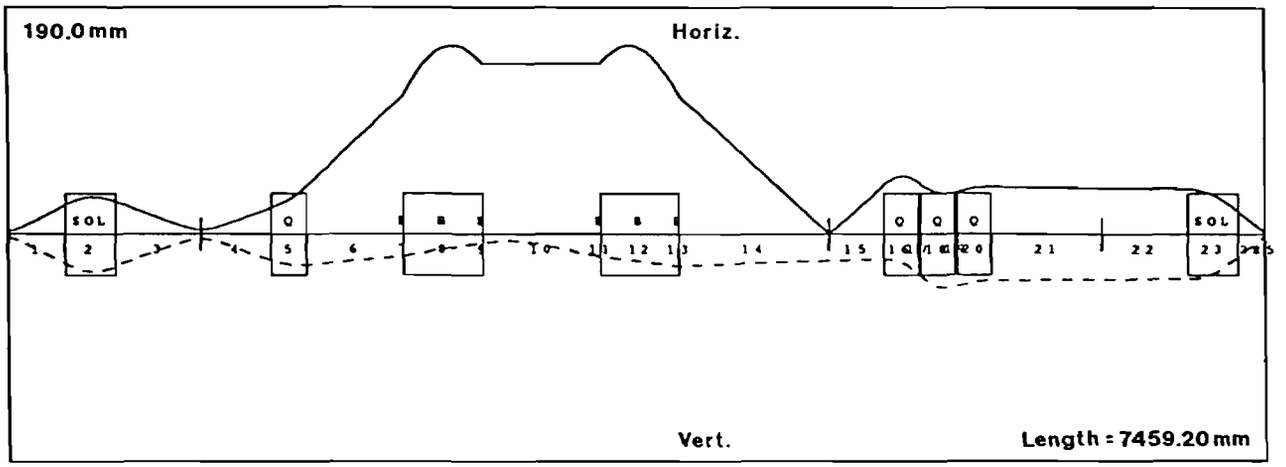

Fig. 2.8 Typical Beam Envelopes in the LEBT

2.3.7 Component Design and Layout in LEBT

The LEBT contains various beam diagnostic and measurement devices. Starting from the ECR source there is a diagnostic box containing the grids for the beam profile monitoring and the input slits of the spectrometer. The following diagnostic box is placed in the image point of the spectrometer and it contains, following the beam path, the beam profile grids, the analysing slits and a Faraday cup. Between the quadrupole triplet and the final solenoid there is room for a beam transformer for an on-line beam current measurement. The last diagnostic device is a segmented monitor to be placed in front of the RFQ.

Concerning the vacuum systems, the LEBT is separated from the connected part of the injector by vacuum valves placed before the solenoid SOL01 and before the solenoid SOL02. The vacuum pumps foreseen for this section are: an ion pump of 60 l/s connected with the first diagnostic box; a pumping station containing a two-stage primary pump and a turbo pump of 240 l/s capacity connected to the vacuum pipe after the second bending magnet. If necessary a third pump, an ion pump of 60 l/s can be placed between the quadrupole triplet and the solenoid SOL02.

Details of the parameters of the LEBT bending magnets, quadrupoles and solenoids are given in the appendix in tables A2.3.1, A2.3.2, A2.3.3, and A.2.3.4.

2.4 RADIO FREQUENCY QUADRUPOLE (RFQ, IAQ)

2.4.1 Specifications and Choice of Parameters

Downstream of the LEBT, an RFQ structure accelerates the ion beam from 2.5 keV/u to 250 keV/u; it has been specified to have a length smaller than 2.8 m. The source works in 'afterglow mode', giving pulses 400 μs long and 10 Hz repetition rate; thus the RFQ, pulsed with the same rate, has a duty cycle below 1%.

The design frequency has been chosen to be 101.28 MHz. The beam dynamics analysis showed that this value is a good compromise between the required focusing strength and the maximum achievable surface electric field (twice the Kilpatrick limit, 22.8 MV/m).

Due to the low beam current intensity delivered by the ECR (below 1 mA), the space charge effects are negligible in the RFQ beam dynamics analysis; nevertheless the limited current from the ions source demands a high transmission (at least 90%) and a good beam quality for the following accelerator (normalized acceptance of at least 0.8 π mm mrad, and emittance of 0.5 π mm mrad).

Table 2.4.1: Specifications for the RFQ

Particles	Pb^{25+}
Input energy	2.5 keV/u
Ouput energy	250 keV/u
RF frequency	101.28 MHz
Max. surface field	< 23 MV/m
Acceptance	$\geq 0.8\pi$ mm mrad
Longitudinal emittance	$< 1.08\pi$ keV ns/u ($< 40\pi$ deg keV/u*)
Transmission	> 90%
Output energy spread	< ±2%
Output phase spread	$< \pm 12^{o}$
Repetition rate	10 Hz
Duty cycle	0.4%

* 'Practical' units used in computer program (deg at 101.28MHz)

2.4.2 Beam Dynamics: Computational Methods and Results

Kapchinskij's original proposal for an RFQ accelerator [27] dealt with a high intensity machine; an approach for low intensity RFQs was put forward by Yamada [28]. The above considerations, combined with an extensive study of different kinds of bunching techniques, led to a novel design procedure [29] in which the structure is divided into six different logical sections and there is a quicker change of parameters, like the accelerating field strength and the synchronous phase along the structure.

These six sections are: the radial matching section (following the Crandall design procedure [30]), the shaper (where the bucket is created), the prebuncher (fast phase compression with constant bucket area), the adiabatic buncher (completion of bunching and more efficient acceleration, following a more recent proposal by Kapchinskij [31]), the booster (fast rise of acceleration), and the accelerating section (up to the final energy).

By optimizing the bunching part of the RFQ, it is possible to design a 2.5 m long structure, with a transverse acceptance, a surface electric field and a transmission that fulfil the requirements of table 2.4.1. and are given in table 2.4.2.

The ratio ρ/r_0 between the transverse radius of curvature of the electrodes and the average aperture is usually in the range 0.75 to 1.0, where the smaller value gives a higher accelerating field, the bigger one a lower multipole component in the field. In this design it has been possible to choose $\rho = 0.95\ r_0$.

Figure 2.9 shows how the parameters, relevant to beam optics, vary along the RFQ; in Fig. 2.10 the transverse envelope, the phase profile and the energy spread profile are represented.

According to simulations, beam losses are concentrated in the RFQ during the bunching process. No significant emittance increase has been observed; nevertheless the emittance value used in the simulation of the RFQ dynamics (0.5 mm mrad) has been assumed bigger than the output of the source (0.35 mm mrad), while the acceptances increase from one section of the RFQ to the next one. This gives a safety margin to cope with misalignments and mismatch of the source.

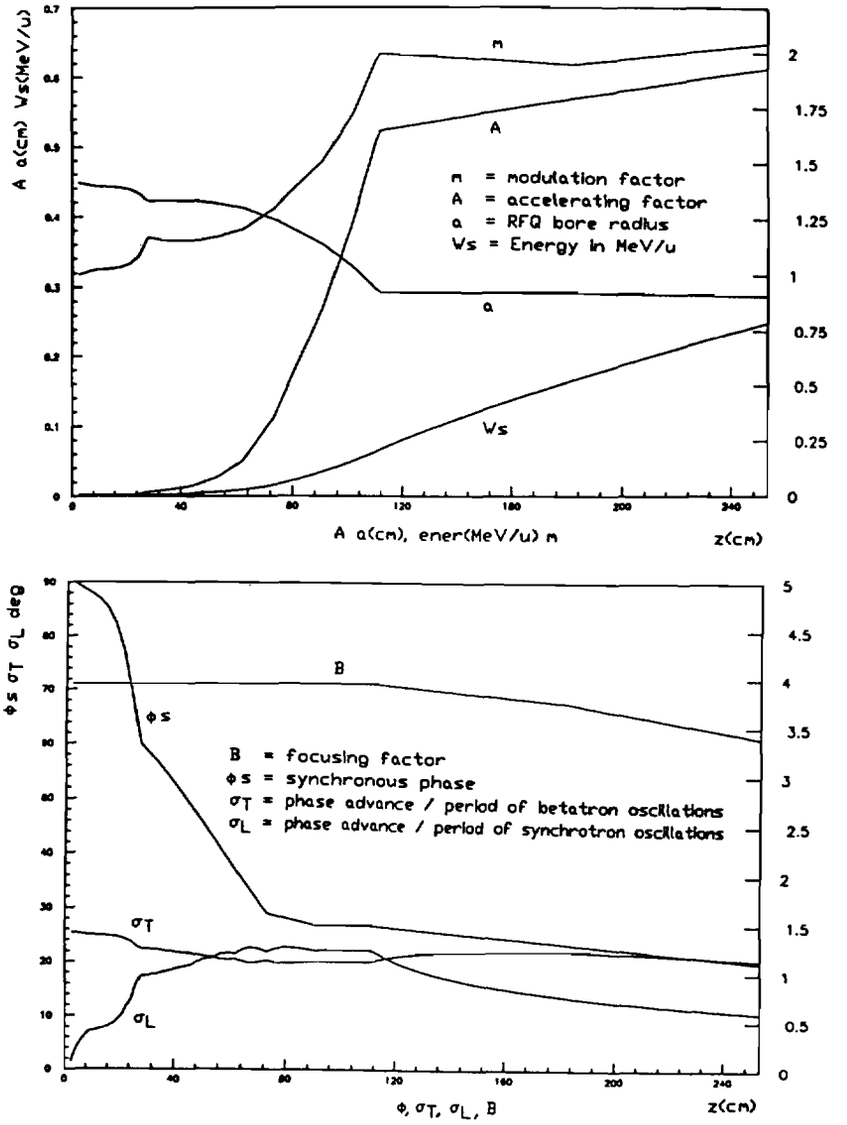

Fig. 2. 9 Optimised Design Parameters for the RFQ

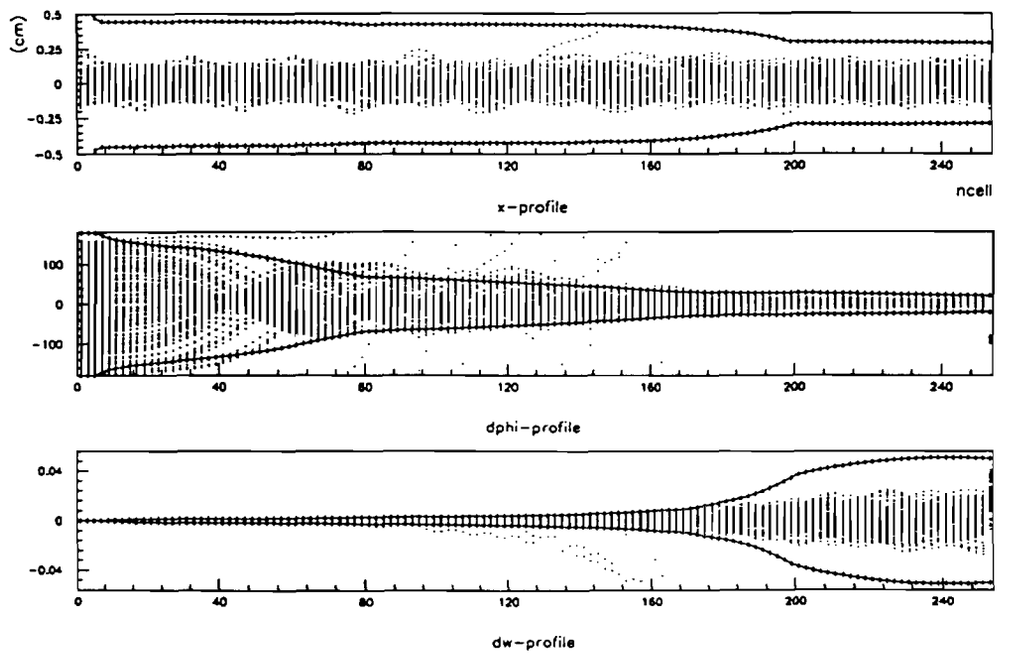

Fig 2.10 Variation of X-Profile, Phase-Spread and Energy Spread Profile Along the RFQ

Table 2.4.2: Computed dynamics parameters of the RFQ

Vane length	2500 mm
Vane voltage	70 kV
Average aperture radius r_0	4.5 mm
Transverse vane tip curvature radius ρ	4.28 mm
Transmission	93%
Transverse emittance increase	–
Longitudinal output emittance (5×rms)	0.94π keV ns/u*

* Equivalent to 34π deg keV/u from computed results.

2.4.3 RF Design and Modelling

Because of the relatively low resonant frequency value, the choice of a '4-rod'-like resonator was quite natural [32]: clear advantages of this structure, when compared to a design of the '4-vane' type, are its compactness at the low frequencies required for ion acceleration and its reduced sensitivity to perturbing modes which compensates for its lower shunt impedance, Z_{sh}.

Nevertheless, two main changes have been considered necessary with respect to the standard design: a double support design [33] and 'vane-like' shaped electrodes [34] have been chosen. The first design choice gives a structure which has no electrical dipole moment in the beam region (without affecting the shunt impedance), as confirmed by numerical simulations and cold modelling of the cavity. The second one makes the alignment of the electrodes in the structure more reliable with the presence of a reference plane for each electrode and also increases the rigidity of the electrodes.

The electrode cross-section has been studied to increase its mechanical rigidity and to give a large surface for the high longitudinal current. The drawback of the vane-like shape is the higher inter-electrode capacitance, which reduces Z_{sh}; however, a careful optimization of the resonator could compensate for this. Opposite pairs of electrodes are connected to frames that force them to the same potential by acting as 'Vane Coupling Rings'; each frame is connected to two supports.

2.4.4 Mechanical Design

The RFQ external tank consists of a cylindrical stainless-steel tank, copper plated with a thin layer (10 μm), with internal diameter of 440 mm and an overall length of 2660 mm. It contains the accelerating structure, the electrodes, made out of a chromium-zirconium-copper alloy, 2500 mm long. The supports connecting the electrodes with the external tank can be made of stainless steel as well as copper alloy depending on the thermal conductivity needed for the heat dissipation in the structure. If the supports are made of stainless steel, a copper plating is needed for proper electrical conductivity.

The required vacuum level inside the RFQ is of the order of 10^{-7} Torr. As the inner surface is more than 8 m^2, and the volume more than 450 l the vacuum system foreseen for the RFQ consists of a standard roughing station with turbo-pump of 240 l/s and 2 ion pumps of 60 l/s.

The RF power source at 101.28 MHz is delivered by an amplifier at 350 kW; the maximum RF pulse length required is 1 ms with 10 Hz repetition rate. A rigid, 100 mm diameter, coaxial line has been chosen for the feeder between the output amplifier and the RFQ.

Two piston tuners, with a diameter of 80 mm, are foreseen to be able to cover the tuning range of ± 70 kHz mantaining the proper field level along the structure within ± 1%.

The design of such an RFQ is shown in Figs. 2.11(a) and 2.11(b) and the computed dimensions are given in table 2.4.3 (repeated as table A2.4.3).

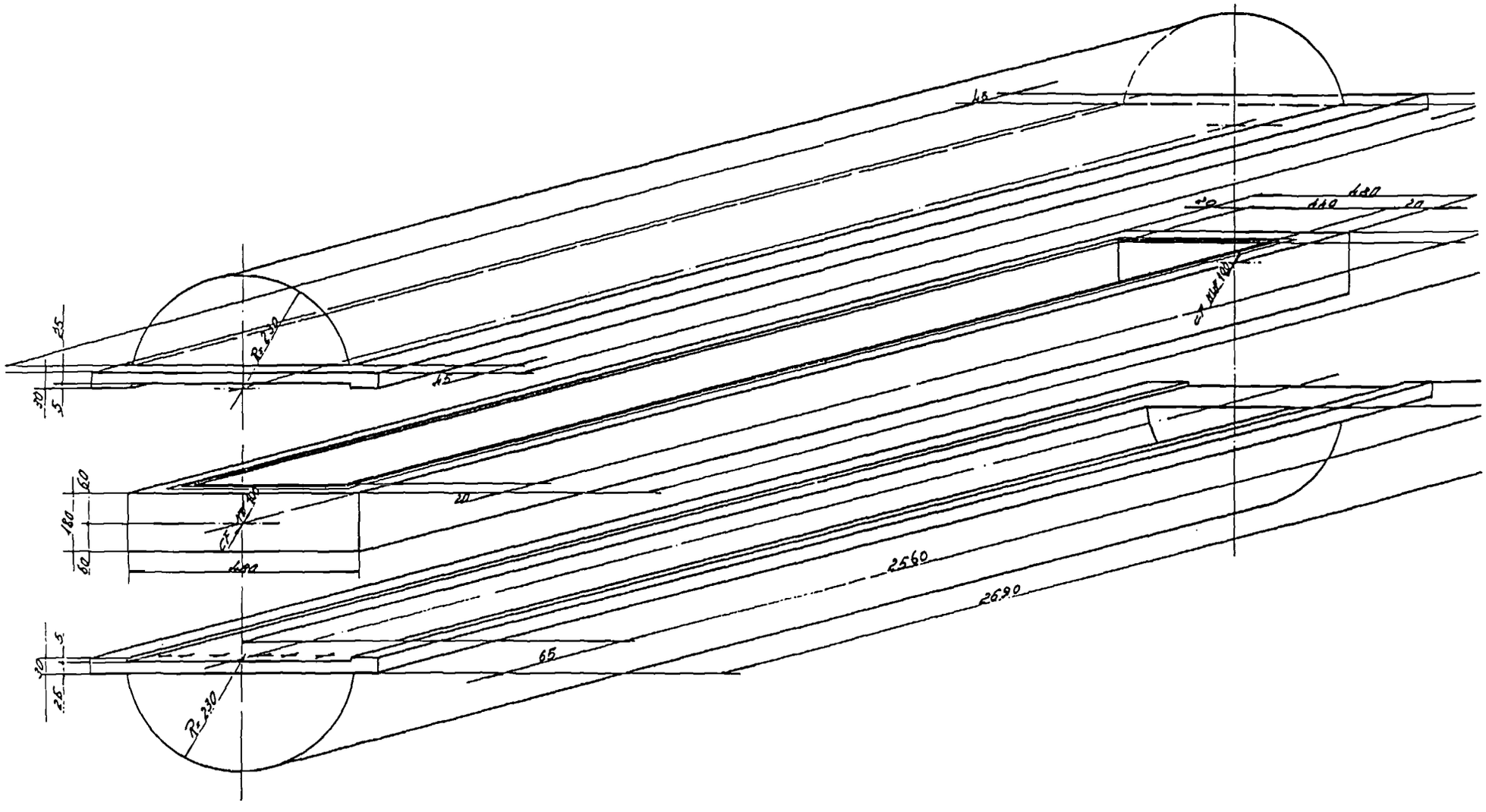

Fig. 2.11(a) Preliminary Design of RFQ: A Three-Dimensional OutsideView

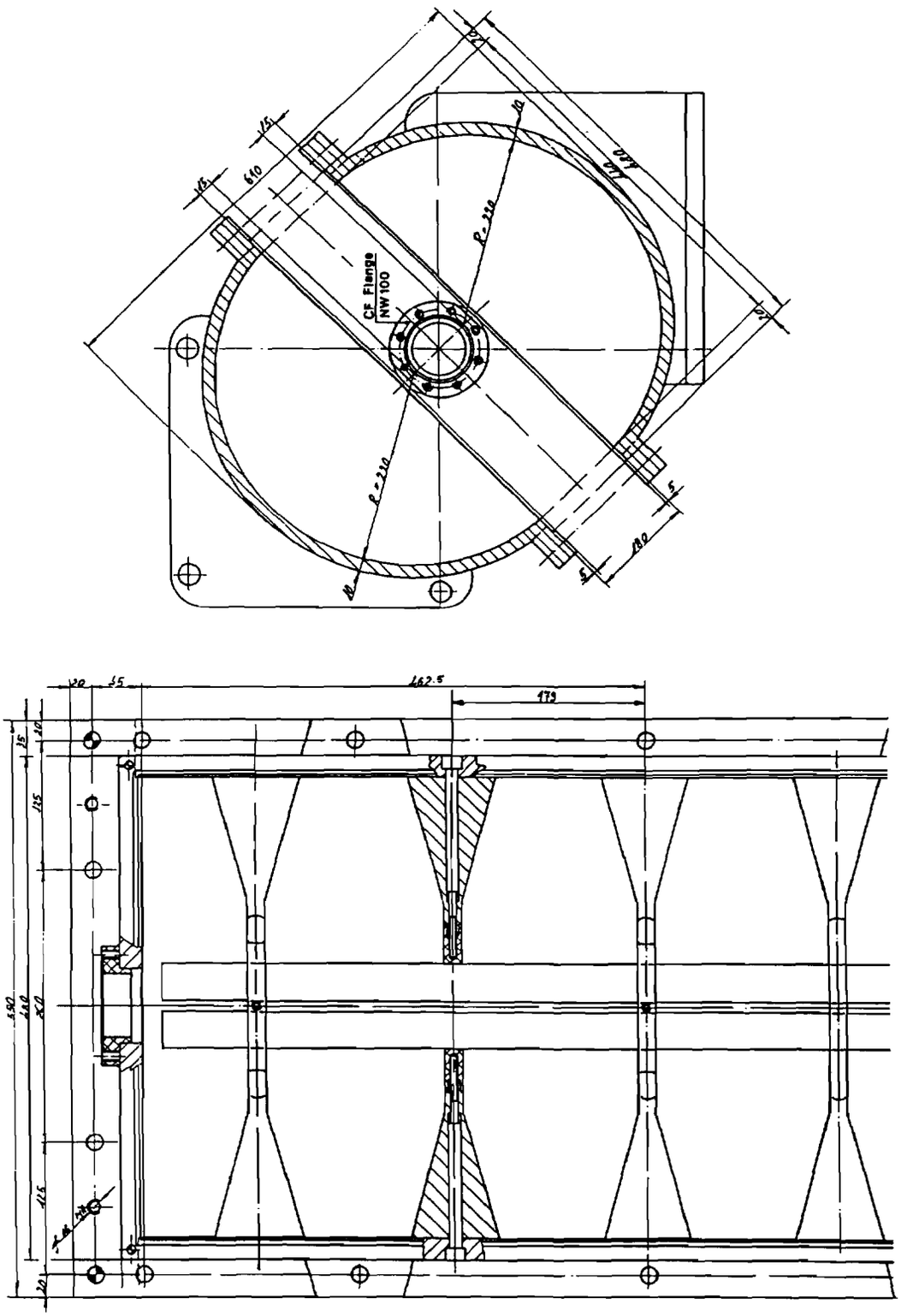

Fig. 2.11(b) Preliminary Design of RFQ: End View and Side View Cross- Sections

Table 2.4.3: RFQ dimensions

Overall tank length	2660 mm
Int. tank dimensions	590 × 440 mm
Ext. tank dimensions	610 mm × 480 mm
Number of supports	14
Cell length	179 mm

2.5 MEDIUM ENERGY BEAM TRANSPORT (MEBT, ITM)

The MEBT matches the beam between the RFQ and the IH structure both longitudinally and transversally. In order to do this, it contains four magnetic quadrupoles and a four-gap RF cavity operating as a buncher. In the section there are also a diagnostic station and a pumping station. The total length of the structure is 1.6 m.

Both RFQ and IH work at the same frequency, but have a different transverse focusing structure. The first is a FODO with $\beta\lambda$ period; the second is a triplet-drift-triplet effectively with greater than $6\beta\lambda$ period. Moreover the bunches have to enter the IH longitudinally convergent.

Therefore the beam matching in the MEBT requires action on six independent machine parameters: the voltage and the position of a buncher and the fields of four quadrupoles. The total length of the MEBT has been kept as small as possible in order to reduce the length of the pulse at the buncher ($\pm 44^{o}$) and the consequent non-linearity in the longitudinal phase-plane.

The buncher is a four-gap (inter-digital) quarter wave resonator. This choice has been made to have the maximum shunt impedance and to get the required voltage ($\approx$ 100 kV) with the available RF-power.

In Fig. 2.12 the envelopes of the beam in the MEBT are shown; the main beam parameters are listed in table 2.5.1 and table A2.5.1. A particular effort has been made to have a round beam inside the buncher and to reduce its transverse dimensions to make the longitudinal emittance growth as small as possible.

A schematic layout of the MEBT is included in Fig. 2.6. The design parameters of the magnetic elements are detailed in table A2.5.2, including the names of the steering dipoles.

In the diagnostic box in the MEBT a beam profile monitor, a Faraday cup and a capacitive probe to obtain a measure of the time structure of the micro-pulse will be located.

Table 2.5.1: Beam parameters in LEBT, RFQ and MEBT

	LEBT (ITL)	RFQ (IAQ)	MEBT (ITM)		
Length	7.05	2.50	1.60		m
Acceptance	0.46	0.80	1.00		mm mrad
Energy	2.5	2.5	250	250	keV/u
$\varepsilon_{x,y}/\pi$	0.35	0.50	0.50	0.50	mm mrad
α_x	0.0	0.8	−1.5	1.7	–
α_y	0.0	0.8	1.2	0.5	–
β_x	0.025	0.024	0.23	0.96	m
β_y	0.025	0.024	0.24	0.55	m
ε_l/π	–	–	0.94	1.08	keV ns/u
ε_l/π	–	–	35	40	^{o}keV/u
β_l	–	–	3.3	4.77	^{o}/(keV/u)
$\Delta\varphi$	–	–	10	13.8	^{o}
α_l	–	–	0	−1.28	–

The quoted emittance and acceptance values are normalized and correspond to the total beam. These emittances are 5 times the r.m.s. value from computer simulations of the beam in the RFQ and MEBT, and can be defined as the product of the semi axes of a right ellipse or more generally as the area of the ellipse/π.

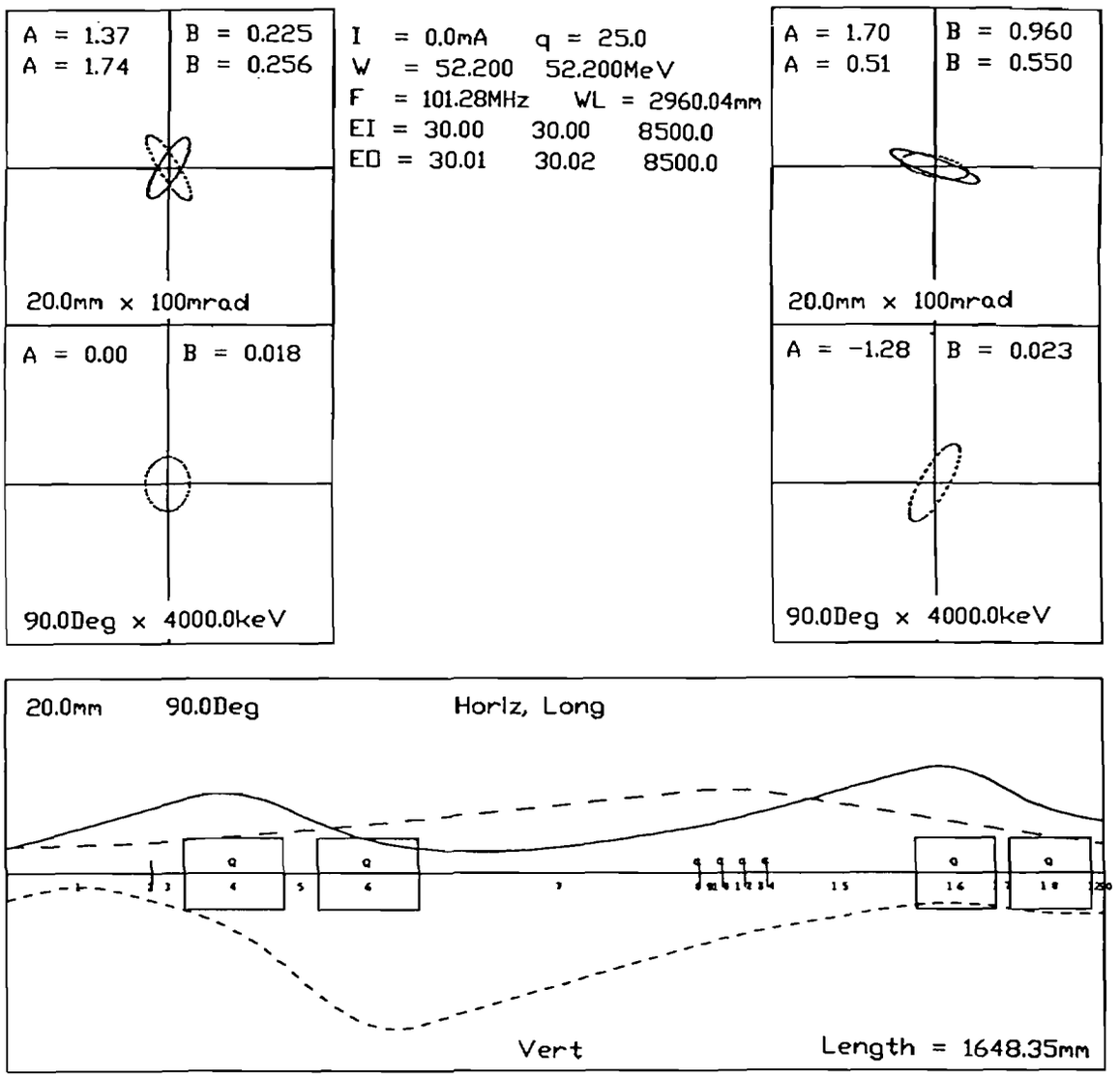

Fig. 2.12 Typical Beam Envelopes in the MEBT

2.6 IH LINAC (IA1, IA2 AND IA3)

2.6.1 Layout

The IH Linac consists of three tanks accelerating from 0.25 to 4.2 MeV/u, Tank 1 at 101.28 MHz and Tanks 2 and 3 at 202.56 MHz making a total length of 8.129 m with an effective accelerating voltage of 32.9 MV. This linac design is an extension of the GSI 'High charge state injector' (HLI) [24] in which the beam dynamics concept of 'combined zero degree synchronous particle sections' is used [35].

2.6.2 Description of IH Principles and Design

A complete description of the operation and beam dynamics of the IH structure exists in several papers (e.g. [35]) and a brief recall is given here. The beam dynamics with 'combined zero degree synchronous particle sections' is illustrated in Fig. 2.13 where the effective phase of the bunch centre varies from positive to negative along a section (1 to 2), and the subsequent drift space, including triplet focusing (2 to 3), and a few longitudinally focusing drift tubes, restore the working point and the beam orientation (2 to 4^-) to that required at the input of the next accelerating section (4^+ to 5). Note that due to operation around $\varnothing_s$=0 the average RF

defocusing is much reduced and that the mean energy of the beam is somewhat above that for synchronous motion.

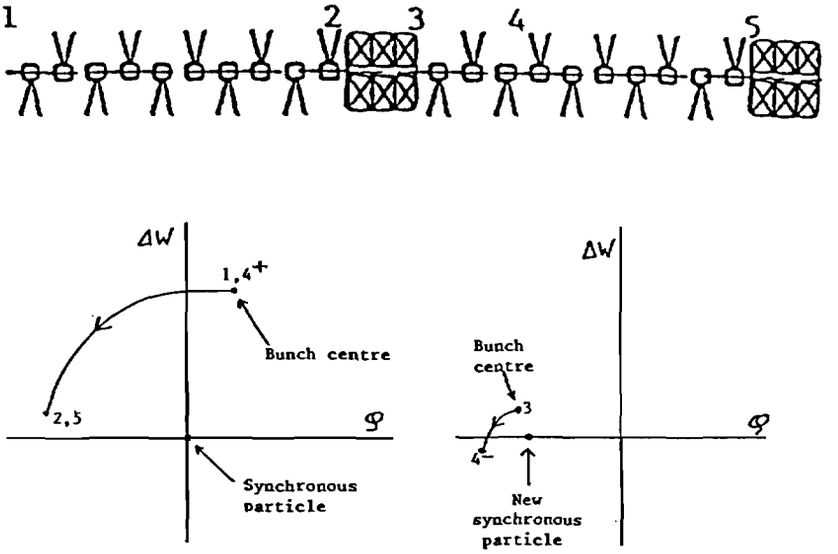

Fig. 2.13 Principles of IH Dynamics

The design follows from these principles. The cavity H mode, loaded by drift tubes, has a mainly accelerating field component on the axis. As RF defocusing is weak, there is no need for focusing within the thin-walled accelerating drift tubes, which leads to low capacitive loading i.e. high shunt impedance and modest RF power requirements. These drift tubes can stand exceptionally high fields, reducing the length of structure required. Longitudinal and transverse acceptances are closely matched to the beam from the RFQ. When the RF field is increased in the IH structure, there is a well-defined threshold level where a small amount of beam is accelerated at about the design energy. Operation at 1% to 2% above this threshold RF field level ensures good beam transmission.

2.6.3 Choice of Maximum Gap Voltage

The maximum fields on the axes of tanks 1 and 3 will be 13.5 MV/m and 11.5 MV/m. respectively. At the entrance of tank 2, 15 MV/m will be reached. By this choice, the RF power consumption as well as the effective voltage gain in tanks 2 and 3 are comparable.

Power tests on the GSI IH cavity showed that for this type of drift tube structure on-axis electric field strengths up to 15 MV/m can be held stably at 5% duty cycle.

2.6.4 Gap Voltage Distribution Along Each Tank

The velocity profile corresponding to the gap voltage distribution along the drift tube structure will be obtained by an iterative tuning procedure using the following design features.

Firstly the construction allows the position of each drift tube to be adjusted along the beam axis. Then the gap voltage distribution can be influenced by changing the effective area of magnetic flux inducers at the tank ends and by changing the capacity distribution between adjacent drift tubes (g/L variation, with g the geometrical gap length and L the period length).

2.6.5 Tuning Range of the Plungers

To reach the required resonance frequency f_r of 101.28/202.56 MHz each cavity will have the tuning range $\Delta f_r/f_r < 5.10^{-3}$, provided by two capacitive plungers (tuners) mounted on each tank. The master plunger, which is located near the midplane of the cavity, will be connected

to the resonance control loop, the other one (identical set-up) will stay in a fixed position and can be used as a replacement in case of mechanical damage to the master. Additionally, the second plunger, which is located at the high energy end of each cavity can be used to do fine tuning of the gap voltage distribution by optimising the beam quality at the exit of each tank.

2.6.6 Quadrupole Triplet Lenses

It is desirable to make the lenses as short as possible as they cause a distortion of the acceleration process. In particular the advantages of short lenses are that the longitudinal and transversal acceptance areas become bigger, RF power can be saved in the case of lenses inside the cavity and the total machine length is reduced. By careful design the number of triplets has been limited to four, two in Tank 1 and one between each tank (see Fig. 2.16 and Table A2.6.1).

To reach 1 T field strength at the pole surface VACO Flux is used for the fabrication of the poles. The pole aperture is 28 mm so the bore hole diameter will be 26 mm. The maximum field gradient requirement of 69 T/m for $^{208}Pb^{25+}$ results from the beam dynamics calculations, and can be compared with the design value of 71 T/m. The first and third quadrupole of each triplet have identical field gradients and will be operated in series by one power supply.

2.6.7 Beam Diagnostics

A 4-segmented capacitive pick-up probe will be installed in front of tanks 2 and 3 to observe the longitudinal bunch shape (differentiated signal) and the transverse beam position. The transverse position sensitivity derived from the difference signals from the x-plane segments and y-plane segments respectively should correspond to an offset of 0.1 mm for beam currents above 10μAe. The cavity RF signal is attenuated by the 60 mm long beam tube (ϕ=22 mm) by about 120 dB so that at the probe the effect of the noise, at 202 MHz, on the beam signal at 101 MHz is either tolerable or can be completely eliminated by switching off the RF power in the following tank. If the beam monitors detect that the beam is off-axis, corrections can be made by steering coils which are mounted in the centre quadrupole of both inter-tank lenses and are independent of the quadrupole main coils.

Selected parameters of the IH Linac are given in table 2.6.1 while a more complete set is given in a form which emphasises the sequence of components in table A2.6.1. Some details of the accelerating structures are given in table 2.6.2.

Table 2.6.1: Parameters of the IH Linac

Design ion	$^{208}Pb^{25+}$
Energy range	250 keV/u - 4.2 MeV/u
Effective voltage gain(MV)	32.9
Total length (mm)	8129
No. of 0° synchr. particle sections	5
No. of cavities	3
No. of quadrupole triplets	4
No. of segmented capacitive pick-up probes	2
No. of xy steering units	2
No. of accelerating gaps	99

Table 2.6.2: Parameters of accelerating structures

No. of Tank	TANK 1	TANK 2	TANK 3
RF Frequency (MHz)	101.28	202.56	202.56
Length between end flanges (mm)	3567	1549	2019
No. of synchr. particle sections	3	1	1
Total no. of accelerating gaps	41	28	30
Synchronous particle phase	see below	5×-30^{o}, 23×0^{o}	7×-30^{o}, 23×0^{o}
Effective voltage gain	13.50	9.88	9.79
Eff. shunt impedance (MΩ/m)	270	265	200
RF power (kW)	205	250	285
Inner drift tube diameter (mm)	18, 20, 22	22	22

N.B. For Tank 1 the synchronous particle phases in the three sections are respectively:
(i) 13×0^{o} (ii) 3×-30^{o} and 11×0^{o} (iii) 4×-30^{o} and 10×0^{o}.

2.6.8 Beam Dynamics Calculations

Figures 2.14(a) and 2.14(b) show calculations with 100% beam transmission of bunches with emittances of $E_x = E_y = 35\pi$ mm mrad and $E_l = 1.54\pi$ keV ns/u (56 deg keV/u) at injection. Figures 2.15(a), (b), (c) and (d) show the 100% beam envelopes for the case of 500 particles transported along the linac. These results were obtained with the computer code, LORAS (R) [32].

2.6.9 Tolerances

Emittance growth and transfer rate as function of tolerances have been investigated in numerous runs using the computer codes DYNAC and LORAS [33]. For the RF voltage and phase stability between tanks we expect tolerances of ±0.3% and we can accept $\pm1^{o}$. Neglecting misalignment errors and beam position errors, particle losses should be < 13%, the increase of beam phase spread < 8^{o} at 200 MHz, the increase in transversal emittance < 14% and the increase in longitudinal emittance < 15%.

Particle losses are defined as the difference of the number of particles contained in the phase ellipse at input and output, divided by the number at input.

The observed increase of phase spread occurs at emittance growths below 50% as the aspect ratio of the phase space ellipses is a function of tolerances as well.

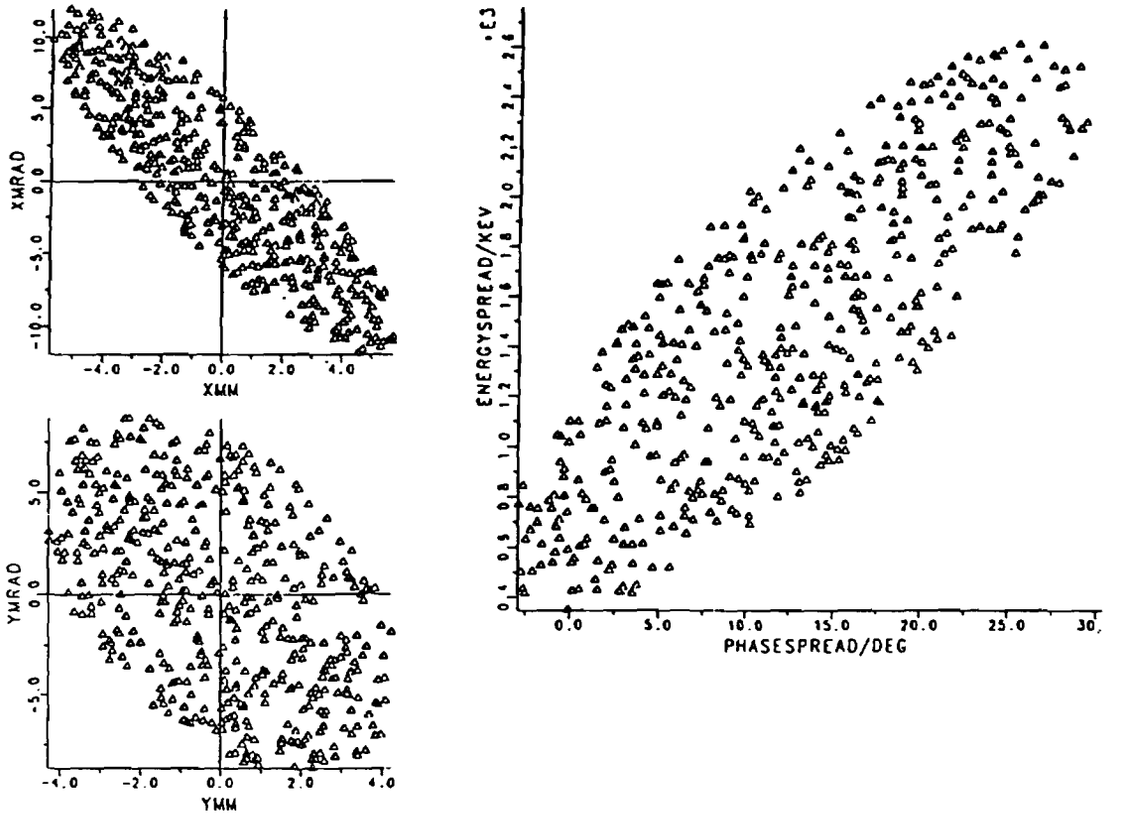

Fig. 2.14(a) Scatter Plots of Injected Bunch In Three Phase Planes at 0.25 MeV/u

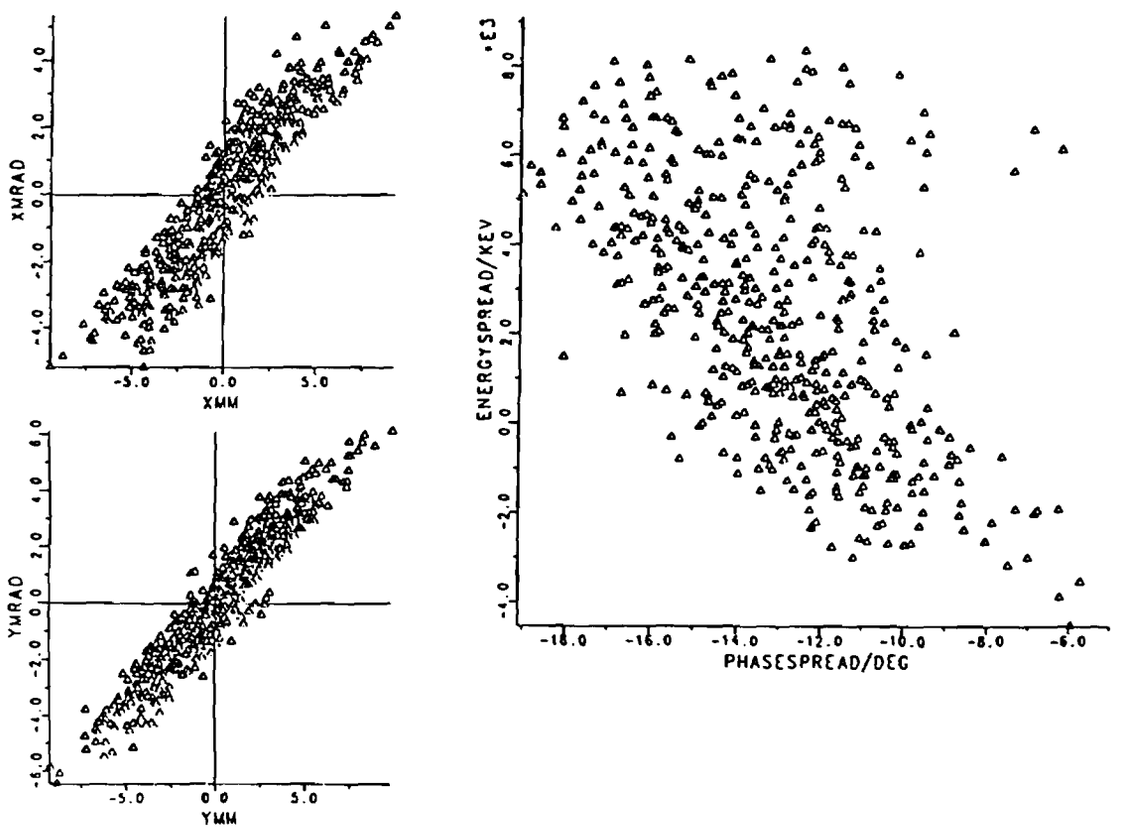

Fig. 2.14(b) Scatter Plots of Output Bunch in Three Phase Planes at 4.2 MeV/u

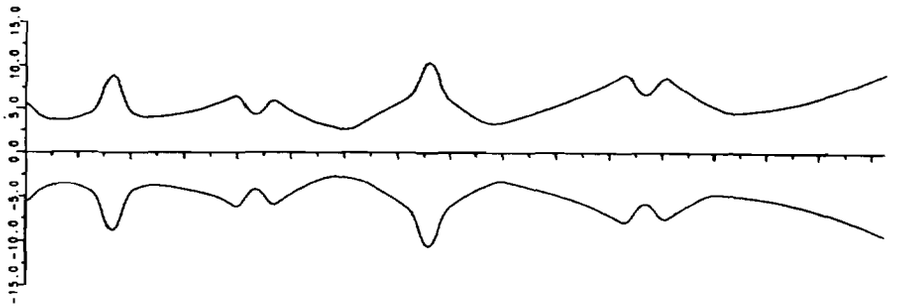

Fig. 2.15(a) Beam Envelope for 100% Beam in x,z Plane

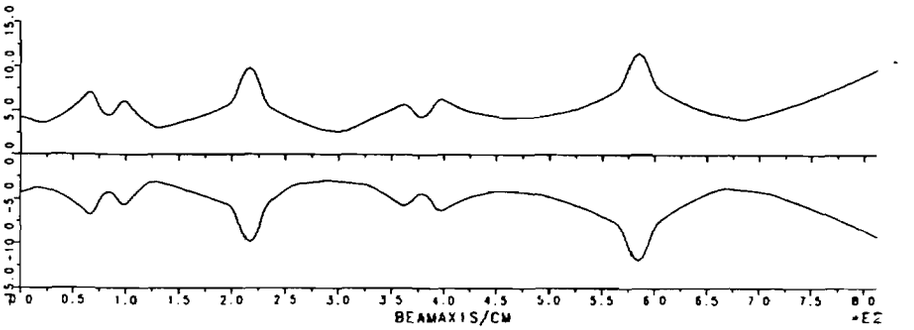

Fig. 2.15(b) Beam Envelope for 100% Beam in y,z Plane

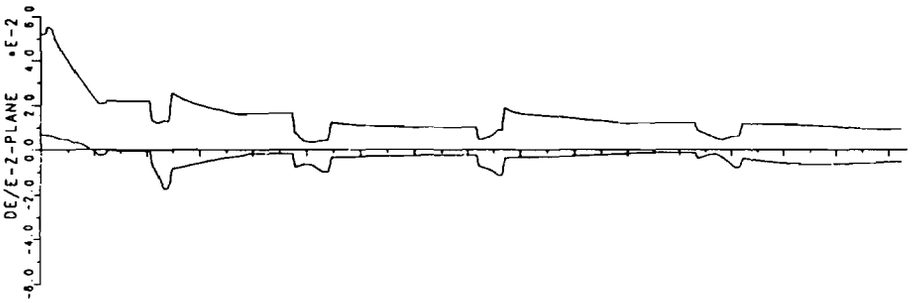

Fig. 2.15(c) Beam Envelope for 100% Beam in dW/W,z Plane

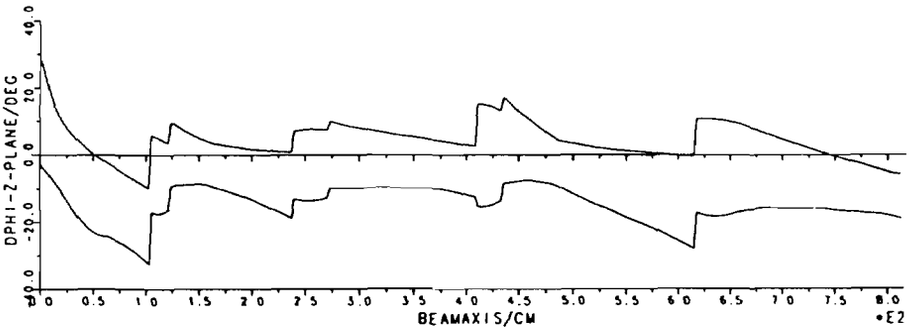

Fig. 2.15(d) Beam Envelope for 100% Beam in dϕ,z Plane

2.7 MECHANICAL CONSTRUCTION OF IH LINAC

2.7.1 General Mechanical Design

The mechanical design has benefited significantly from the IH-structure already operating successfully in the new HLI-Injector at GSI. In order to facilitate copper plating, machining, handling and mounting, each tank unit is assembled from one centre frame and two tank half shells (Fig. 2.16). The lower tank half shell is bolted to the sub-frame which is supported by three alignment screw jacks (5 ton rating).

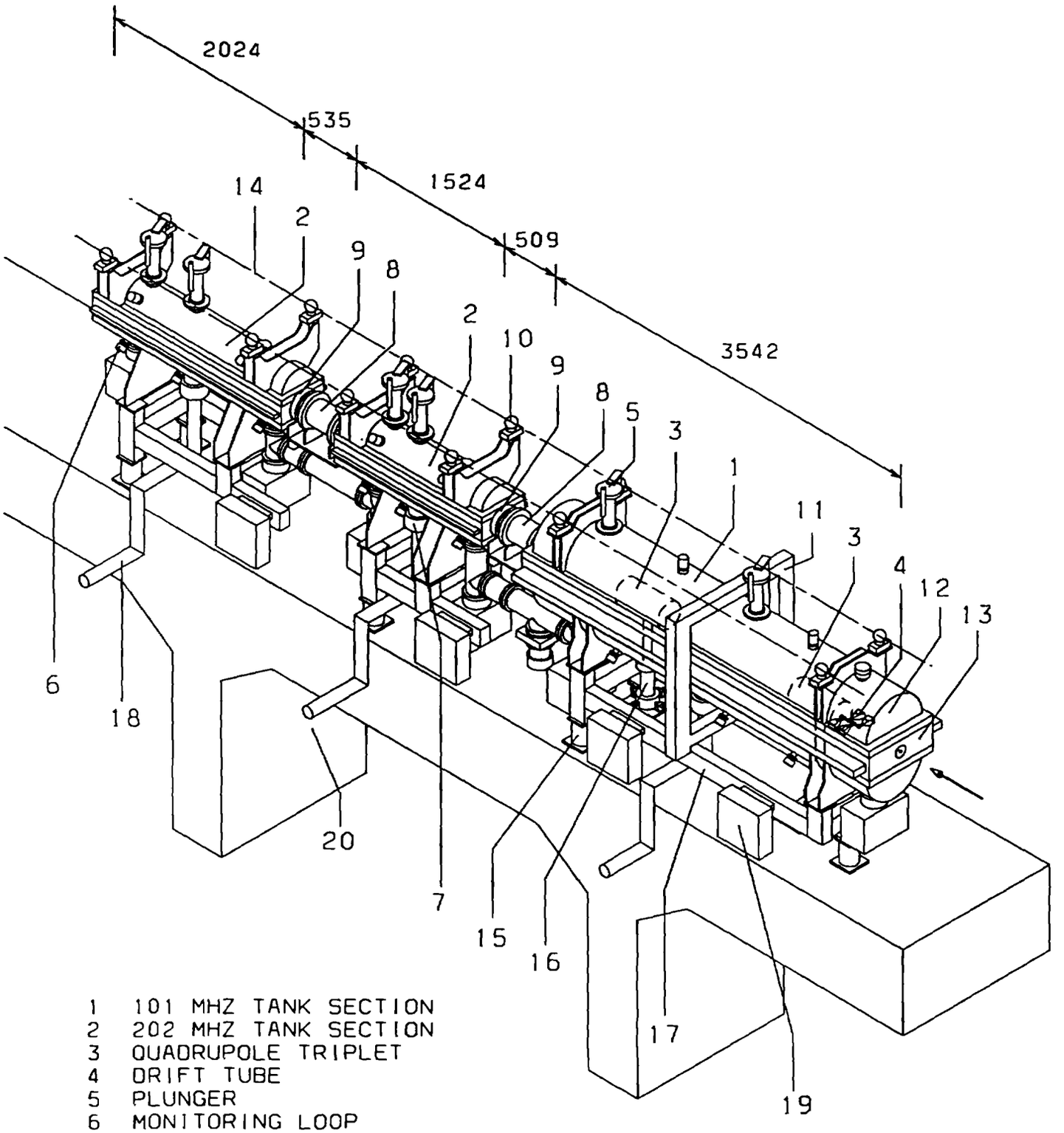

Fig. 2.16 Mechanical Layout of Interdigital-H Linac

There are no separate supports for the inter-tank quadrupole triplets. These two triplets are adjustable by elements which are mounted on brackets on tanks 2 and 3 respectively. The two drift tubes, containing triplets in tank 1 are assembled on the subframe, therefore ensuring independent alignment of these elements relative to the entire tank unit. In the case of tank 1, atmospheric pressure exerts high static loading causing lateral compression of about 0.3 mm which is compensated by pulling back the centre frame with screws incorporated in the alignment frame.

After interpretation of X-ray measurements around the similar GSI structure, it was decided to provide local shielding for personnel protection on all tanks. This will consist of 5 mm thick lead sheet which will completely cover the outside surfaces of the structures and will be mounted at GSI.

2.7.2 Mechanical Features of Tanks

The mechanical design for the three tanks has been fully developed by an experienced manufacturer. These tanks are made of mild steel and all non-machined inner surfaces are ground in order to prepare them for the copper plating process. The mounting surfaces on the centre frame have to be machined very precisely because no transverse adjustments are foreseen to align the small inner drift tubes; however it is possible to adjust these tubes in the longitudinal direction.

2.7.3 Small Drift Tubes

The small drift tubes which do not contain triplets can be adequately cooled through the contact surfaces by heat conduction, as they are bolted to the water cooled centre frame Fig. 2.17. A good thermal conductivity should be obtained in spite of the poor mechanical properties of copper after heat treatment.

2.7.4 Large Rectangular Tank Flange

Figure 2.18 shows a detail of the large rectangular flange. This flange is the most critical mechanical detail and it has to be designed very carefully. RF contact and vacuum tightness are ensured by a 1.5 mm silver wire which has to be compressed to half of its diameter. To generate the necessary force, 236 screws are required with the distance between screw axis and gasket minimised. Otherwise the bending moment would distort the flange and the required compression of the gasket could not be guaranteed. The rough-vacuum slot allows vacuum leak checking and, in combination with the rubber O-ring joint, acts as a backup if a leak opens up during operation.

2.7.5 Intertank Triplets

There is very little space between adjacent tanks to incorporate a triplet and a phase probe but the triplet can be disassembled without needing to disturb the tanks (Fig. 2.19). The bellows at the ends allow only a small transversal movement. A useful design feature is that the alignment of the triplet with reference to its supporting tank, can be done before the tanks are finally installed.

2.7.6 Drift Tubes of Tank 1 Containing Triplets

These drift tubes, containing quadrupole triplets, are technologically the most complicated components, (Fig. 2.20). Their stems pass through the lower part of the tank via bellows and are mounted with their adjustment mechanisms on the sub-frame. The quadrupole triplet is supported by the thin beam tube only. Stem and drift tube bodies are water cooled with all the body parts made of welded stainless steel and then copper plated. The most difficult design task was to feed 12 water-cooled current leads from the drift tube body to the outside.

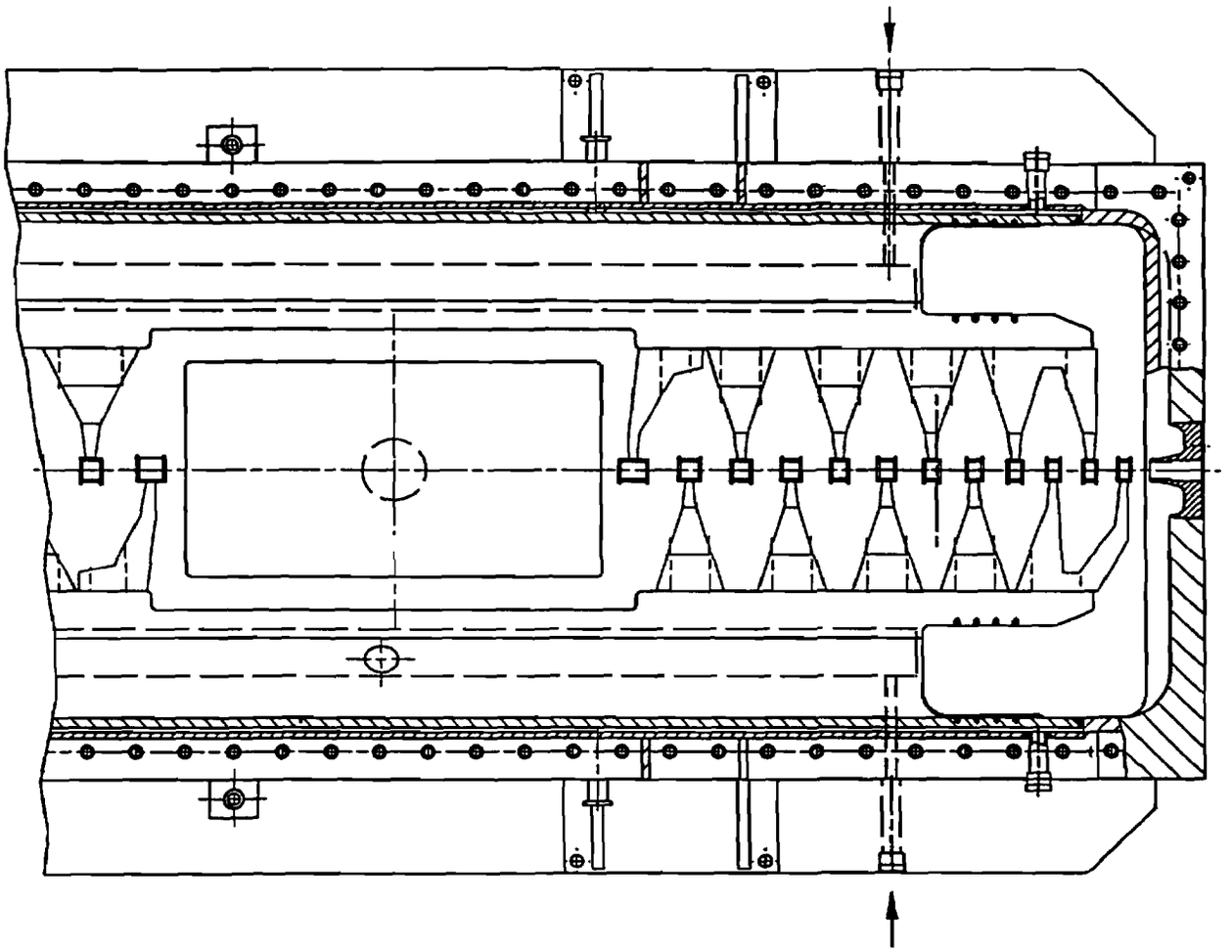

Fig. 2.17 Cross Section of Tank 1 Showing Small Drift Tubes

2.7.7 Vacuum, Gaskets and Surfaces

In order to obtain the required good vacuum conditions the entire IH-structure is metal sealed, as most vacuum equipment now is at GSI, and to reduce the number of different sealing principles CON FLAT flanges are preferred. As 90% of the entire inner surface will be copper plated by the well known GSI method, any final machining or finishing is not necessary and a final cleaning process can be saved. The stainless steel surfaces of the triplets, bypass vacuum pipes etc. will be cleaned by the usual ultrasonic bath for vacuum components.

The layout of the vacuum equipment is under CERN responsibility and will be described in section 3.4

2.7.8 Water Cooling

Manufacturing the tanks of mild steel instead of stainless steel is preferred as it reduces costs, eases the copper plating process and reduces distortions after welding. One disadvantage is that a special closed cooling circuit, temperature controlled to ± 1°C and with maximum pressure of 6 bars, is needed for the tank cooling jacket. This must be independent of the circuits used for quadrupoles, drift tubes, etc. which are connected to a high pressure cooling circuit with a water quality of < 10 μS/cm especially needed for the quadrupoles and in which other materials like stainless steel, copper and plastic are used.

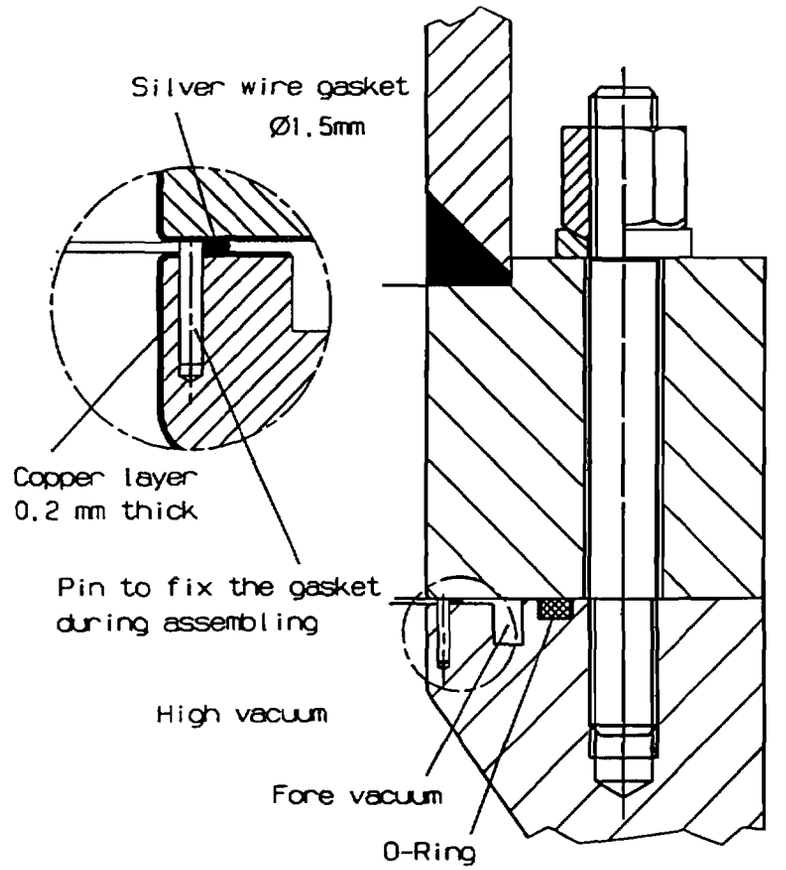

Fig. 2.18 Details of Vacuum Sealing on Large Tank Flange

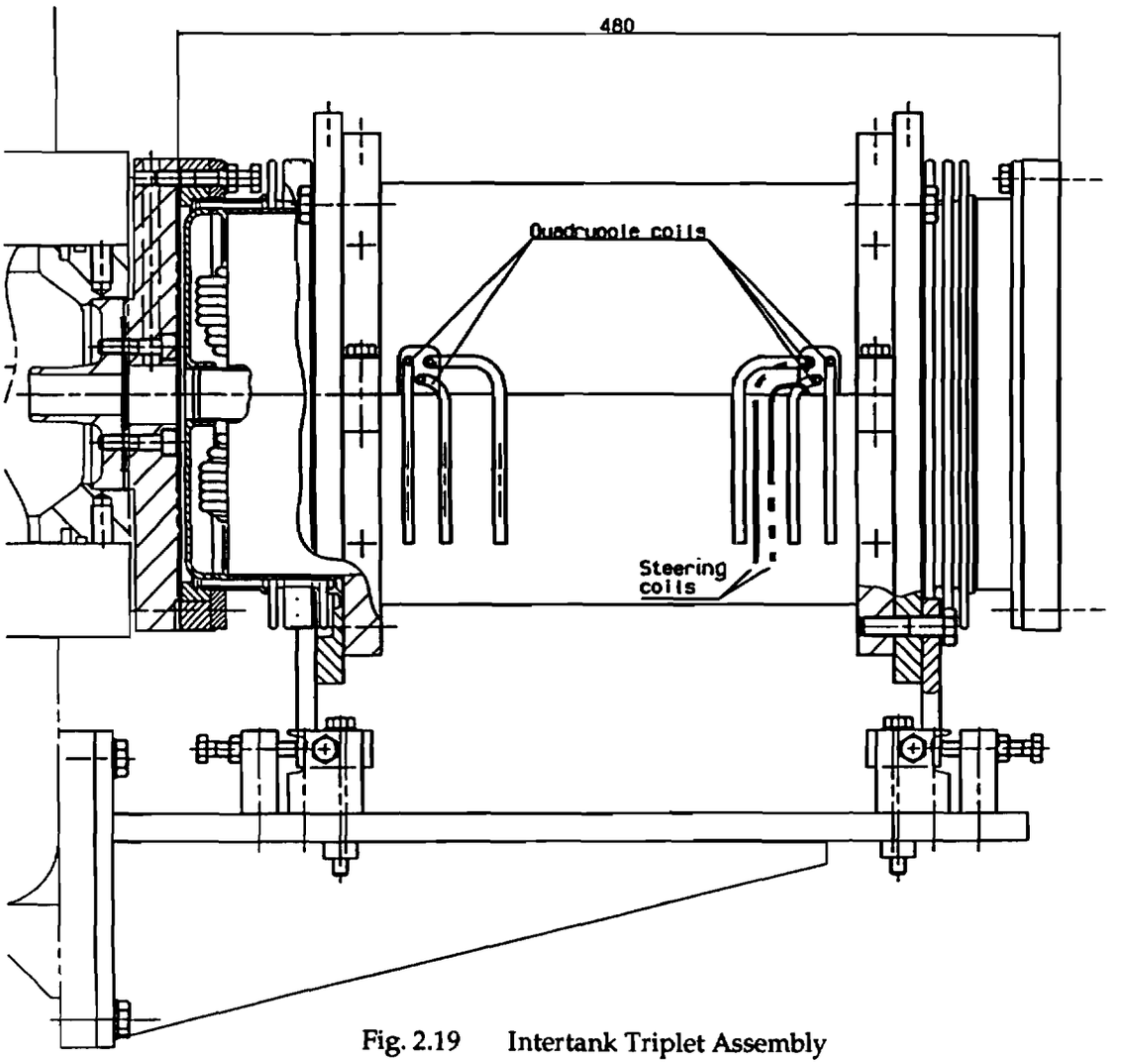

Fig. 2.19 Intertank Triplet Assembly

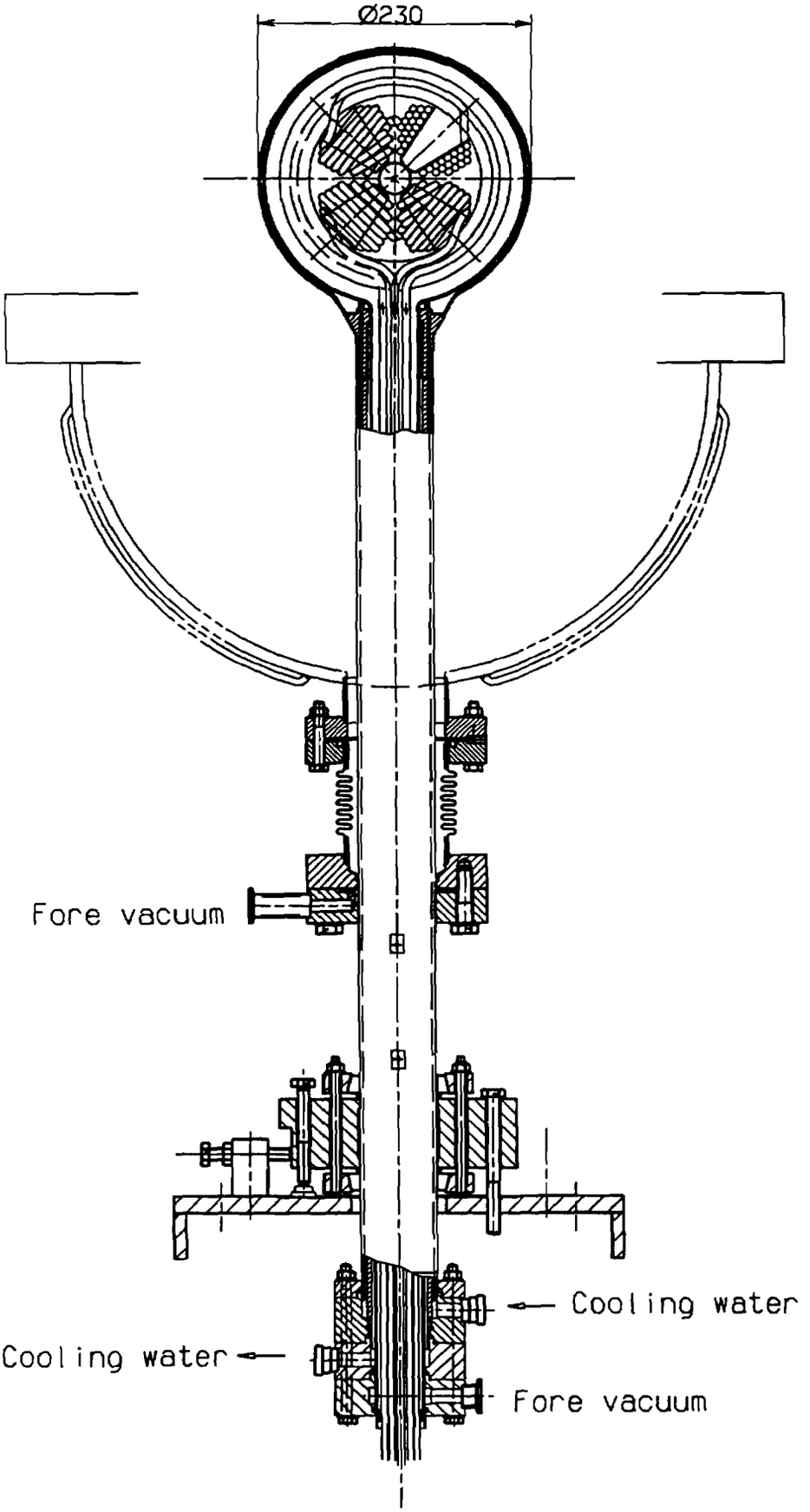

Fig. 2.20 Cross Section of Drift Tube with Triplet

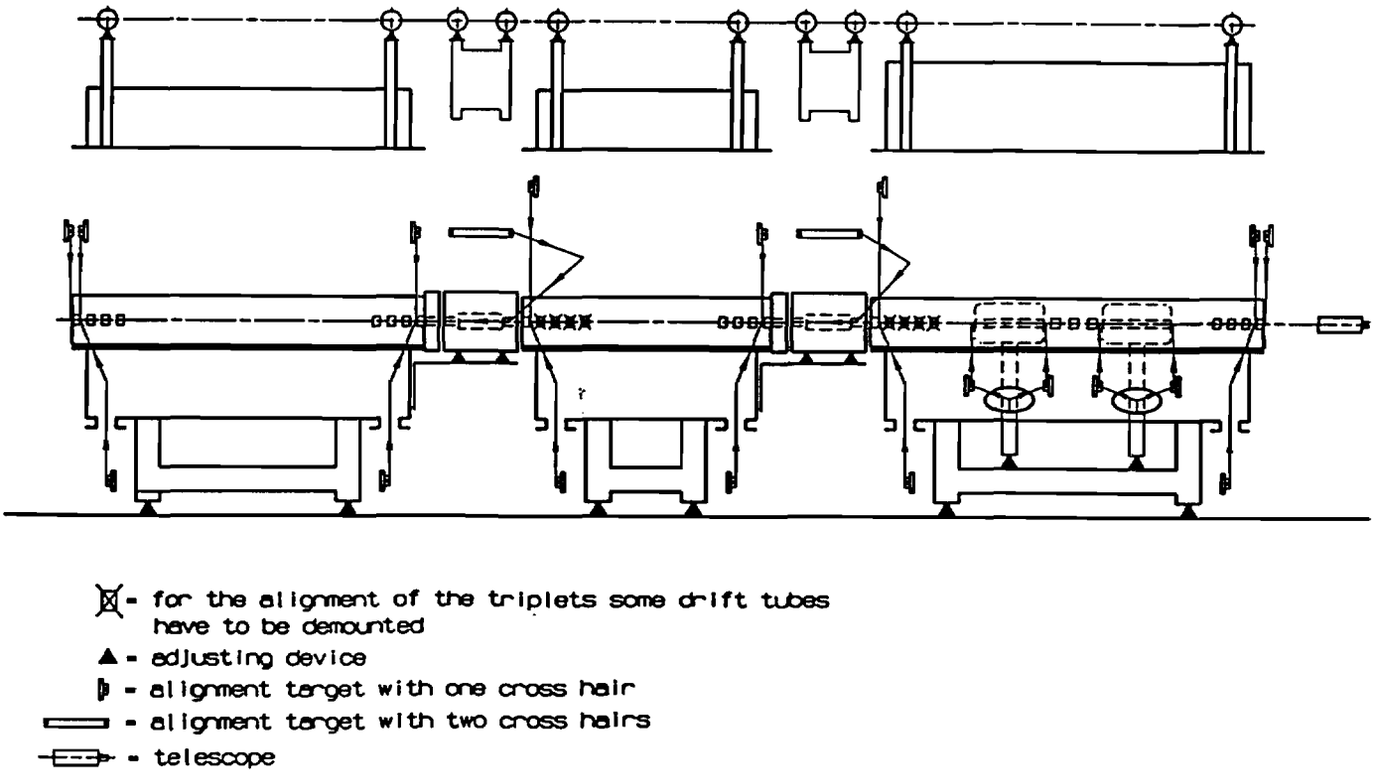

Fig. 2.21 Schematic of Alignment Procedure

2.7.9 Alignment

An accurate procedure which is realizable when the entire IH-structure is initially set up in the right place is shown at the bottom of Fig. 2.21;

a) Remove the upper tank half shells from tank 1 and tank 2

b) Disassemble some drift tubes next to the output end of tank 1

c) Use a telescope at one end of the linac structure to align all triplets and tanks.

It is a lengthy process to remove the upper tank half shells just to place the alignment targets in order to check the position of triplets, e.g. if there were doubt on the alignment during operation.

The upper part of Fig. 2.21 shows the position of the six off-axis targets which are fixed directly to the tanks with other targets on two jigs resting on the inter-tank triplets. This is the preferred CERN approach allowing an alignment check of the IH Linac in its operational state (under vacuum). However two important components, the tank 1 drift tubes with quadrupoles, are not directly accessible then. It is proposed to have reference marks on the support stems below the IH tank which can be used to check the alignment using triangulation with theodolites mounted on brackets on the adjacent wall of the linac tunnel.

2.8 MEASUREMENT, STRIPPING, FILTERING AND BEAM TRANSFER AT 4.2 MEV/U (ITF)

2.8.1 Introduction

At the output of the ion linac there is a region of about 12 metres up to the shielding wall that separates the linac from the PS. This region will allow adjustments, measurements and optimisation of the ion beam to be made independently of the following accelerators.

After stripping the different charge states of the beam are mixed randomly, and, as the magnetic fields act differently on each charge state, specific measurements cannot be made. It is necessary to define a strategy which allows the measurement of beam parameters without the influence of the unwanted ions, then the transfer of an ion beam having the required charge state to the booster. Knowing the beam current before stripping (with the help of the beam transformer) it is expected to be able to make the following measurements:

i) To measure the emittances in the horizontal and vertical phase planes. Energy spread and microbunch profile in the longitudinal plane.

ii) To measure the effect of the increase in beam size due to the stripper as a function of its composition, thickness and imperfections. These measurements to be made in the transverse and longitudinal planes in order to optimise the Pb^{53+} beam.

iii) To measure the beam currents in the different charge states, the energy spread of the Pb^{53+} beam as well as its angular extension at the debuncher. This particle beam, having only ions of the required charge state, can be transported towards the booster via the measurement lines LBS and LBE.

iv) To centre the beam, measure its profile and study the beam current stability. To do this quasi-non-destructive 'SEM fils' in the line leading to the booster are used. The beam matching in the horizontal and vertical planes will have been adjusted in the LBE line, and with the help of the debuncher, the energy spread will be optimised by studying the beam in the LBS line.

The layout and nomenclature of the transport lines between Linac 3 and the PSB is given in Fig. 2.1.

2.8.2 Beam Characteristics

The beam parameters at entrance of the ITF Line are given in table 2.8.1. As the measurements will be done using the beam delivered by the installed ECR source (section 2.2.1) the following data correspond to an initial charge state, Pb^{28+}.

Table 2.8.1: Beam at input to ITF line

	Before stripper	After stripper
Type of particle	Pb^{28+}	Pb^{53+}
Energy (MeV/u)	4.20	<4.20
Current (μAe)	65	20

Transverse phase planes

	Horizontal	Vertical
Emittance (Π mm mrad)	8.5	8.4
Normalised emit.(Π mm mrad)	0.81	0.80
Alpha	-2.3	-2.6
Beta (mm/mrad)	4.3	4.6

Longitudinal phase plane

	Before stripper	After stripper	After Debuncher
Emittance (π keV ns/u)	1.82	>1.82	>1.82
dW(keV/u); dW/W (%)	23; 0.5	>23; >0. 5	<2.1; <0.05
dt(ns); dϕ(deg.)	0.23; 17 (at 200 MHZ)	>0.23;>17 (at 200 MHZ)	1.07;39 (at 100 MHz)

The length of beam pulse will be 400μs (max. 600μs) with a repetition time 1.2s.

Note that a complete set of parameters of beam elements and measuring equipment is given in the appendix as table A.2.8.1.

2.8.3 The Optics of the Line

The line consists of two quadrupole triplets and four bending magnets (Fig. 2.22). The first triplet (symmetric) focuses the beam which is strongly divergent at the output of the IH structure, onto the stripping foil (STR01) in order to obtain there a beam ellipse of small dimensions and in principle axes in the vertical and horizontal phase planes. This leads to a minimisation of the growth of the emittances due to scattering of the beam on the stripper. The second triplet (3 independent quadrupoles) matches the beam to the filter section, and thus an image of the object slit can be obtained on the analysing SEM-grid MSGH10, for the measurement of the energy spread. The four bending magnets have different functions i.e. (i) the first magnet (BHZ11) is used as a spectrometer to analyse the beam before and after stripping (ii) the first two magnets (BHZ11 and BHZ12) allow the separation of different charge states which are analysed at the centre of the filter so that only the required charge state for the booster is accepted in the second part (iii) there, the magnets BHZ13 and BHZ14 align the beam onto the downstream line and ensure an overall non-dispersive transfer i.e. no increase in horizontal emittance nor increase of the length of the micro-bunch compared to a rectilinear trajectory of the same length (iv) the focusing effect of the magnets in the horizontal and vertical planes provides a beam which can be easily be matched to the downstream line.

Figure 2.23 shows the beam envelopes in the filter and the output emittances as a function of the input emittances.

2.8.4 Debuncher

The energy spread after the stripper is about ± 0.6%, but the PSB has much less acceptance than this in the longitudinal plane. An RF cavity acting as a lens in the longitudinal phase plane allows the reduction of the energy spread.

This debuncher has to provide a peak voltage modulation of 200 kV and should need only 2kW RF-power from a transitorized driver amplifier. A multigap structure with high efficiency can be used because the cavity length can be up to 700 mm. Based on the development of post-accelerator structures a compact spiral loaded resonator with four gaps operating at 101.28 MHz has been chosen (length 700 mm, diameter 500 mm, drift tube aperture 60 mm). The cavity is made of copper plated stainless steel, the spiral drift tube support which is a L/4 resonator is made of a 45×45 mm Cu bar. Model measurements have shown that this cavity has the high shunt impedance required.

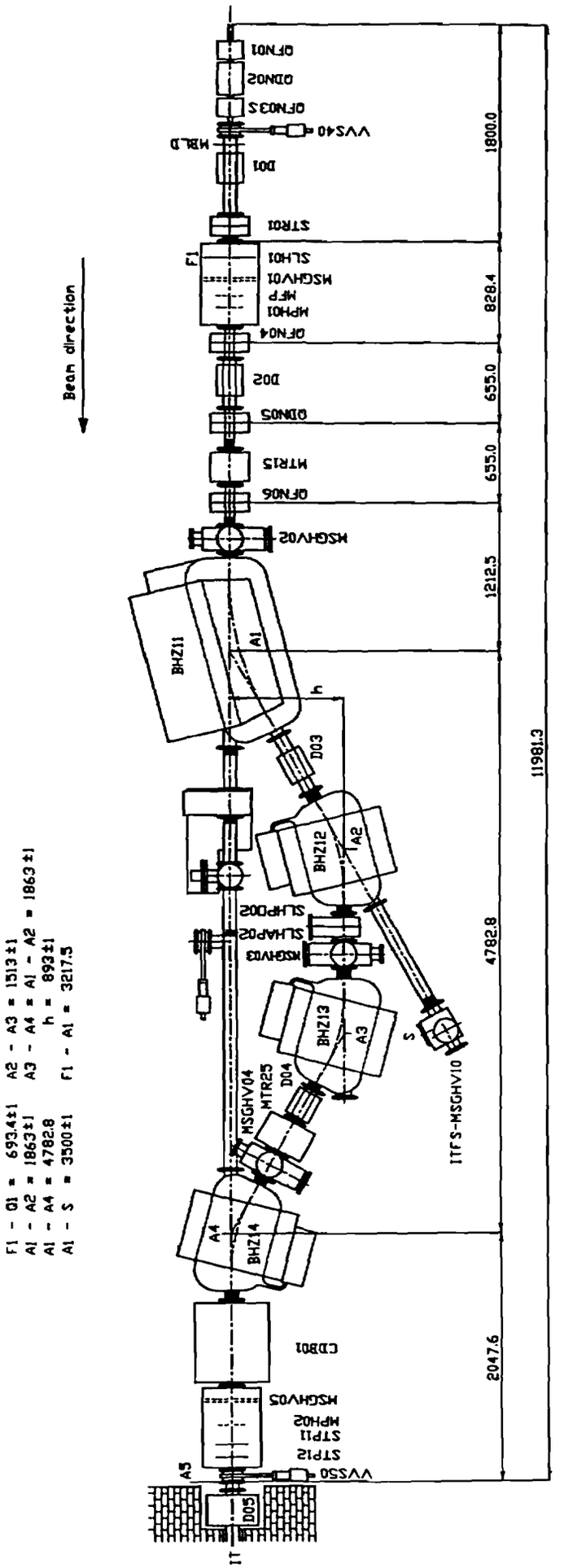

Fig. 2.22 Layout of Magnetic Elements in the ITF Line

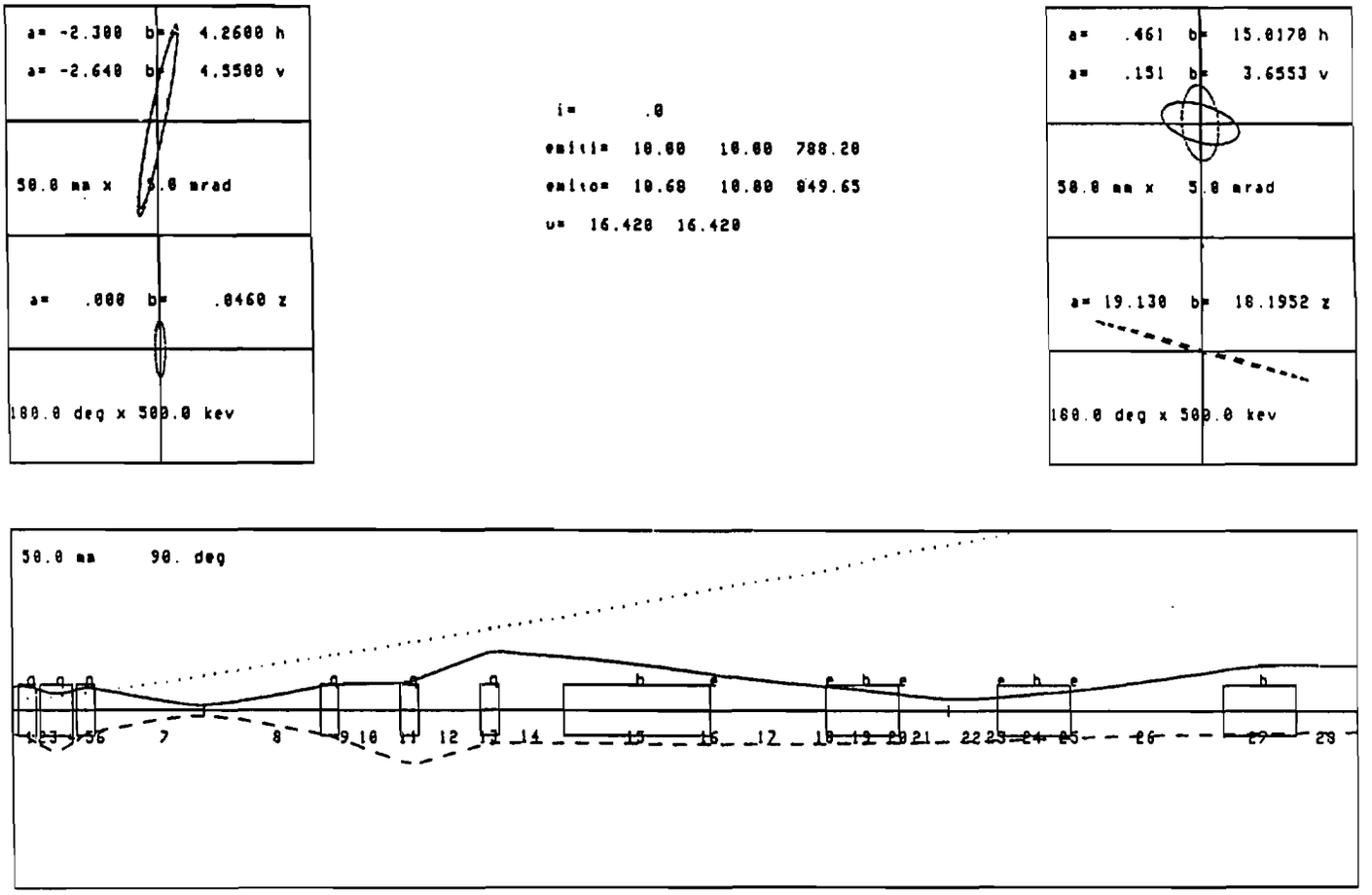

Fig. 2.23 Computed Beam Envelopes in ITF

2.8.5 Description of Beam Measuring Equipment

Beam Current Transformers

It is necessary to study continually and in a non-destructive manner the beam current at the out-put of the linac and the number of Pb53+ ions which are obtained after the filter section. A new, highly sensitive beam measuring transformer is being developed.

Profile Measurements by SEMgrids and SEMfils

This equipment is used to measure the transverse profile of the beam in order (i) to align the beam (ii) to measure its dimensions and possibly to deduce the energy spread and the emittance. Two types of movements are possible, fast with fixed steps and slow with variable steps. The signals obtained are amplified by identical electronic systems for all the measuring stations including SEMgrids before the IH structure. The interface and the software are identical to those on the PS.

Measurement of Phase and Profile of the Microbunch

There are two types of measurement

(i) with a fast Faraday cup (destructive) matched to 50Ω and with a resolution of about 10° at 100 MHz

(ii) with a fast phase pick-up (non-destructive, provided by GSI); two positions are foreseen, one at the output of the IH structure and the other before the debuncher, to measure the length of the micro-bunch.

Energy Spread Measurement

This consists of an object slit which is imaged on MSGH10 using quadrupoles QFN04,05,06 and BHZ11 as a spectrometer magnet. One can both measure the charge states without stripper (Pb28+) and with stripper (Pb53+). The expected resolution is 4.2 keV/u.

Emittance Measurements

Precise emittance and PSB matching measurements are made in the LBE line which is downstream from the ITF line. In LBE we measure in one pulse the collection of densities in either the horizontal or vertical phase plane. During the commissioning of the linac an apparatus placed in the continuation of BHZ11 and based on the principle shown in Fig. 2.24, will be used. A plate with equidistant (6 mm) narrow slits in either the horizontal or the vertical plane defines precise positions in the corresponding phase plane. At approximately 600 mm there is fluorescent screen on which the width of the luminous spots is proportional to the angles in the beam. The light is analysed and the signal read by a flash ADC. The emittance is reconstructed using special software.

2.8.6 The Stripper

This consists of thin carbon foils (0.5–1 μm or about 100 to 200 μg cm^{-2}) with a diameter of about 8 mm. The apparatus can hold about ten foils whereby foils of different thicknesses and quality can be tried for optimisation.

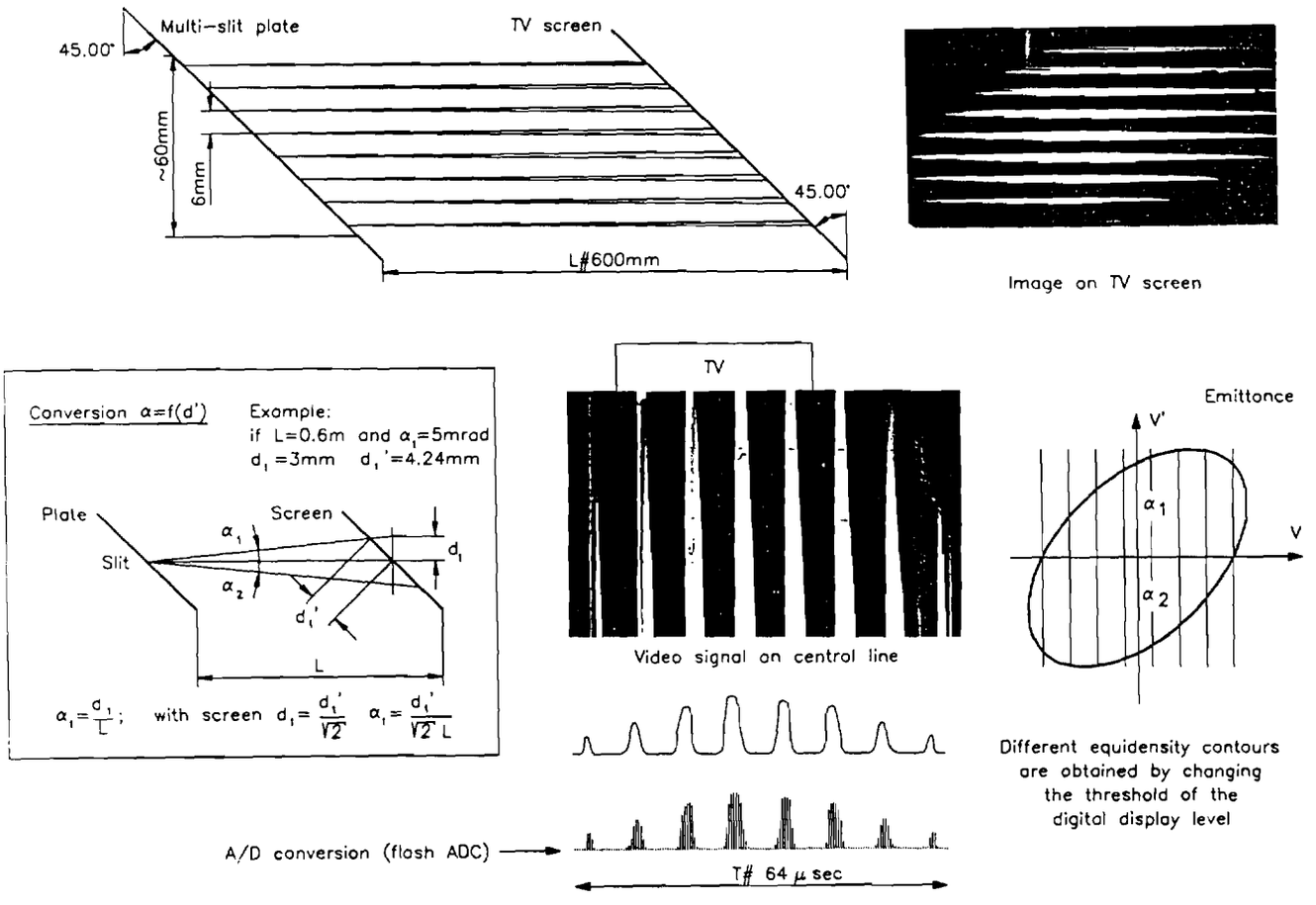

Fig. 2.24 Principle of Emittance Measurements in Direct Beam Line

2.8.7 Mechanical Assembly and Vacuum

The mechanical assembly of the line has been developed by INFN Turin. Except for the first triplet which will have a special support, all the elements up to BHZ11 will be aligned using a girder with a precisely aligned central slot. The same type of girder is used at the centre of the filter. The four bending magnets will be on screw jacks of the type used throughout the lead linac.

The ITF line is considered as an independent vacuum sector and is defined by sector valves at its two extremities. The backing system is in the straight line BHZ11 to BHZ14 while the four ion pumps are installed along the normal beam line.

2.8.8 ITH and LTB Lines

These lines are used for the transfer of the ion beam either towards the measuring lines (LBE and LBS) or towards the (Booster Synchrotron) PSB.

ITH:

Three quadrupole triplets are used for focusing and two sets of steering magnets and SEMgrids allow centring of the beam and observation of the profile.

LTB:

This transfer line works in pulse-to pulse mode with either ions or protons being transferred to the PSB. The steering magnets and the first two quadrupoles in the line are powered accordingly. Two beam current transformers are used to measure the (high intensity) proton current. A high sensitivity transformer (MTR55) as used in the ITF line, allows measurements of the ion beam currrent. Two SEMfils (MSG30 and 40) measure the profiles of one or the other beam.

2.8.9 The Measuring Lines LBE and LBS

These two lines allow single pulse measurements (in 12μs) of the parameters of the three phase planes relevant for the correct injection of the beam into the PSB.

LBE:

A new development allows measurements (in 12μs) of the beam density in each element of a 48 by 24 matrix covering the phase plane. The two unit vectors determining the area covered by the matrix are separately adjustable and so allow the instrument to cover the complete area of the beam. From this matrix the following results can be derived: the curve E=f(I) with E= emittance and I=current, Twiss parameters and the display of an emittance surface defined by a chosen equidensity contour. Statistics on beam stability of parameters and immediate observations of the effects of the variation of the focusing or beam steering can also be studied in pulse-to pulse mode.

LBS:

This allows the measurement and adjustment of the energy spread as required by the PSB. Also working in the pulse-to pulse mode, the energy spread can be adjusted using the debuncher installed in the ITF line.

2.8.10 Summary

The ITF line which consists of an assembly allowing the adjustment and measurement of the linac beam can, as far as its beam instrumentation is concerned also be used for measurements of the intermediate energies from the IH Linac. Thus it must be operational before these beams become available. The comprehensive set of measuring lines including LBE and LBS should enable a straightforward adjustment of the beam and rapid fault finding all along the lines.

2.9 TABLE OF PARAMETERS

Table 2.9.1 gives computed beam parameters at 12 places between the ECR source and the (de) buncher output.

Twiss parameters are derived from simulations, done with TRACE 2D, TRACE 3D [26], PARMTEQ [37], and DYNAC [33]. The output values at the ECR are based on experimental results. Emittance growths in the LEBT, the buncher (in the MEBT) and stripper are, like the current losses, expected values in the statistical sense. To ease comparison of the different designers choice of emittance values, all emittances have been converted to 4 rms values. This means that at a waist of a particle beam the axes of the relevant phase space ellipse are 2 rms values.

In some cases, pessimistic emittance values have been considered with the particle tracking programs, to sound out emittance blow-up or particle losses due to non linearities in the devices, so the absolute values should be taken as indicative only.

Table 2.9.1: Beam characteristics throughout LINAC 3

Beam characteristics for a pulse-length of 400 μsec at 2 Hz repetition rate	position 1	2	3	4	5	6	7	8	9	10	11	12
	ECR = LEBT out in	LEBT = RFQ out in	RFQ = MEBT out in	BUNCHER in	BUNCHER out	MEBT out	IH in	IH = ITF out in	STRIPPER in	STRIPPER out	BUNCHER in	BUNCHER out
Particle	208 Pb 25+									208 Pb 53+		
Energy [MeV/u]	.0025		.25					4.2				
Relativistic beta	2.31 E-3		2.31 E-2					9.43 E-2				
Pulse current [μAe]	80		72					65		20		
Accelerating frequency [MHz]		101.28	101.28	101.28	101.28		101.28	202.56			101.28	101.28
Horizontal acceptance /π [mm mrad]	200	350	45	45			44					
Horizontal emittance /π [mm mrad]	120	150	17.3	17.3	17.3	17.3	32	8.5	8.5	10	10	10
Normalized hor. emitt. /π [mm mrad]	.28	.35	.40	.40	.40	.40	.74	.81	.81	.95	.95	.95
Horizontal alpha	0	.8	- 1.37	- 2.09	- 3.84	1.70	1.69	- 2.29	0	0	.46	
Horizontal beta [mm/mrad]	.025	.024	.225	.777	1.337	.960	.94	4.26	1.02	.87	15.0	
Vertical acceptance /π [mm mrad]	200	350	45	45			44					
Vertical emittance /π [mm mrad]	120	150	17.3	17.3	17.3	17.3	32	8.4	8.43	10	10	10
Normalized vert. emitt. /π [mm mrad]	.28	.35	.40	.40	.40	.40	.74	.80	.80	.95	.95	.95
Vertical alpha	0	.8	1.75	4.17	2.26	.510	.47	- 2.64	0	0	.151	
Vertical beta [mm/mrad]	.025	.024	.256	1.757	1.081	.550	.55	4.55	1.03	.88	3.65	
Longitudinal accept. /π [deg MeV/u]							.105					
Longitudinal emittance /π [deg MeV/u]			.028	.028	.032	.032	.053	.135	.135	> .135	> .068	> .068
Longitudinal emittance /π [keV ns /u]			.76	.76	.86	.86	1.43	1.82	1.82	> 1.82	> 1.82	>1.82
Energy spread [MeV/u]			.0028	.0028	.0042	.0042	.0054	.0224	.0224	> .0224	> .0224	< .0021
Phase spread [deg]			10	32	33	12.4	15.9	6.2	17		39	> 39
Tilt [deg]			0	- 30	32	9.8	12.6	- 1.2	- 16		- 39	0

In this table the horizontal plane = x - plane
Longitudinal emittances and phase spreads are given w.r.t. the frequency of the (in some cases preceding) accelerating device
Longitudinal emittances are also given in MKS units
Tilt = phase spread for the maximum of E - Emean

3 GENERAL SERVICES AND SYSTEMS

3.1 LINAC BUILDINGS AND INFRASTRUCTURE

3.1.1 Buildings

Building 351

Linac 3 which consists of ECR source, LEBT, RFQ, MEBT, IH tanks and stripper/filter line is housed at the place of ex-Linac 1 (plan view Fig. 3.1). A reinforced concrete support with hollow arches has been chosen so the pedestal of Linac 1 has therefore been extended to support the first part of the complex (ECR source, LEBT, RFQ, MEBT); in addition a solid cast concrete corner block has been included to accommodate the 135° bend in the LEBT (3 D view Fig. 3.2). A lateral extension of the pedestal has been built to support the stripper/filter line. The floor has been rebuilt to cope with these extensions of the pedestal; this new construction leaves enough height between the basement and the floor to house power supplies and control racks. All the RF equipment is lodged at ground floor level, adjacent to the main linac structure (Fig. 3.1). Cuttings in the concrete below the RF equipment were made to house the RF feeder lines. Other equipment, for example power supplies for the filter magnets and the IH quadrupole triplets will be housed in the basement.

Building 236

This assembly hall has been built near B351 because the existing buildings are already congested. It has a concrete base of 7.6 x 16.3 m, is 5.6 m high and is equipped with a 3.2 T crane.

3.1.2 Electricity

For this project, a rationalization of the mains electricity supplied to the buildings (all from one transformer building) is being implemented. Only one source of mains electricity will be supplied; special low noise screened mains and secure mains (backed up by a diesel generator) will not be available. Two exceptions to this general rule are, the controls system and the vacuum pumps of the source which will have a separate non-interruptible power supply. The distribution within the building and provision of separate and lockable circuit breakers for the high power equipment are foreseen for each main high power equipment e.g. modulators for the RF amplifiers. For the new equipment the new norms (C15100) and Safety Instruction concerning PVC free cables (IS 23) are respected. In addition one aim of this new layout is to ensure the coherence of the electricity systems used on the accelerators of various ages i.e. LEP, SPS and PS. As all old cables in the region had to be removed, a complete new design of the secondary mains cable layout has taken into account the new machine requirements.

3.1.3 Air Conditioning and Cooling Water

Air conditioning

The heat to extract from the air has been estimated to be 85 kW, (more than Linac 1), taking into account that water cooling is foreseen for most elements and there is a peak in the heat dissipation distribution in the region of the source. Most of the ducts of the Linac 1 air conditioning, and the chilled water distribution could continue to be used but some extensions of the air conditioning ducts had to be made in order to cope with this new heat distribution. The electrical regulation equipment and the monobloc air conditioning/ventilation unit will be replaced in order to ensure the coherence of the installations amongst the various accelerators of CERN.

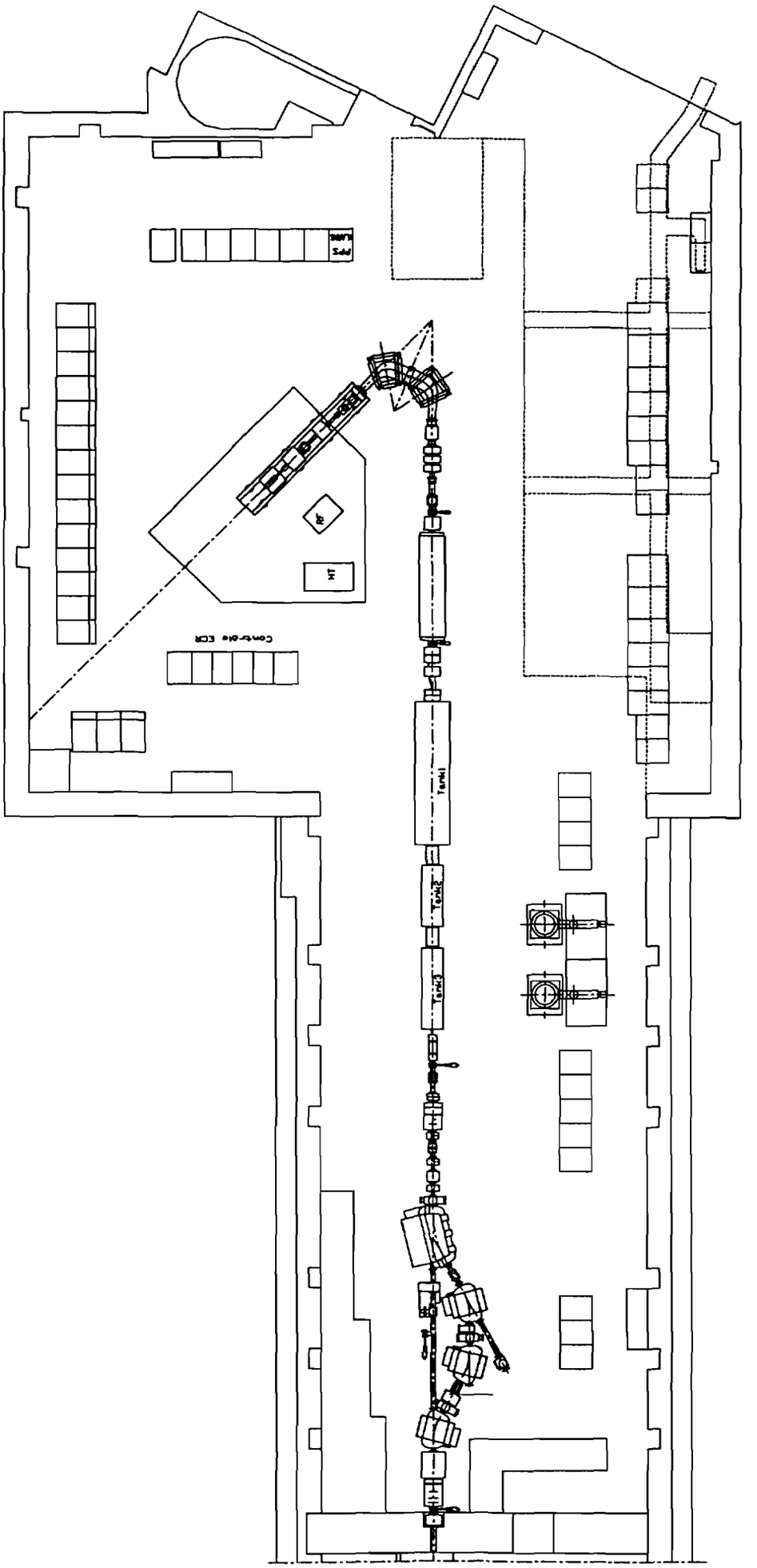

Fig. 3.1 Plan of Building 351 with Linac 3 Layout

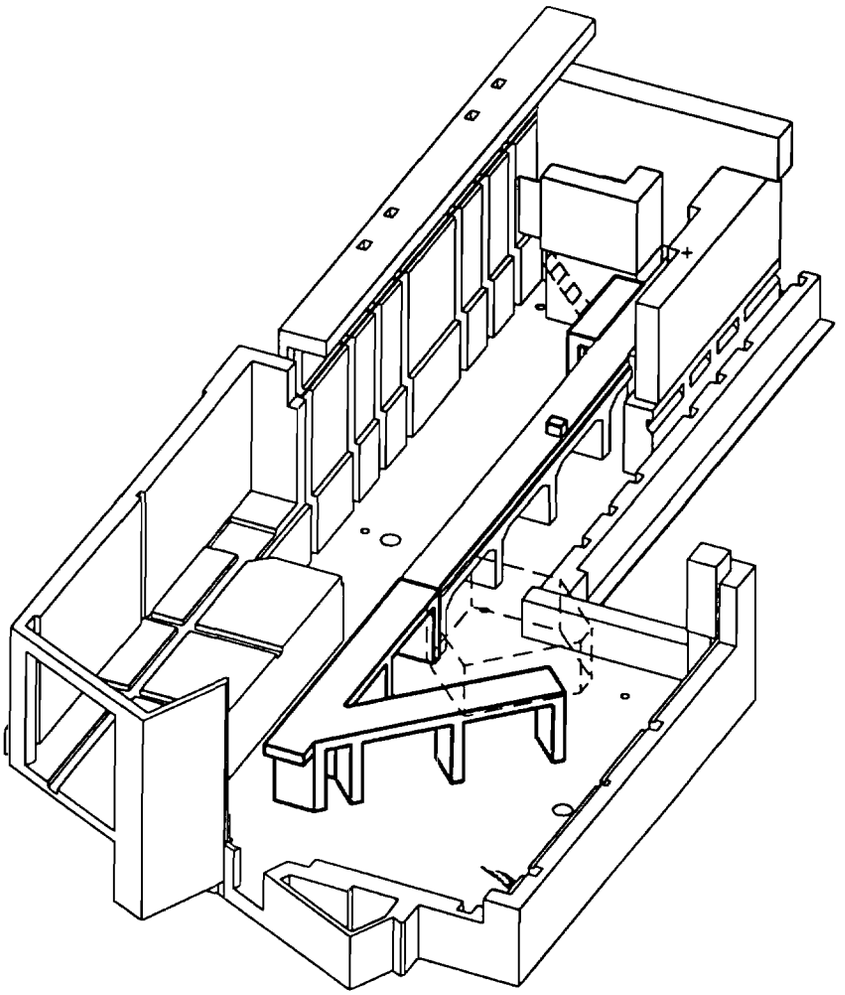

Fig. 3.2 3D View of (empty) Linac 3 Building

Cooling water

Much of the heat load in the building will be taken by the water cooling of the elements e.g. magnets and power supplies.

Two main circuits are foreseen:

One of demineralized water with 25 bars pressure at input and 2 at the output, with a temperature of 25 ±1° (maximum in summer: 28°-29°), and a conductivity of 0.5 μS/cm. The total flow rate available is 12 m3/h and this seems enough if there is some use of raw water in parallel. From the main circuit, secondary ones with suitable pressure reduction will be derived.

One closed circuit of raw water cooled by chilled water via a heat exchanger. Maximum input pressure is here 6 bars and the return should not be lower than 2 bars. The temperature of the water can be maintained in the range 25 ± 1° with a particular application to the mild steel cooling jacket of the IH structure where a corrosion inhibitor will be added and upper pressure strictly limited to 6 bars.

3.1.4 Fire Detection

The old fire detection ducts had to be changed as they were not in accordance with Safety Instruction IS 23. No fume extraction system will be installed but a valve in the exhaust circuit of the air conditioning will be opened by a trigger coming from the fire detection system.

3.1.5 Radiation Protection

The following operating characteristics were assumed [38]:

Table 3.1.1: Assumed operating conditions of Linac 3 for radiation estimates

Ion:	208 Pb^{25+}
Maximum energy:	E= 4.2 MeV/u
Maximum intensity:	100 μAe (of ions) with 1 % duty cycle
Maximum average beam:	0.25 10^{12} ions/s

It is important to note that the radiation coming from the beam can be completely neglected in comparison with the high X-ray level produced by the RF fields in the cavity and the highest electric fields will correspond to the lowest charge states. These maximum conditions are expected to apply only while setting-up. During normal running the duty cycle is expected to be 0.25 % or less and the nominal charge state for the lead ions (+28) requires lower accelerating voltages. Taking into account measurements made at GSI and the layout of Linac 3, the X-ray dose rates in mSv/h to be expected in the surrounding area if no shielding is added when the RF is set to operate with 25+ ions, are indicated in Fig. 3.3 (dose rates assume a factor of 3 attenuation by the thick steel frame of the IH structure, and that tanks 2 and 3 both emit X-rays at 50 % of the level of tank 1).

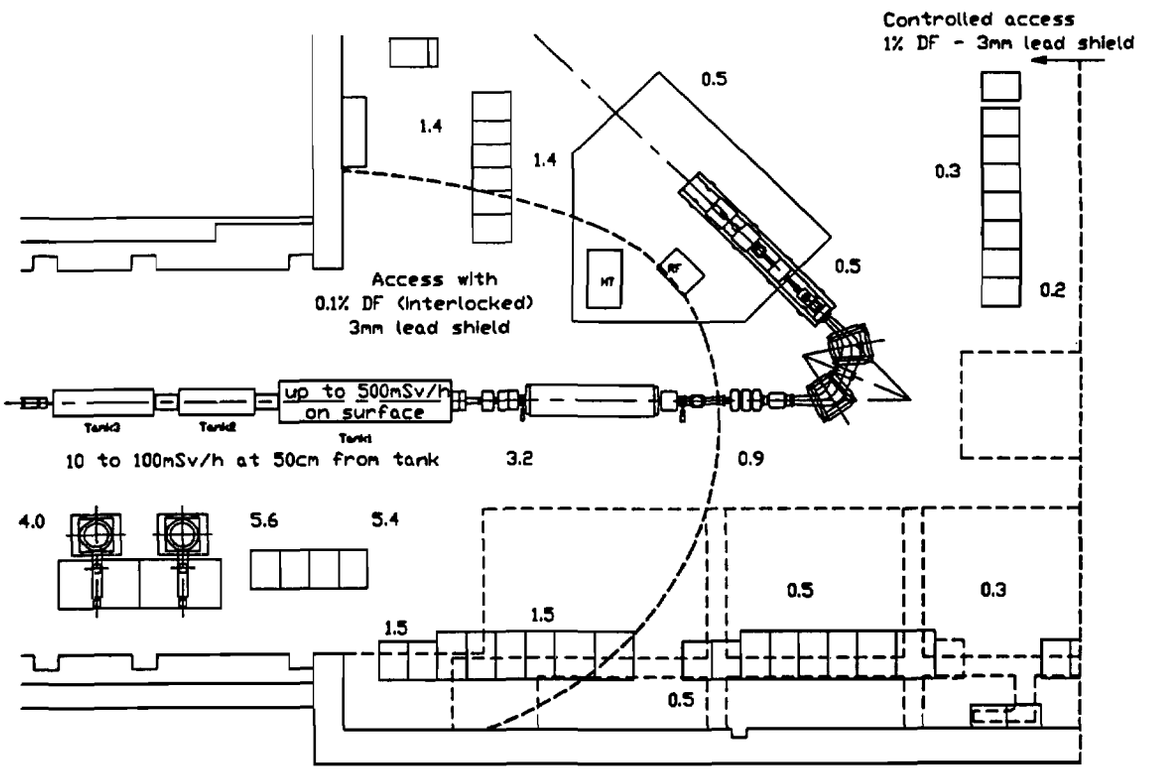

DOSE RATES NEAR CERN LEAD LINAC
(mSv/h)

1) 208 Lead + 25 (8.88 reference Volts)
2) 1% Duty Factor (DF)
3) Factor of 3 self-shielding at large distances
4) 25% decay of dose rate with time
5) Tanks 2 and 3 emit only 50% of X-rays of tank 1

 Fig. 3.3 Estimated X-ray Dose Rates near Linac 3

The dose rates near the accelerator tanks are such that some interlocked barrier, possibly coupled to the RF voltage, would be necessary for access to the vicinity of the accelerator. To avoid these operational constraints and to minimize possibilities for irradiating personnel, it has been decided to surround the IH accelerator tanks with a close fitting 5 mm thick lead jacket, which will reduce the dose rates in the area by up to two orders of magnitude.

The concrete shielding at the end of the filter/stripper line, near the PS has been also reinforced because measurements had shown this was needed given the proximity of the high flux proton ejection line TT2 just beyond it.

3.1.6 Alignment

The refurbished concrete support pedestal has been made with its top surface plane at 1.27m below the ideal beam level (433.660 m above sea level). Up and downstream of the main line, the vertical and horizontal positions defining the beam axis are marked on monuments already used in the past for Linac 1; on the main part of the pedestal four built-in concrete blocks are equipped with steel alignment monuments to define an off-axis line 600 mm above and 300 mm. to the right of the ideal beam axis. Adjacent to the intersection point between the off-axis line at 135° to the main line, there will be another fixed monument which will be used with a temporary monument beyond the source to define a line 600 mm vertically above the axis (no horizontal offset). Alignment strategies for all parts of the linac region have been defined using the fixed monuments mentioned above and some temporary ones. The precise supports, 'douilles' (for the Taylor Hobson alignment targets), which will be installed and pre-aligned on the off-axis jigs attached to the individual beam transport elements, are of standard CERN design.

3.2 CONTROLS SYSTEM

3.2.1 Architecture

The controls system uses a 3 level system architecture (see Fig. 3.4). On the highest level, the user interaction level, UNIX based Workstations are used. On this level all applications programs are implemented as X-Windows applications. The workstations are connected to front end computers through ETHERNET. The front-end computers, based on VME equipment (DSC = Device Stub Controller), constitute the second level of the architecture. They run a Posix compliant Real-time operating system named LynxOS. On this level equipment driving software (equipment modules) is installed controlling an accelerator subsystem e.g. power supplies, RF, timing, instrumentation and the like. The Equipment module is called from the application through Remote Procedure Calls (RPC) and remotely executes subroutines, so called stubs. The physical equipment is finally controlled over a field bus (Mil 1553, serial CAMAC) by G64 controllers or directly through VME interfaces. The software running in G64 controllers is under the responsibility of the equipment expert and communication between the DSC and the G64 crates is done through a mutually agreed protocol.

The Workstations as well as the DSCs are booted over ETHERNET from a file server, which is also used for storage of all permanent information for these machines. While the Workstations use local disks for swapping, the DSCs are completely disk free, which constitutes a great advantage considering the harsh environment they must work in (close to the equipment).

3.2.2 Software

Each level of hardware has a level of software associated to it (see Fig. 3.5). On the workstations the software is mainly concerned with user interactions. A console manager allows application programs to start, shows acquisition orders of lists of parameters and permits control of individual parameters. The control panels are generated by a 'knob server'

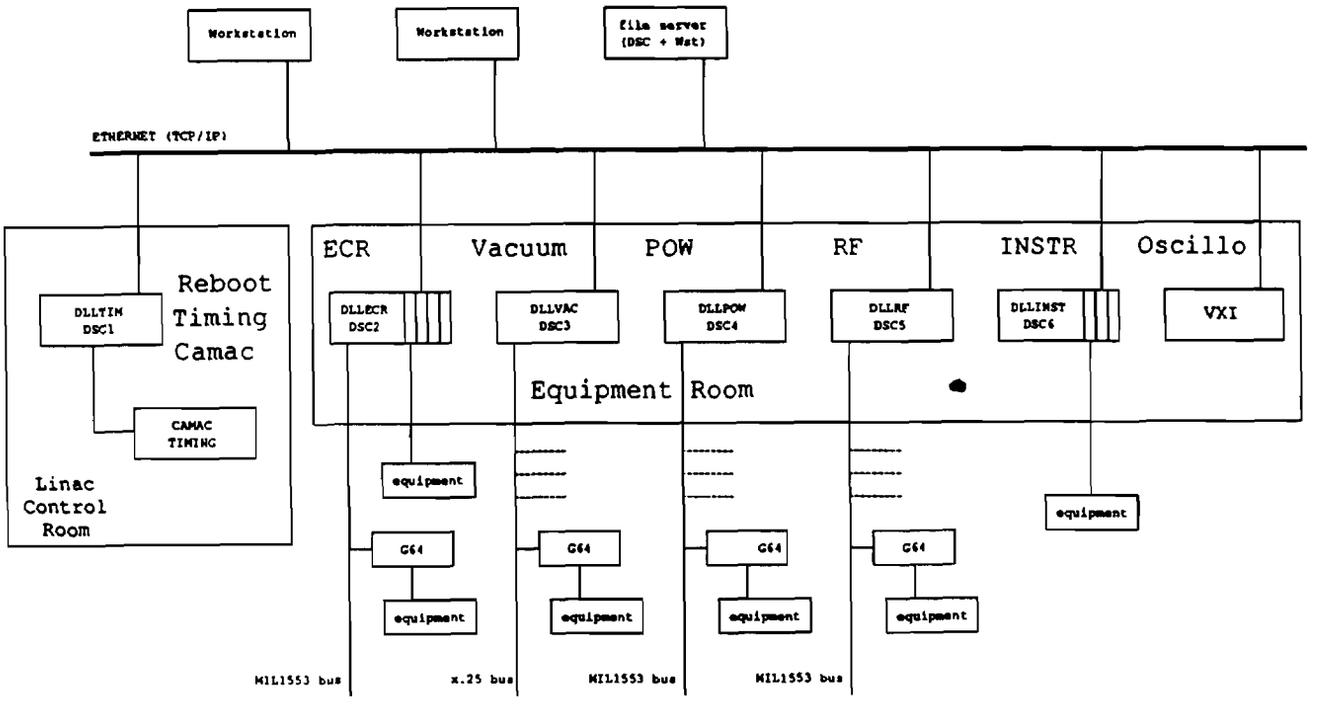

Fig. 3.4 Controls System Schematic Showing Three Level Architecture

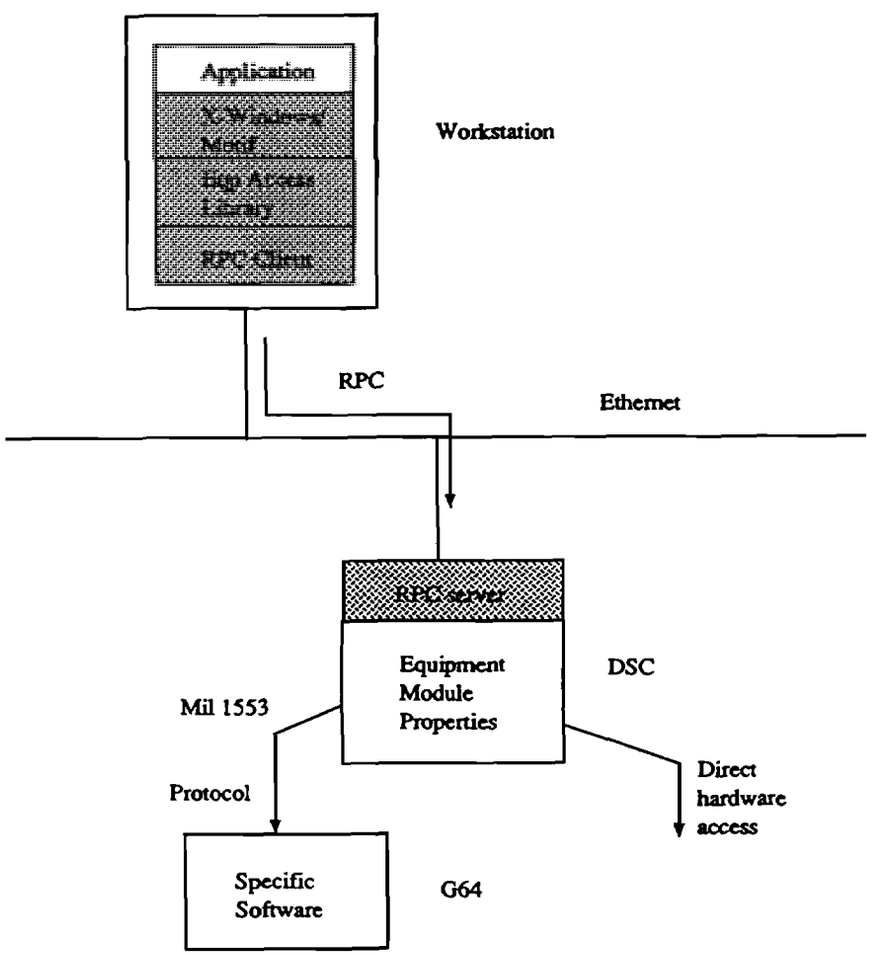

Fig. 3.5 Software Architecture

which takes the request for control of an equipment and puts a window with control buttons onto the screen. The use of a server ensures that all controls panels for the same type of equipment will look the same, thus enforcing uniformity for all applications in the system. All errors are treated by a common error server which displays error information in a consistent fashion and logs them for later inspection.

Applications are based on the Motif user interface giving the same look and feel for all of them. In addition the layout of certain menus and buttons are fixed and certain panels (for date and time, freeze/unfreeze display etc.) will always appear in the same form and at the same location on the screen.

Application programs access the second software level through an equipment access library, which calls (on the DSC) remote equipment-driving subroutines, the so-called equipment module properties.

The access library gets all information needed for parameter access (e.g. the DSC address where the equipment module property resides) from a real-time data base, which in turn contains tables extracted from a central Oracle data base. The central data stores all information needed by the access library as well as the equipment modules (e.g. interface module addresses, min/max values etc.)

The access library calls the remote subroutines via an RPC mechanism which is hidden from the programmer. The EM properties either send messages over the equipment protocol to the specific software in G64 controllers (MIL1553 case) or control the interface hardware directly.

3.2.3 Analogue Signals

An analog signal observation scheme consisting of a VXI crate, 3 screenless oscilloscopes, modules offering up to 12 oscilloscope channels and an analog multiplexer is used. Twelve out of 96 signals may be connected through the multiplexers (MUX) to the 12 oscilloscope traces. The signals are digitized in the scopes and are then transferred over the network to the workstations, where they are displayed. A 'virtual scope' program on the workstations allows interactions with the scope in order to control any of the scope parameters.

3.2.4 Timing

The injection of ions into the PSB is sychronized with a signal related precisely to the magnetic field of this machine (SIP = Start Injection Pulse). SIP precedes the beginning of the transfer of the beam by 2 ms. Individual timings for driving the users' equipment are derived therefrom with a sufficient precision (100 ns) by using digital delays, located in a central CAMAC crate.

For triggering slow processes, like the bending magnets in the beam transport lines, one uses an earlier prepulse from the PS/PSB timing system (FLI = Forewarning LInac), preceeding the beam by 660 ms with a precision of ±10 ms.

Alternate injection of ions and protons from Linac 2 and optional observation of either beam in the common measuring lines is controlled on a pulse-to-pulse base according to information received from a central Programme Line Sequencer (PLS).

The timing system will run under the controls system through a serial CAMAC loop from a VME chassis. Appropriate equipment modules (EM) provide the user interface to control the setting of the timing parameters, as well as remote diagnostics to allow for solving operational problems.

3.3 RADIO FREQUENCY (RF)

3.3.1 Introduction

Six RF-amplifiers including all the amplitude and phase regulation, phase setting and cavity frequency tuning will be needed to feed the two RF bunchers at 101.28 MHz, one RFQ and one IH-structure at 101.28 MHz and two more IH-structures at 202.56 MHz of Linac 3 (Fig. 3.6). CERN is responsible for the low level part up to 1 Watt, using standard CERN techniques as far as possible. The GSI contribution to the RF-system consists of the power amplifiers for all the RF-structures of Linac 3, except the two 202.56 MHz amplifiers which will be made in collaboration with CERN.

3.3.2 Low-level R.F.

The reference for each tank shall be provided by an eight-way power-splitter delivering 200 mW at 101 MHz to each station. This goes directly into a high-resolution phase-shifter which can be adjusted remotely. An optional frequency-doubler is included in the phase-shifter to allow operation at either the fundamental or at 202 MHz (resolution at both frequencies being approximately 0.2°). The power-splitter option was considered practical for the relatively short linac length. A reference-line with a pulsed amplifier and directional-couplers (such as used in Linac 2) was also considered. It was discarded both due to the cost and the stringent demands made on the phase and amplitude stabilities required (±0.3° R.F. phase, $\pm 3\ 10^{-3}$ for amplitude). It was thought that a C.W. reference would find it easier to produce a stable, reproducible output than a medium power (4-600W) pulsed amplifier.

The calculated temperature dependence for the linac length has been estimated at 202 MHz to be less than 0.1° per degree of temperature change.

Figure 3.7 shows the layout for one RF station. This is very similar to that used in CERN's Linac 2 and existing modules will be used where possible. The phase and amplitude requirements demand that certain modifications be made - the most important being to the detector boxes which have to be regulated to avoid thermal drift. Amplitude-levelling circuits may also need to be added to the phase-detector to minimise output variations as the tank voltage is varied. However the tank voltages for a given ion type, will essentially be fixed after initial setting-up, and with the phase-loops in the low-level, acting so that the phase detectors in the detector box work around zero volts; any amplitude dependence is, in theory, removed. Measurements on the existing hardware show that amplitude variations around the nominal working voltage may be tolerated for a 0.5° magnitude error as the detector rest point moves away from nominal zero phase. Also, assuming that the detector rest position is no more than 2.8° from the nominal zero, then the measurements show that a variation in tank voltage magnitude of +0.95 dB results in errors of 0.1° phase or less.

3.3.3 Amplifier Specifications

Three different amplifier types at the two frequencies, will satisfy the power requirement of the cavities and an additional beam load of about 7 mA, with a proper reserve for tube ageing, mismatches and regulation of amplitude and phase. All amplifiers are specified for 1 ms pulses with 10 Hz repetition frequency, i.e. for 1% duty cycle, to guarantee a relaxed operation with shorter pulses and lower repetition rates which applies during initial operation (table 3.3.1). The specifications for the three amplifier types are very detailed and as similar as possible to get uniform controls, power supplies and analogue measurement equipment. Cooling circuits with water quality of < 1 µS/cm are used for the power amplifiers.

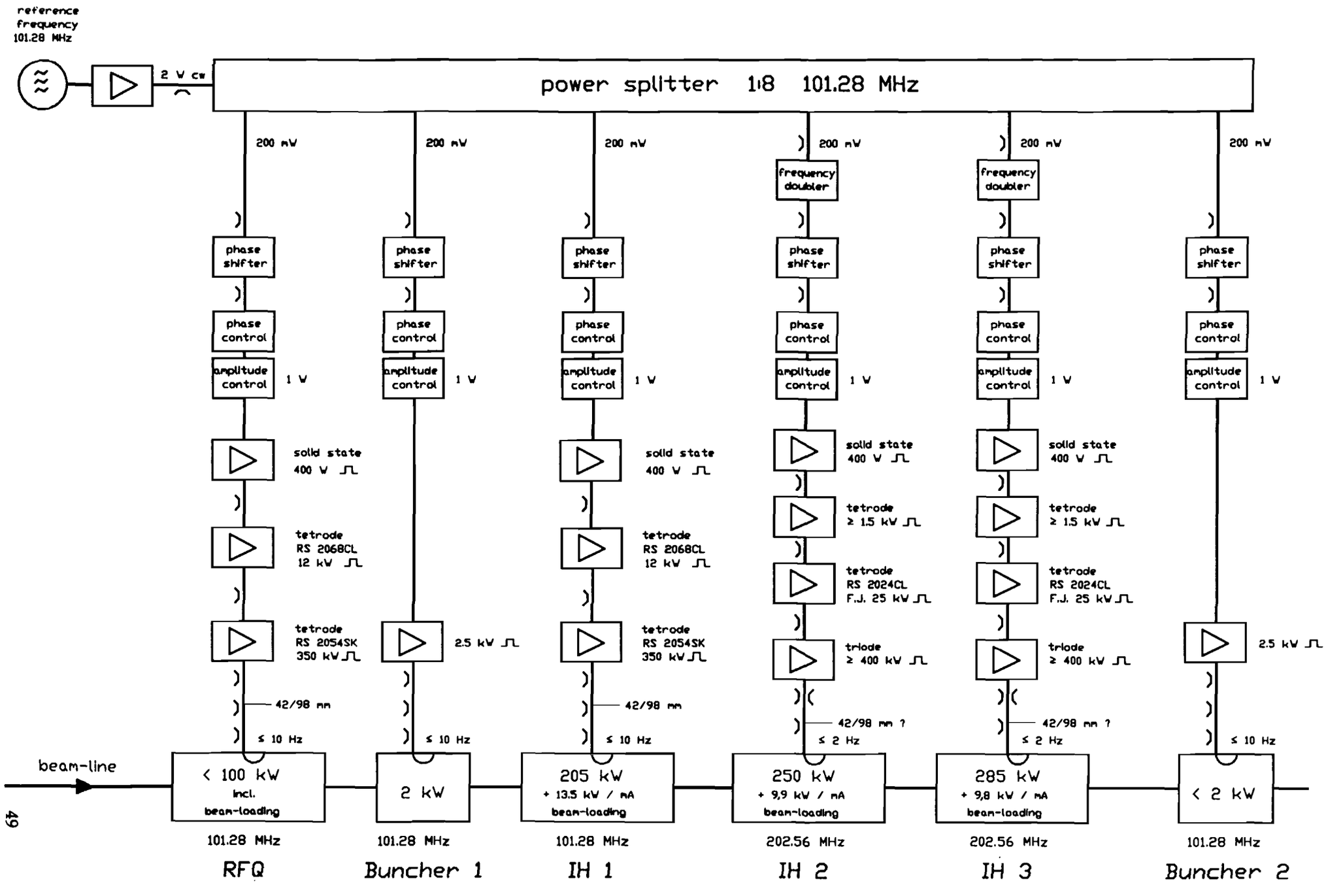

Fig. 3.6 RF Distribution and Amplifier Chains for Linac 3

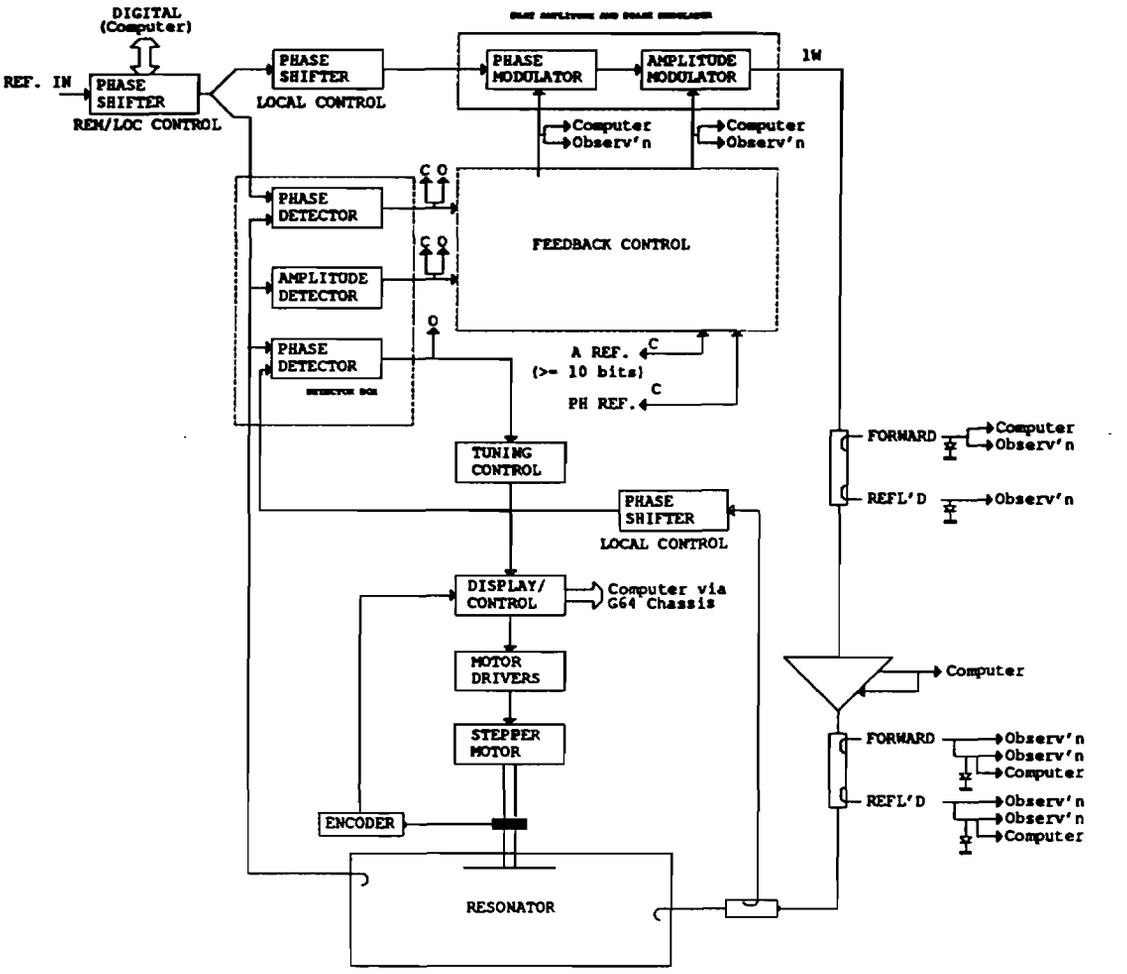

Fig. 3.7 Block Diagram of One RF Station

Amplifiers for Bunchers

The two amplifiers for the bunchers at 101.28 MHz will be solid state devices as they have to deliver only pulses of 2.5 kW, a power that has already been demonstrated by solid state amplifiers of the HLI at GSI with a duty cycle of 60%.

101.28 MHz Power Amplifiers

For the two high power 101.28 MHz structures, the RFQ (IAQ) and the IH1 (IA1), two equal amplifiers will be used, even though the power consumption differs by a factor of more than three (100 kW to 350 kW). Thus the number of spare parts is reduced, maintenance is easier and tubes which do not fulfil their specified power can still be used in the first amplifier. A modified broadcast amplifier could be used as driver, but most of the bidding companies prefer their own specific design. Existing circuits with a full, a $3\lambda/4$ and a $\lambda/4$ anode-resonator will be helpful for the final amplifier design. Tetrodes in the power range of 350 to 400 kW are available from several companies.

202.56 MHz Power Amplifiers

The two amplifiers for IH2(IA2) and IH3(IA3) are identical and consist of the old Linac 1 amplifiers improved for reliability, especially in the final stage. The latter is a water-cooled triode amplifier working in grounded grid mode, using a capacitor bank power supply of about 30 kV and a pulsed cathode configuration. The output power will be at least 400 kW.

As driver the so-called 'Frank James Amplifier' delivering 25 kW at 1 ms pulse length will be used, with an air-cooled tetrode in grounded grid mode, a capacitor bank HT supply and screen grid pulsing. The tube-type pre-driver operates using a tetrode in the same mode as the driver, to which it delivers an output power greater than 1.5 kW at 1 ms pulse length. To bring the power level up from the low level/control system to that required at the input of the pre-driver there is a solid state amplifier with maximum output 400 W for 1 ms pulse length.

3.3.4 Controls and Power Supplies

The control of all the six amplifiers will be standardized, using a SIMATIC free-programmable unit (produced by Siemens AG) for each amplifier, which differs only in the size needed for the small buncher amplifiers, but uses the same programming language 'Step 5'.

The anode power supplies will use dc voltages with a stored energy of about 10 to 12 kJ per capacitor bank. The crowbar system for the discharge of the capacitors will use a GSI development.

Table 3.3.1: Parameters of amplifiers

	BUNCHERS* (ITM.CRF & ITF.CRF)	RFQ &IH1 (IAQ & IA1)	IH2 & IH3 (IA2 & IA3)
Centre frequency (MHz)	101.28	101.28	202.56
Pulse duration (ms)	1.0	1.0	1.0
Pulse repetition frequency (Hz)	10	10	2
Peak input power (W)	1	1	1
Pre-driver (W)	–	600 (solid state)	1500 (tetrode)
Driver (air-cooled tetrode) (kW)	–	20	25
Final stage	Solid state	water-cooled tetrode	water-cooled triode
Power Output (kW)	2.5	350	400

* CERN nomenclature in brackets

3.4 THE VACUUM SYSTEM OF LINAC 3

The two completely different activities which had to be undertaken in the framework of this project concern the design of a new system for Linac 3 (this section) and the comprehensive upgrading of the PSB and PS vacuum systems in order to ensure adequate transmission of partially stripped ions (section 3.5).

Since Linac 3 is being built in collaboration with various member state laboratories and institutes, CERN's main role concerning the vacuum system design, its components and its control options, is to ensure compatibility with the design philosphy of the up-graded PS complex. The following areas are therefore important:

3.4.1 Vacuum Quality Standards

CERN's experience with ultra-high vacuum systems has led to the development and choice of materials which have low outgassing rates especially after proper cleaning and sometimes vacuum firing to 950° C (stainless steel). Of course where RF, mechanical strength and manufacturing ease are also as important, other materials e.g. copper alloys and aluminium, may be chosen but then special attention must be paid to surface cleanliness, porosity and virtual leaks which can occur when joining materials without allowing proper pumping slots or clearances.

3.4.2 Choice of Equipment

Much of the vacuum equipment can be standardized relative to the rest of the PS complex. For example the backing pumps, turbo pumps and ion pumps have standard pumping speeds and flange sizes and are assembled into pumping stations together with standardised ion gauges, shut-off valves and manifolds. (see details in Table 3.4.1). Also the controls for this equipment has to be compatible with the existing CERN installations. Standardised metal seals (mostly aluminium) are fitted to standard flanges on the ports of the apparatus or to a bellows/flange combination, when necessary.

3.4.3 System Design

Each sector will have at least one pumping station. The division into sectors by gate valves is generally conditioned by the vacuum technical requirements. For an intervention on a single component it is undesirable to bring the whole machine to atmospheric pressure, and the sectors follow the natural operational separation between different types of accelerator equipment. In the region up to 250 keV/u, where the space is limited, this is not entirely possible. Figure 3.8 gives a schematic layout and table 3.4.1 lists the vacuum equipment.

3.4.4 Controls Philosophy

Standard CERN logic for automatic pump down (handling of pressure data) and automatic letting up to nitrogen has been used throughout. This includes protection against power cuts and false manoeuvres.

3.4.5 Maintenance Possibilities

Maintenance must be able to be done efficiently by hired labour in shutdowns with minimal supervision from CERN supervisors.

3.4.6 Spare Parts Policy

Standardisation allows rational selection of spares which can be used in the whole of the PS complex.

Table 3.4.1: Summary of type and number of vacuum components

Getter Ion pump of 230 l/s for larger volumes	9
Getter ion pump of 60 l/s for small diameter beam pipes	7
Roughing station with turbo molecular pump and dry N2 inlet	5
Roughing stations on source and air-lock	2
Turbomolecular pumps with magnetic bearings on source	2
Sector valves between 60 and 160 mm	5
Pirani Penning vacuum gauge pair, also for controls interlocks	10
Penning gauge for specific element surveillance	5
Pressure read-out equipment	7

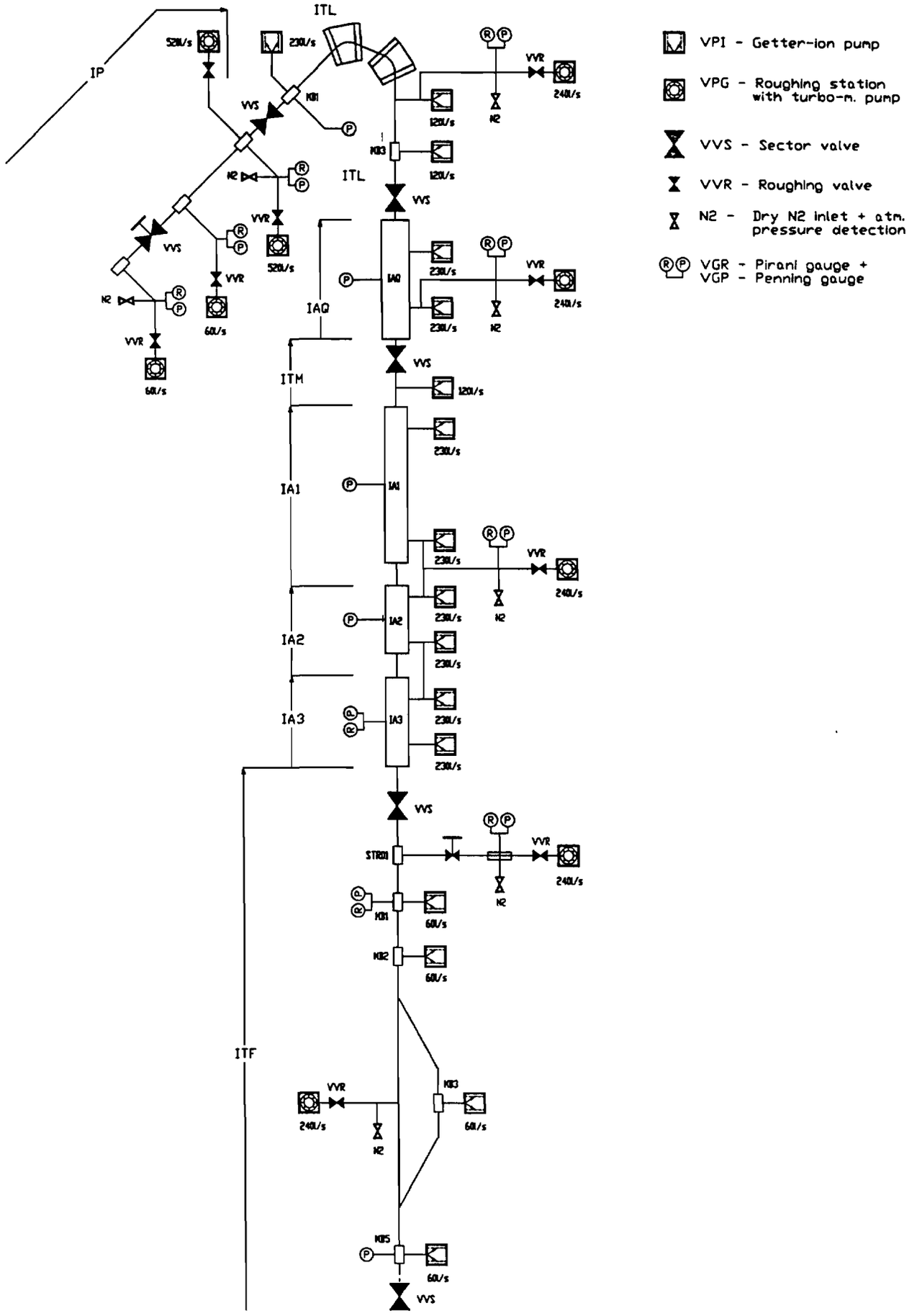

Fig. 3.8 Schematic Layout of Vacuum System in Linac 3

3.5 UPGRADING THE VACUUM IN THE PSB AND PS

This is necessary to obtain an acceptable transmission rate in those machines where the partially stripped ions will be accelerated. The transmission against pressure curve of Fig. 1.2 shows that an acceptable combined transmission rate of better than 50% through both machines requires on the beam path a partial pressure from the non-hydrogen gas components lower than 1×10^{-9} Torr in the PS and below 9×10^{-10} Torr in the PSB. At those pressures one can reasonably suppose a rest gas composition of 80% H_2 and 20% mostly H_2O, N_2 and some CO, so the real total pressure will be around 5 times that value in both machines. Due to the gas composition, the real partial pressure of non-hydrogen gases is 30% of the pressure indicated on the gauge, which is calibrated for N_2. This means that the pressure, as read, has to be below 2.8×10^{-9} Torr in the PSB and 3.5×10^{-9} Torr in the PS. At present the gauge pressure in the PSB is close to 2×10^{-8} Torr and in the PS 1×10^{-8} Torr; an improvement factor of more than seven has to be aimed for in the PSB and more than three in the PS.

This desired lowering of the vacuum pressure in the PS and in the PSB can be treated under five headings. The assessment of the possible improvements attainable and the evaluation of the results will depend on the diagnostics means in the rings, which are being installed now in the frame-work of the vacuum consolidation projects. In the table 3.5.1 the separate actions are denoted by T(i), T(ii) etc as in the headings in the text but the actions belonging to each accelerator are grouped.

3.5.1 Vacuum Chamber

In the PS (T(i))

The PS already has new vacuum chambers in its 100 bending magnets made out of stainless steel, 316L+N, and vacuum fired before installation. An average total pressure along the beam path better than 5×10^{-9} Torr as read is obtained. It is not foreseen to apply bake-out to these vacuum chambers.The tanks in the straight sections in between magnets will be discussed below.

In the PSB (T(ii))

The stainless steel used for the beam envelope is generally 316L or 304L, not vacuum fired. The 4 parallel beam channels give a good conductance and an average pressure just above 1×10^{-9} Torr (as read) is reached here. The vertical manifolds that interconnect the 4 beam pipes can be dismounted reasonably easily and they will still undergo the vacuum firing in the first stage of the upgrade work.

3.5.2 Components in Vacuum

PS Machine Tanks (T(iii))

In most of the straight sections in between the magnets of the PS machine tanks are installed which often contain equipment with a high outgassing rate. In these tanks a pressure in the low 10^{-7} Torr is reached after a week pump down.

In some straight sections this equipment is recent, with Wheeler^R type end flanges. They are already designed for an improved vacuum, and can undergo a soft in-situ bake-out. The pressure will go below 1×10^{-8} Torr, an improvement of a factor of more than 10 compared with the old situation.

This new design no longer allows interventions in-situ. In case of problems the whole tank with its contents and attached equipment has to be exchanged for a well prepared spare. The situation in the PS will be further improved by replacing a 1 metre tank and its equipment in straight section 58 and a two metre one in straight section 16 by tanks in this new design. For both these tanks, the main reductions in outgassing concern the contents i.e. the pulsed septum magnets and beam observation equipment.

PSB Septa and Kickers (T(iv))

Due to its 4 beams the PSB needs injection or ejection equipment for each beam. This creates heavy out-gassing sources which require urgent action. Also the four stacked septum magnets, kicker magnets or other types of equipment need improvement. Due to this quadruple design replacement of injection and ejection equipment is expensive. There are several sections with high gas loads in the PSB ring, with a major problem the presence of pre-'UHV' old ferrites in different places. The replacement of these ferrites is under consideration and might take place in the 1994 shut-down. A soft bake-out after installation will be necessary after installation to diminish the degassing of the new ferrites.

3.5.3 Eliminating Unnecessary Outgassing

In some places in both machines rarely used equipment is still installed in vacuum and this load on the vacuum system should be diminished where possible. Also any installation of equipment for tests in the PS or in the PSB should be weighed against the risk of perturbation of the vacuum conditions (action T(v)).

For new manufacturers the respect of the requirements for UHV equipment has to be stressed.

3.5.4 Optimizing Installed Equipment

In some places pumps are connected to the beam vacuum chamber via long and/or bent conductances. In one typical case which is repeated 22 times it is proposed to use a smaller pump via a better connection and gain in pumping speed and in pressure (action T(vi)).

3.5.5 Pumping Speed

Once the existing installations have been improved by lowering the gas load, one has to consider the best options for the increase in the pumping speed needed. Out of the different possibilities for high volume pumping for the first stage only two have been retained:

Getter-ion pumps (T(vii))

These will be added in certain places, also to leave as few gaps as possible in the regular pumping distribution. This extension of the existing system does not pose any new operational or exploitational problems. Also it is planned to replace a large number of these pumps, many of which have been in frequent use for more than 20 years and have lost a substantial part of their capacity, (T(viii)). With the new manifold for the sublimation pump in the PS, the conductance for the getter pumps will be slightly reduced.

Titanium Sublimation Pumps (T(ix))

CERN has a large experience with Titanium sublimation pumps both on the mechanical design side as well as on the control side. They offer a capacity of more than 1200 l/s for an easily handleable size and their maintenance is simple.

It is planned to add a 1200 l/s Titanium sublimation pump to every Getter Ion pump in the PS and in the PSB pumping system. Figure 3.9 shows how the mechanical design is foreseen in the PS giving a maximum conductance between the new pump assembly via the existing manifolds to the downstream end of each magnet vacuum chamber. The new inter magnet tank design also foresees around two sublimation pumps per meter length. In the PSB most vertical manifolds will receive a sublimation pump, Fig. 3.10. On tanks with high outgassing equipment these pumps will also be added.

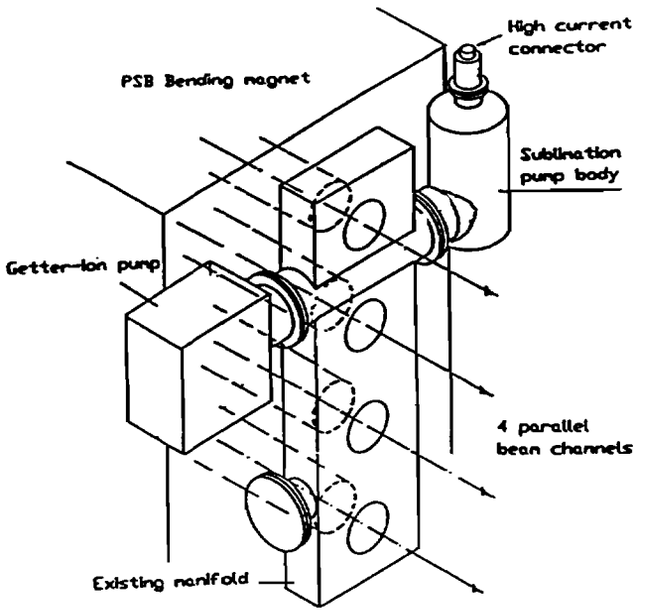

Fig. 3.9 New Pump Manifold for PS

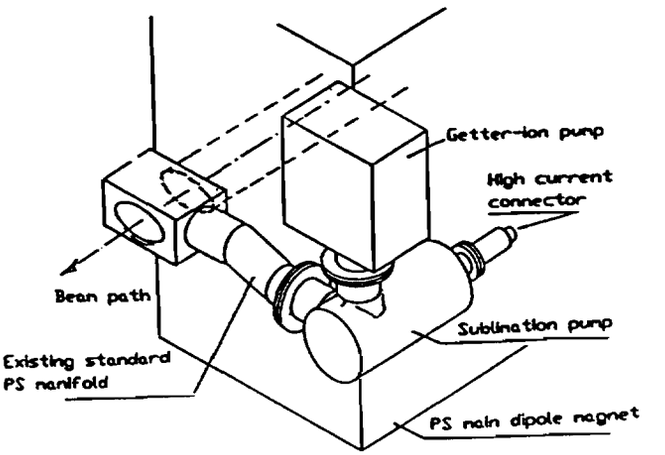

Fig. 3.10 Proposed Pump Connections for PSB Manifold

3.5.6 Summary of Actions

The (very) approximate expected improvements are not cumulative linearly.

Table 3.5.1: Actions to improve the vacuum and predicted effects

Action:	Machine:	Effect on Q:[1]	Effect on S:[2]	Effect on P:[3]
T(i)	PS			- nil -
T(iii)	PS	-6×10^{-6}		-0.5×10^{-9}
T(v)	PS, effects are small but see note 4 below.			
T(vii)	PS, not yet defined, in any case small.			
T(viii)	PS		-500 l/s	$+ 0.5 \times 10^{-9}$
T(ix)	PS		+ 22'000 l/s	-4.5×10^{-9}
T(ii)	PSB	-1.2×10^{-5}	indirect	-1.5×10^{-9}
T(iv)	PSB	-5×10^{-5}		-5×10^{-9}
T(v)	PSB, effects are small but see note 4 below.			
T(vi)	PSB		+ 660 l/s	-1.8×10^{-9}
T(vii)	PSB, not yet defined, in any case small.			
T(viii)	PSB		+ 700 l/s	-2×10^{-9}
T(ix)	PSB		+ 16'000 l/s	-1×10^{-8}

1 Q = total outgassing in Torr l/s.
2 S = pumping speed in l/s.
3 P = average gauge pressure difference on the beam path in Torr.
4 This has more influence on operational safety and on risk of lost time due to break-down.

An extremely approximate estimate of the static pressure to be reached after the improvements as listed above gives as a result gauge pressures around 3×10^{-9} Torr, slightly lower in the PS, slightly higher in the PSB. This means that for the PSB it will be necessary to provide a soft bake-out of the new ferrites after they are installed. Also a maximum of extra pumping speed is to be considered, to lower the pressure bump in between two pumps in as many places as possible. In this way the pressure of the 'heavy' non-hydrogen components should be reduced to an acceptable value of about 9×10^{-10} Torr in the PSB (see section 4.3.1).

3.5.7 Effect of Operating Conditions on PS Vacuum

One cannot discuss vacuum in a machine like the PS without mentioning the difference between static pressure after a a few weeks pumping and the pressure rises brought about and influenced by the different types of particles and by their intensities in the circulating beam. In the early days of the discussion on heavy ions in the PS complex some observations were made, with the following results.

In the case of lepton acceleration in the PS a sharp rise to the 1×10^{-6} Torr level is observed which falls back to a slightly higher than base pressure in a few seconds only. Full recuperation occurs in one hour.

In the case of intense proton beams for antiproton production, the pressure rises to about twice its base value to 2×10^{-8} Torr. It will take a few days after that before the desorption rate and the pressure are back to their base values.

It will require some development effort on the newly installed diagnostic equipment and on the interpretation of the measurements to refine these observations. In particular, the planned improvements treated above (summarised in 3.5.6) should alleviate these pressure rise problems. It may still be necessary to separate lepton and ion cycles in the PS super-cycle or in the extreme cases, to avoid incompatible vacuum conditons by optimal scheduling of the ion runs, lepton runs and antiproton runs.

4 PROTON SYNCHROTON BOOSTER (PSB)

4.1 INTRODUCTION

The Proton Synchrotron Booster (PSB) is a stack of four synchrotrons sharing a common main magnet and focusing quadrupoles, a common main power converter and vacuum system. The machine has a radius of 25 m (one quarter the radius of the CERN PS) and accelerates up to $9\ 10^{12}$ protons/ring from 50 MeV to 1 GeV in about 450 ms at a repetition time of 1.2 s. Protons are injected by the classical multiturn process (up to 17 turns), which is intrinsically lossy: Injection efficiencies exceeding 40% are hardly possible if one wants to inject the maximum possible number of particles.

Although the PSB has accelerated light ions over years and the related problems due to low intensities and low energies per nucleon (entailing large acceleration frequency swings) are well known, accelerating highly but not completely ionized heavy ions would be impossible without substantial modifications. The most significant effects are due to the large cross-sections of charge-exchange processes between the circulating ions and the molecules of the residual gas at low energies. The obvious cure is improving the vacuum, but as already outlined in chapter 3.5, achieving gas pressures guaranteeing negligible transmission losses, is out of reach. One remedy is to accelerate as fast as possible, at least during the low-energy phase, where charge-exchange processes are most likely and the ensuing loss rate extremely high. Figure 4.1, showing the computed lifetime of the nominal Pb ions as a function of their energy, illustrates the importance of the low-energy phase.

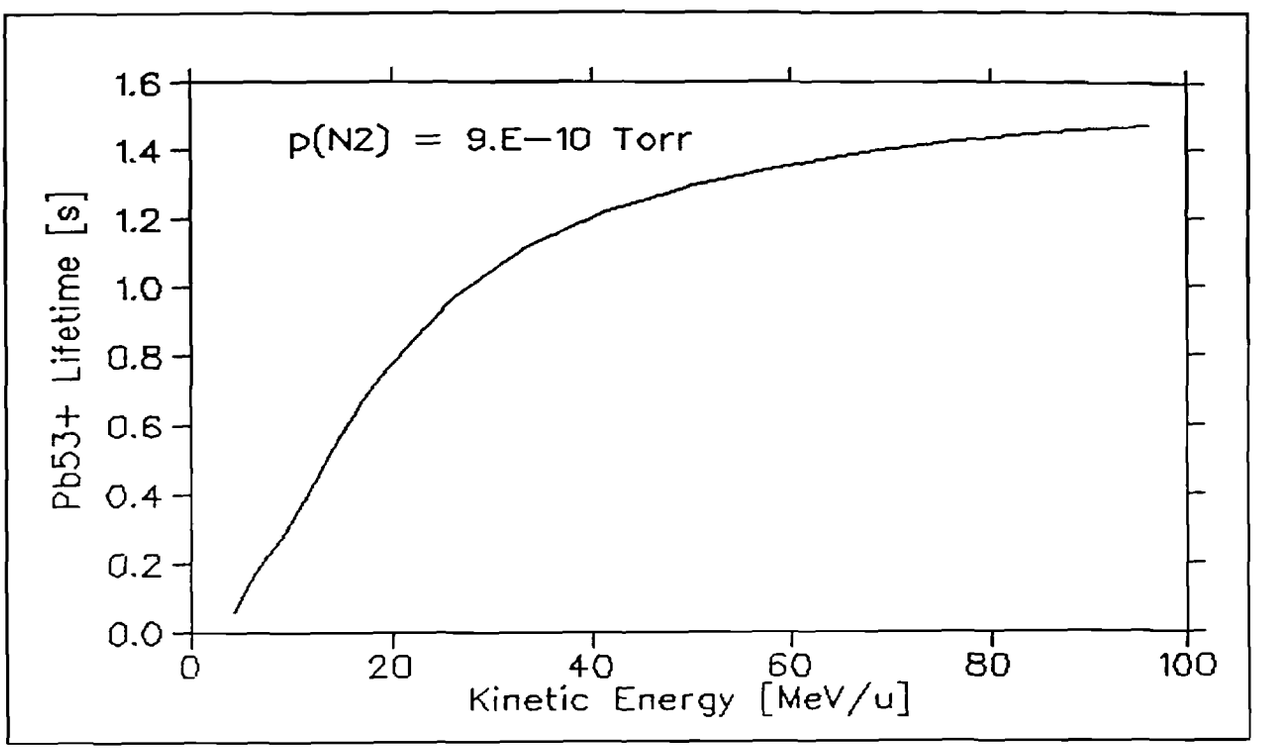

Fig. 4.1 Lifetime of Pb^{53+} versus Kinetic Energy in the PSB

4.1.1 PSB acceleration parameters

Table 4.2.1 compares the basic parameters relevant for acceleration of lead ions and protons. A more detailed compilation is given in Table A4.2.1 of the Appendix.

Table 4.2.1: Compilation of PSB parameters relevant for acceleration of Pb^{53+} and protons

Parameter	Pb^{53+} Ions	Protons	Unit	Comments
Charge State	53	1		
Injection				
Kinetic Energy	4.2	49.6	MeV/u	i.e. 50 MeV protons
$\beta = v/c$	0.0946	0.314		
$(B\rho)$	1.159	1.0353	T m	
Bending Field B	0.141	0.1255	T	
Revolution Period	5.536	1.668	μs	
RF Frequency	3.61	3.0	MHz	
Ejection Flat Top				
Kinetic Energy	95.40	993	MeV/u	i.e. 1000 MeV protons
$(B\rho)$	5.66	5.66	Tm	
Bending Field	0.689	0.689	T	
β	0.421	0.875		
Revolution Period	1245	599	ns	
RF Frequency	8.05	8.35	MHz	
Total Duration of Acceleration Cycle	257.6 (computed)	415 (measured)	ms	
Global Transmission due to Charge Exchange Loss	0.62	1		Eff. non-hydrogen pressure 9 10^{-10} torr

4.2 IMPROVING THE PSB

4.2.1 Summary of Improvements

The modifications aiming at minimum losses due to the above process are: vacuum improvements (4.2.2), modifications and improvements of the Main Power Converter to operate at highest possible dI/dt to shorten the acceleration time (4.2.3), and injection and RF-capture of the ion beam from the linac on a rising magnet field at the highest possible dB/dt (4.2.4).

As the $(B\rho)$ of the reference ion is 12% greater than that of the 50 MeV protons, the currents of the optical elements in the injection line BI.XXX as well as of the Main Power Converter, have to be modulated according to the type of particle. This is already possible with the exception of one quadrupole: BI.QNO20.

Other complications arise due to the need to deal with the low velocity of the ions. All pulsed injection/extraction elements have to cope with the longer revolution period, which for elements BI.XXX in the injection beam, is in addition to the pulse-to-pulse modulation of +12% with respect to proton values. In particular, this implies a new staircase pulsed magnet ('Distributer') to subdivide the linac beam pulse (in time) over the vertical levels of the four Booster rings (4.2.5); lengthening of the flat tops of the existing one is more expensive. Further modifications required are: lengthening the flat tops of the pulsed septa in the injection line BI.SMV (vertical) and BI.SMH (horizontal), stack of four in the Booster ring (4.2.6), pulse-to-pulse modulation of the slope of the four slow (multiturn) injection kickers BI.KSW (4.2.7), lengthening the flat top of the ejection kickers BE.KFA14L1 (again a stack of four in the ring) and of the vertical recombination kickers BT.KFA10,40 and BT.KFA20 (4.2.8).

The lower intensity of the ion beams (three orders of magnitude below the weakest proton beams) creates problems in the RF beam control system and for all beam diagnostics. The relevant modifications are: a new digital beam control system (4.2.9), operating only on ion cycles and, in the beam diagnostics sector, five new beam current transformers in the injection line and a stack of four slow DC beam current transformers in the Booster ring (4.2.10-11) with a dynamic range extending down to ion intensities. These transformers will also allow extension of the range of emittance measurements (Beamscope) to ions. As beam positions in the beam lines cannot be measured directly at low intensity, steering has to be monitored by TV observation of scintillator screens (4.2.12). Their movements (in and out) will be synchronized with the ion cycles (pulse-to-pulse modulation) in order not to interfere with proton cycles. Video signals will be digitally processed to enhance readability.

4.2.2 Vacuum

This is the most important and costly modification; section 3.5 is devoted to it. In all calculations of loss due to charge exchange processes with the residual gas we have assumed an average total pressure of 4.5 10^{-9} Torr with a content of 80% hydrogen. As the cross-sections for H_2 are about two orders of magnitude smaller, their contribution is neglected and hence we have chosen a reference non-hydrogen pressure of 9 10^{-10} Torr to calculate the transmissions displayed in the Table above and in Figure 4.1.

4.2.3 The Main Power Converter

The Main Power Converter (commonly abbreviated MPS, S for Supply) of the PSB consists of five SCR type modules ('Groups') in series of which at present only three are used while the remaining are spares or available for test and repair. To speed up acceleration of heavy ions it is proposed to operate with four groups, which implies only minor modifications of the controls. Not considering initial transients, their maximum dI/dt (needed to shorten the acceleration time) is given by the tolerable induced voltage V_{max}=L dI/dt + I R = 900 V per group. But even to reach this maximum from zero, a limit to its derivative dV/dt has to be imposed to avoid excessive peak currents in the DC filter elements and/or pertubations of the power grid. The result is an initial parabolic increase of the magnet current, the so-called 'round-off'. Although the computed transmission of 0.74 displayed in Table A4.2.1 for the first acceleration phase appears acceptable as it corresponds to a global transmission of 0.62, one should bear in mind that this figure has been computed assuming an initial voltage rise of the MPS at 150 kV/s, more than three times the present rate of 45 kV/s. With the latter, the duration of the acceleration cycle would be 320 ms, transmission for first acceleration, 0.59, and the global transmission would drop to, 0.50. As the impact of the length of the initial round-off is more dramatic at higher gas pressures, and because of the uncertainties in the prediction of the final average nitrogen equivalent pressure, raising the dV/dt limit is an important precaution. In fact, in dedicated machine studies a rate of 150 kV/s has been achieved with modified control circuitry, and peak currents of filter capacitors have been measured; their operational limit is being checked with the manufacturer. Figure 4.2 shows the fast ion cycle and the standard proton cycle (with three power converter groups).

4.2.4 Injection and RF-capture with Increased dB/dt

Transmissions tabulated above have been calculated on the assumption of injection and RF capture on a flat bottom magnet field. Further reduction of acceleration time can be achieved if multiturn injection and capture are performed at the same time during the initial parabolic rise (one could even envisage starting the magnet cycle from a lower bottom and capturing after the round-off, in other words at a maximum dB/dt of 3.5 T/s - unfortunately not a realistic possibility). Indeed, a method of profiting from the biggest possible RF bucket for capture at non-zero dB/dt has always been applied in the PSB for the capture of protons; during adiabatic capture, i.e. for 300–500 μs, the RF frequency is programmed, so as not to accelerate the protons at all, tracking the revolution frequency of the freely spiralling beam. Capture then profits from the full 360 degree-long bucket of a non-accelerated beam.

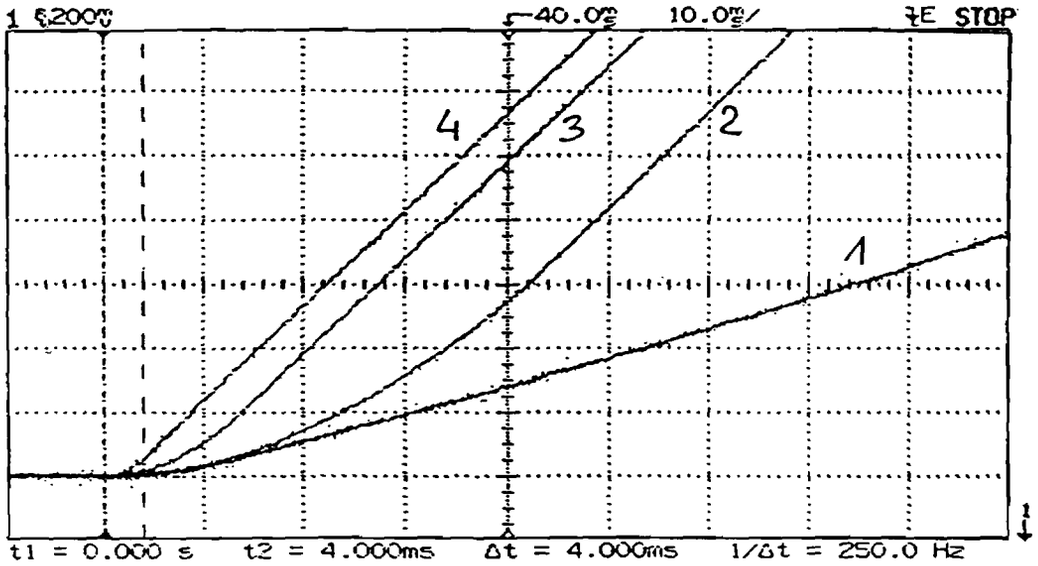

Fig. 4.2 Initial Current Rise in PSB Magnet Versus Power Converter Conditions
Three groups of the Main Power Converter with different limits to the voltage rise:
#1 Standard proton cycle for comparison
#2 Fastest possible rise with present rate limit of 45 kV/s
#3 Modified rate limiter at 125 kV/s (maximum envisagable with DC filter)
#4 Rate limit pushed to 475kV/s without DC filter (effect of bypassing it, on proton acceleration still to be tested

Machine studies [39] have been performed at dB/dt = 2.1 T/s with low-intensity proton beams to optimize voltage programs. At this slope, capture efficiencies of 75% (to be compared to 92% on a standard dB/dt of 0.4) have been achieved so far. Theoretical studies are under way [40] to understand better the dynamics of this variant of adiabatic capture, hoping to improve further these figures. The loss in capture efficiency is of the same order as the computed early loss due to interaction with the residual gas, and it is uncertain whether this method will actually yield higher transmission, because the steeper the field slope, the larger the variation in the mean orbit position during spiralling. At 3.5 T/s the beam spirals at -38 m/s, i.e. about 3.8 - 5.7 mm during injection (100 to 150 μs) and 12 to 19 mm during capture (300 to 500 μs). Both contributions summed up, the ensuing reduction of radial aperture is inadmissible, as injection efficiency would suffer.

4.2.5 Dedicated New Vertical Distributer for Ions

Trying to adapt the present high-voltage proton distributer which allows injection for about 35 μs in each ring, is considered difficult and manpower and cost intensive. It has therefore been proposed to build a new, dedicated ion beam distributer [41] aiming at a design without gas thyratron switches. In Fig. 4.3 the present and the proposed layouts of the distribution area are shown. The present separate horizontal and vertical post-deflectors BI.DHZ40 and BI.DVT40 will be replaced by one combined standard PSB 'type 1' dipole. The necessary restriction of a vacuum chamber section of 130 mm external diameter is easily tolerable.

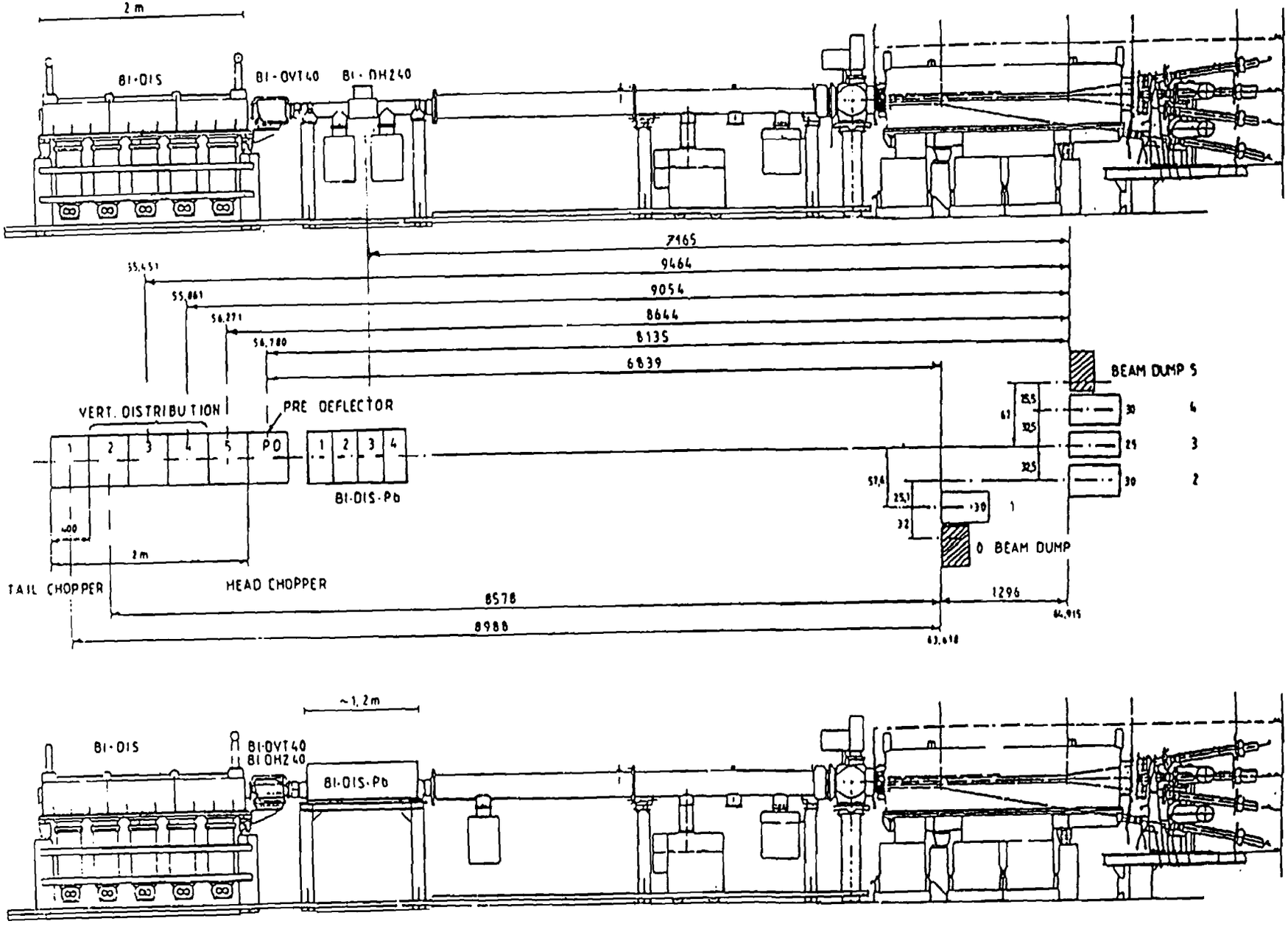

Fig. 4.3 Present (a) and Future (b) Layout of PSB Beam Distribution Area

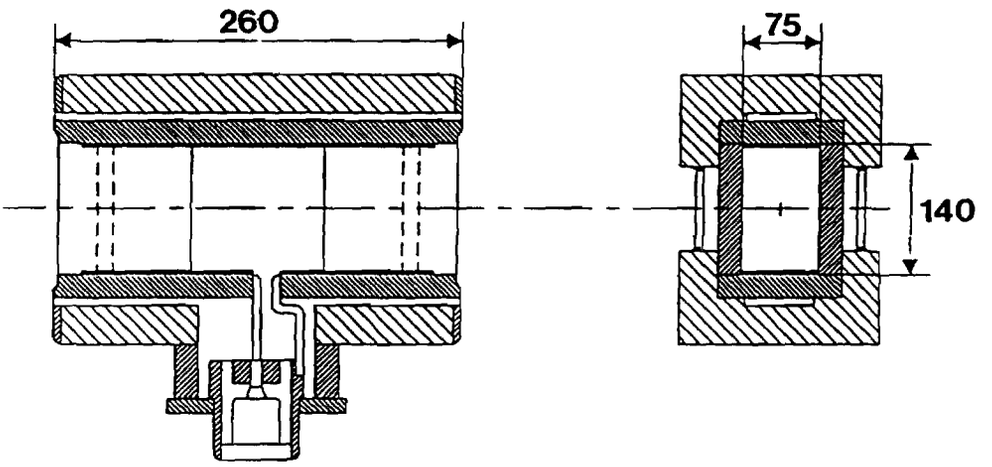

Fig. 4.4 Layout of Ion Distribution Module

More critical is the aperture of the new distributer itself: 60 x 110 mm is required for operational safety. As the proton device, the ion distributer configuration consists of a static dipole (the aforementioned post-deflector common to both particle beams) and fast-rise (5 μs) modules, one for each switching step. For clean operation (sharp beam rise) a head clipper is required; whose function can be assumed by the leading edge of the injection kicker of Ring 4. In this way a minimal configuration with only 4 modules can be envisaged. Figure 4.4 shows the schematic layout of a module.

The tentative parameters of the ion distributor can be found in Table A4.3.1 (see appendix).

4.2.6 Pulsed Septa

Tests performed on the power supplies for the septa BI1.SMV, BI2.SMV, BI4.SMV and BI.SMH have indicated that for an extension of the flat tops to >500 μs the active filters have to be modified. Interface electronics has to be replaced to allow pulse-to-pulse modulation. The choice, consistent with the on going standardisation, is:

Active Filter	Chassis of PS and EPA septa
Interface Electronics	G64 Bus, 2 cards (for active filter and ppm compensation)

4.2.7 Slow Injection Kickers

The four individual pulsers operate by the resonant discharge of a capacitor into the magnets (inductance 20 μH). Once the entire energy is stored in the latter, they are aperiodically discharged into an RC network, yielding an almost linearly decaying current pulse of about 50 μs length. Extending this decay to 150 μs requires an extra choke of 25 μH and a capacitor of 280 μF, entailing stronger deviation from linearity, but having negligible influence on the injection process. The new resonant circuit requires higher charging voltage as well as the necessary 12 % increase of the peak current. The ensuing higher voltage of 9 kV (at present 6 kV) is at the limit of the charging supply ratings. Switching between ion and proton pulses is done by an extra CX1140 thyratron. The modulation of the amplitude is done simply by trigger delay variation; different parts of the slope will be used for different species. Figure 4.5 shows the two pulse shapes for protons and ions.

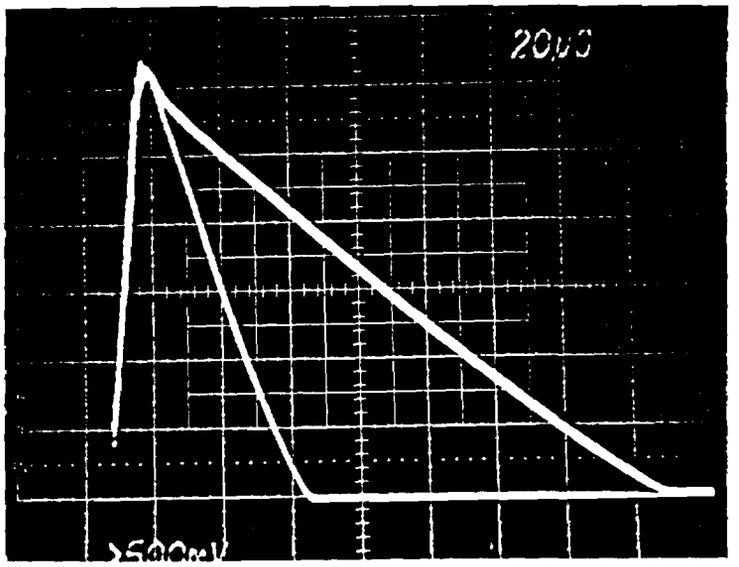

Test of modified slow injection kicker module : Short slope (50 μs) for protons, long slope (150 μs) for future ion injection

Fig. 4.5 Slow Injection Kicker - Pulse Shapes for Protons and Heavy Ions

4.2.8 Ejection and Vertical Recombination Kickers

Seven kickers are operating in the extraction and vertical recombination system of the PSB: Each ring has its own ejection kicker BE1-4.KFA. Recombination of rings by pairs into two beam levels requires the kickers BT1.KFA10 and BT4.KFA10 and finally BT.KFA20 to recombine these two levels. The pulse length is determined by the ion revolution period of 1245 ns, with the exception of BT.KFA20 which has to provide twice this unit length [42]. The pulse length being essentially determined by (twice) the electrical ('PFN') length, all kicker cables need to be replaced by longer ones, and, to benefit fully from the change, better quality (e.m. shielding, loss) ones. To these cable delays one has to add the distance between magnets and pulsers (feeders) plus an extra equal length for compatibilty with future LHC beam extraction. Each magnet array has four cables in parallel. The five different cable lengths which are to be manufactured, are designated in Table A4.3.2 with total cable lengths including a spare coming to 7500 m. More details can be found in the full cable specification [43].

As a consequence of the extended cable length, the present CX1154 switching thyratrons (rated 3000 A peak) have to be replaced by the more powerful (6000 A peak) CX 1174 type and their housings adapted.

4.2.9 New Digital Beam Control System

It has been decided to separate the beam control systems for protons and ions, in order to (i) decouple the functioning at the very different intensity levels and RF harmonics of the two species, (ii) allow open-loop acceleration of ions and (iii) build a system compatible with the future standard PS digital beam control system using identical building blocks as far as possible. The RF frequency is computed from the B-Train, a pulse train representing the main bending field clocked at 1 Gauss intervals.

Figure 4.6 shows a block diagram of the PSB ion digital beam control system. Its essential features are given in table 4.3.1 (A4.3.4).

Table 4.3.1: Essential features of the PSB ion beam-control system

Analog Part	Pure RF signals: Pick-up's, AVC, Superheterodyne, Phase discriminator at fixed IF of 10.7 MHz
Digital Part	Revolution frequency programme, derived from B-Train Control of harmonic number Type of particle control RF direct synthesis (no frequency multiplication) B-Train error correction Common 10 MHz atomic clock for all machines
Mechanical Standards	NIM standard Only front panel connectors RF Connectors: LEMO 00

4.2.10 Injection Line Beam Transformers

There are five transformers foreseen, one before the vertical distributor and one per ring, after the distributor.

Two ranges are provided, one for protons with 200 mA full scale (resolution < 1mA) and one for ions with 20 μA (resolution < 2 μA). The latter range can be increased easily if necessary. The ranges are selected automatically by the PLS control for analogue acquisition and manually for analogue observation (which can be made automatic if desired). There is digital acquisition of the average value of current during injection in the corresponding ring and total charge injected in the ring for transformers after the distributor. Similarly for the transformer before the distributor there is acquisition of the average value of current during injection in each ring and the corresponding charge.

4.2.11 New DC Beam Current Transformers

These current transformers have dynamic range (I_{min} to I_{max}) of 5 10^8 to 2 10^{13} charges/ring and a frequency range from DC to 10 kHz. There are 4 ranges with full scale 2 10^{13}, 2 10^{12}, 2 10^{11} and 2 10^{10} charges respectively with resolution 0.1% of full scale or 2 10^8 charges whichever is greater. This value expected at injection, will improve during acceleration due to the increase in velocity. The range selection is automatic for the digital acquisition and manual for the analogue observation. The circulating charge in each ring is acquired digitally at 5 critical times in the acceleration cycle and at a time which may be freely selected by the user.

4.2.12 Pulse-to-pulse Modulation of Scintillator Screen Movements

The movements of the electro-pneumatic drives of the 16 scintillator screens in the Booster injection line, in the ring and the recombination/transfer line have been analysed (positioning and retracting time, frequency of use versus expected lifetime) [44]. The results being encouraging, a complementary hardware interface (G64 standard) has been designed and added to the existing one. Software of the Video Tree has been modified accordingly to control trigger advance as a function of the supercycle configuration and the measured individual screen characteristics. Digital image processing, which has to be integrated into the architecture and hardware standards of the new PS control system will be added at a later stage.

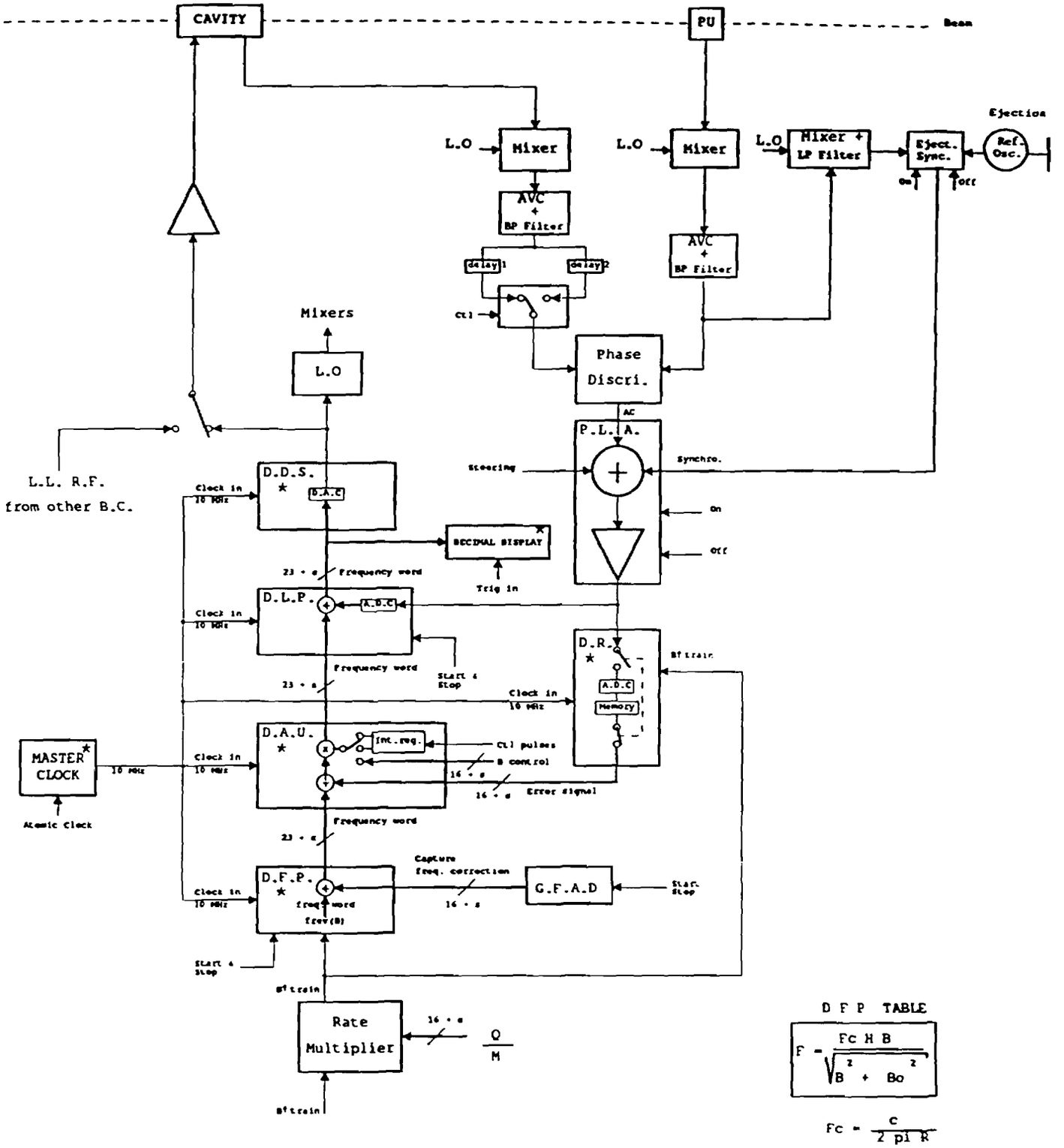

Legend: * = New module
G.F.D.A. = Analogic and Digital Function Generator
D.F.P. = Digital Freq. Program
D.A.U. = Digital Arithmetic Unit
D.L.P. = Digital Loop Processor
D.D.S. = Direct Digital Synthesizer
D.R. = Digitizing Recorder
P.L.A. = Phase Loop Amplifier

Fig. 4.6 Block Diagram of Digital Beam Control System for Ion Acceleration

5 PROTON SYNCHROTRON (PS)

5.1 GENERAL

The PS machine will accelerate Pb^{53+} ions on magnetic cycles of 1.2 s, four cycles at the beginning of a 19.2 s supercycle and in PPM (Pulse to Pulse Modulation) mode, allowing for example antiproton production, e^+ e^- acceleration, etc., on the remaining cycles.

The maximum field compatible with this 'short' repetition rate is 0.95 T corresponding to a momentum of 5.09 GeV/c/u for Pb^{53+} (or 20 GeV/c for protons).

The transport line between the PSB and the PS cannot be pulsed in PPM. As a result, the PSB to PS ion transfer has to take place at the same Bρ as the standard 1 GeV proton transfer (Bρ = 5.66 Tm). This not only sets a maximum energy of the ions in the PSB but also forbids any stripping between the PSB and the PS, consequently imposing the acceleration in the PS of ions with a charge of 53+ and requiring the final total stripping (53+ to 82+) to take place in the transfer line between the PS and the SPS. Stripping in the PS would be undesirable because of additional intensity losses.

5.2 INJECTION

Injection into the PS machine will take place on a 20 ms long flat bottom at B = 0.0807 T. The 40 (= 4 x 10) bunches from the 4 PSB rings will be captured into 20 RF buckets (i.e. 2 bunches into each bucket) making use of the standard ferrite tuned RF cavities.

Some of the main parameters of the PS injection are listed below (a more complete list appears in Table A5.2.1):

Table 5.2.1: PS injection parameters with Pb ions

Bending field	B	0.08073	T
Momentum	p	432.25	MeV/c/u
Kin. energy	T	95.4	MeV/u
	β	0.421	
Revolution freq.	f_0	200.8	KHz
RF freq.	f_{RF}	4.02	MHz
Bet. tunes	$Q_x \sim Q_y \sim$	6.25	
Bunch length	τ_b	45	ns
Long. emitt.	ε_l	$8\ 10^{-3}$	eVs/u
Hor. em. (2σ)	ε_x	26	π mm mrad
Vert. em. (2σ)	ε_y	13	π mm mrad

The revolution time will be 5 μs compared with 2.5 μs for the proton beams. This implies an important modification in the pulse length of the injection kicker. The present system makes use of four modules (i.e. four magnets and the associated power supplies) all pulsing at the same time, each magnet being terminated on its proper terminating resistance. The modification consists in installing triggerable switches (thyratrons) which can short-circuit the magnets on a PPM basis. This allows the current (or the kick) of each magnet to be doubled, in such a way that two modules in short circuit will deliver the same kick-strength as four normal modules. By pulsing the two pairs one after the other, the kicker length will be finally doubled from 2.5 to 5 μs as required.

Such a modification unfortunately will entail also a longer kicker fall time from 45 ns to 75 ns (5-95%) and a possible deterioration of the last injected bunch can be expected. The eventual replacement of the PFN cable by a longer one will permit return to the normal mode with its inherently shorter fall time.

5.3 ACCELERATION

After 20 ms spent on the injection flat bottom, that is after about 50 synchrotron periods, each pair of 8 10^{-3}eVs/u bunches will form a single bunch of ~ 66 10^{-3} eVs/u. The RF voltage will be raised to 200 kV and the acceleration will take place bringing, in about half a second, the ion beam to the extraction kinetic energy of 4.25 GeV/u.

A new digital beam control with a revolution frequency programme derived from the B-train, similar to the one used in the PSB (see section 4.3.9), will be installed.

Note that no transition crossing will be required in the PS, as $\gamma_{tr} = 6.12$.

5.4 EXTRACTION

Extraction from the PS machine will be carried out as a standard single-turn fast extraction. No modifications of the present hardware will be necessary.

Some of the main parameters at the PS extraction are listed below (a more complete list appears in table A5.2.1):

Table 5.4.1: PS extraction parameters with Pb ions

Bending field	B	0.9512	T
Momentum	p	5.09	GeV/c/u
Kin. energy	T	4.25	GeV/u
	β	0.984	
	γ	5.558	
Revolution freq.	f_0	469.3	KHz
RF freq.	f_{RF}	9.39	MHz
Bet. tunes	$Q_x \sim Q_y \sim$	6.25	
Bunch length	τ_b	9	ns
Long. emitt.	ε_l	72 10^{-3}	eVs/u
Hor. em. (2σ)	ε_x	3	π mm mrad
Vert. em. (2σ)	ε_y	2	π mm mrad

5.5 THE STRIPPER

The stripper, a 100x100 mm Cu or Ni foil, will be installed in the transfer line between the PS and SPS (TT10). A mechanism will move the foil in and out in PPM mode. To be compatible with the different beams the rise and fall time will have to be less than 0.7 s. The thickness of the foil, in the range 0.1 to 1 mm, will be optimised experimentally as soon as the beam is available and tests will have to be scheduled accordingly. Each foil replacement will require less than 3 hours, most of this time due to vacuum pumping. The lifetime of the foil is expected to be unlimited for normal operation. Two transformers, one upstream and one downstream of the foil will measure the stripping efficiency.

6.1 GENERAL FEATURES OF LEAD ION ACCELERATION IN SPS

The SPS is currently used as a 450 GeV/c proton accelerator for fixed-target physics while being at the same time the last component of the LEP injector chain, providing positron and electron beams at 20 GeV/c. It has also already been used for high energy physics with oxygen and sulphur ion beams [45].

It is intended to operate with lead ions in a similar way to that used with these lighter ions: on each cycle the SPS will accelerate four batches of lead ions simultaneously, injected consecutively from the PS at 1.2 s intervals (Fig. 6.1). This repetition time, which is standard for proton injection at 14 GeV/c into the SPS, limits the magnetic field on the flat top of the PS magnet cycle to a maximum value corresponding to a proton momentum of 20 GeV/c. In the PS the lead ions have a charge Q = 53+, but, since they are fully stripped after extraction from the PS, they have a charge $Q = Z$ = 82+ in the SPS. The SPS magnetic field at the injection of the lead ions therefore corresponds to a proton momentum of 20×53/82 = 12.93 GeV/c, well above the minimum of 10 GeV/c required from a magnetic point of view. The maximum magnetic field during the flat top of the SPS cycle depends on the desired duty factor. For operation with protons the maximum field is usually 2.025 T in the main dipoles. The latter value corresponds to a momentum of 450 GeV/c per proton or 82×450 GeV/c = 36.9 TeV/c per lead ion.

The relative velocity, β, of the lead ions at transfer is comparatively low (0.984) and its change during acceleration in the SPS exceeds the frequency swing for which the SPS travelling-wave cavities have been designed. Because of the short filling time of these cavities, their phase can be adjusted during the passage of a beam free period, or hole in the beam, if the hole is at least 2 μs long. To circumvent the limitations imposed by the frequency range of the SPS cavities, it is thus foreseen to operate the latter at a constant frequency and to adjust their phase after each revolution of the lead ions (see section 6.2).

The lead-ion program will take place at a time when the SPS is in regular service as injector for LEP and it must be assumed that the lead ions will have to be accelerated on interleaved magnetic cycles during periods of LEP operation. Therefore this operation with lead ions will be subject to the same demands for efficiency as the operation with protons and for this it is necessary to upgrade the beam monitoring in the SPS ring, the proton transfer lines, and the secondary beams (6.3). Furthermore, a number of improvements to the external target stations and the mobile beam dumps of the secondary beams are required (6.4).

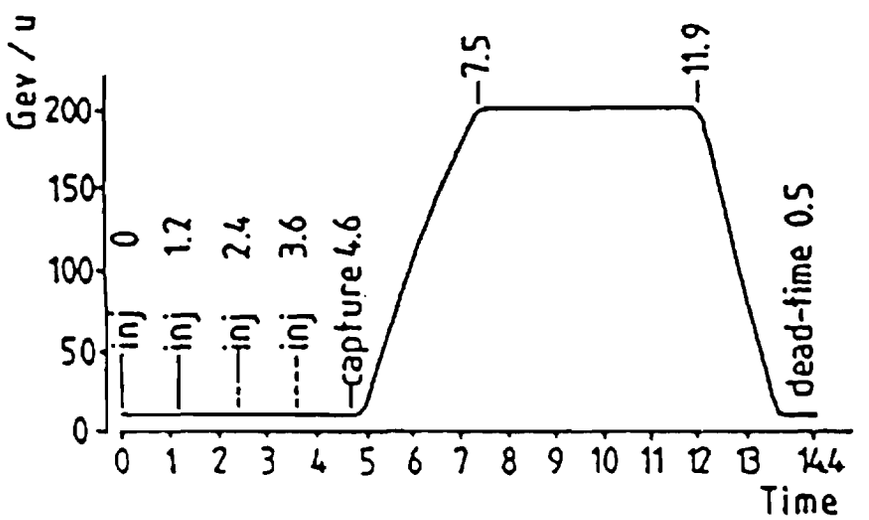

Fig. 6.1 SPS Super-Cycle for Ion Operation
Duration of cycle is 14.4s for the acceleration of $^{16}O^{8+}$ ions to 200 GeV/u, with four-batch injection and flat-top length of 4.4 s

Beams of lead ions can be extracted simultaneously from the SPS towards the West and North Experimental Areas. The lead ions are transported to the areas via the primary and secondary beam lines, after the external targets have been withdrawn. The primary beams to the West and North Areas are equipped, respectively, with one and two splitter stations, which can provide beams to two and to three different experiments. Thus the lead ions from the SPS can be shared simultaneously between six different beams. The sharing ratio between the two areas and between the experiments in the same area can be adjusted in the range 10% to 90%. Because of the long debunching time at top energy, the holes in the beam, which are necessary for acceleration at constant frequency, will persist during slow extraction.

A comparison between the main operating parameters for lead ions and for protons (fixed target physics) is shown in table 6.1.1

Table 6.1.1: Nominal SPS parameters with Pb ions

Mode of SPS operation:	with ions	with protons
	interleaved with lepton beams for LEP	
Cycles in SPS supercycle:	Pb ions e^+ e^+ e^- e^-	(Protons e^+ e^+ e^- e^-)
Nominal length of SPS supercycle:	19.2 s	(14.4 s)
Nominal length of one e-cycle:	1.2 s	(1.2 s)
Nominal length of the ion cycle:	14.4 s	(9.6 s)
Nominal ion energy:	up to 177 GeV/u	(450 GeV)
Injection energy E:	4.25 GeV/u	(14 GeV)
β at injection:	0.984	(0.998)
Horizontal tune:	26.6	(26.6)
Vertical tune:	26.6	(26.6)
Transverse normalized emittances (at 2 σ):	15 π mm mrad	(40)
Foreseen intensity:	3.93 10^8 Pb ions 3.2 10^{10} charges	(3 10^{13}p)
Debunched beam with slow extraction:		
Slow extraction duration	2.5 s at top energy	
$\Delta p/p$ at extraction	10^{-3}	

6.2 CAPTURE AND ACCELERATION

At the proposed injection energy, the revolution frequency of the lead ions with β= 0.984 is too low to allow acceleration in the usual mode, with a variable frequency proportional to the instantaneous revolution frequency of the beam, since the useful frequency range of the SPS cavities is only 0.5%. Fortunately, the latter are travelling-wave structures of which the filling time ($\simeq$ 1 μs) is much smaller than the revolution time (23 μs) of the particles. This feature opens up the possibility of a new method of acceleration in which the four PS batches occupy a total of about 10 μs while the other 13 μs are taken up by four holes, possibly of different lengths. Whenever a batch passes through the cavities, the latter are powered at a constant frequency with maximum accelerating voltage. During the passage of each hole or of one hole per revolution, the instantaneous frequency of the cavities is briefly changed so that the RF phase matches the arrival of the particles on their next passage through the cavities.

The short filling time of the SPS travelling-wave cavities also permits an independent adiabatic capture of each of the four PS batches by means of amplitude modulation of the RF voltage. After a new PS batch has been injected, the RF voltage in the cavities is raised adiabatically during the successive passages of that particular batch only. The batches already injected continue to see a constant voltage, which will hold them in their respective azimuthal positions. In this way, each batch will only be captured once, so that the overall capture losses are minimised.

To implement this new acceleration procedure, which has already been tested with protons [46], a number of electronic circuits must be built to modulate the phase and amplitude of the accelerating voltage at the revolution frequency. Some modifications to the transmitter plants are also necessary to cope with the fast 100% amplitude modulation. Furthermore, previous experience with sulphur ions has shown the necessity for a new high-sensitivity phase pick-up.

6.3 BEAM INSTRUMENTATION IN THE SPS RING AND PROTON TRANSFER LINES

The beam monitors installed in the SPS ring and in the proton transfer lines have been designed for intensities in the range of 10^{11} - 10^{13} charges. Although improvements to some monitors were made for operation with oxygen and sulphur ions, most detectors cannot be used at the expected lead-ion intensities of 10^{9} to 10^{10} charges without a drastic increase in their sensitivity.

In the SPS ring, the 216 electrostatic pick-up stations that are used for the closed-orbit measurements will be equipped with special 200 MHz preamplifiers. They are incorporated in the general multicycle facility provided by solid state switches to allow simultaneous operation with leptons. The preamplifiers are located in the auxiliary building. To achieve sufficient sensitivity it is necessary to limit the bandwidth of the receivers to match the characteristics of the incoming ion beam. This bandwidth reduction will be programmable as well.

In order to permit measurement of the low intensity lead ion beam improvements to the high sensitive beam current transformer have been implemented. Further development is on the way.

The beam monitors in the injection transfer line, where the ion pulses are as short as 2μs, can be adapted without much difficulty to the expected lead-ion intensities. However, in the extraction channels and in the extracted beam transfer lines, the spill will have a duration of several seconds with correspondingly lower instantaneous ion intensities. Moreover, the total intensity is shared among the North and West Areas and between more than one experiment in each of these areas. Therefore, the existing detectors in the extraction channels and in the transfer lines cannot be used for lead ions.

The secondary emission monitors for steering and intensity measurements of the extracted beams will be equipped with high-quality integrating amplifiers, which will be installed close to the monitors in the transfer tunnels in order to minimise the deterioration of the signals in the cables due to electrical noise and radiation-induced ionisation. These integrating amplifiers have already been designed and constructed for the oxygen operation in 1986 and can be used again. They must be mounted and demounted before and after the lead-ion runs to avoid damage during operation with high-intensity proton beams.

Beam-profile measurements are needed for setting up of the extracted beams, for emittance measurements, and for the adjustment of beam splitting. During operation with protons secondary emission grids are used for these measurements. However, at the expected lead-ion intensities, the signals from the individual strips of a grid become so low that the required sensitivity cannot be achieved, even with high-quality integrating amplifiers close to the monitor. It is therefore proposed to use, for the profile measurements, luminescent screen monitors, the screens of which will be observed by highly-sensitive silicon-intensifier target cameras. The signals from the latter will be processed by VME-based electronics to obtain the desired beam profiles. Most of the required luminescent screen monitors, though equipped with only standard Vidicon cameras, already exist and are installed in suitable positions, but additional monitors are needed in the two extraction channels and at the upstream ends of the beam transfer lines TT20 and TT60 to the North and West Areas.

The extracted lead-ion currents are of the order of 3×10^{-11} A. Therefore, highly-sensitive detectors are required for the servo control of the slow spill. Such a detector will consist of a thin scintillator placed in the beam path and observed by a photomultiplier. The output current of the latter will be compared with a reference signal and the difference between the two signals will be fed, after amplification, into the power converter of a quadrupole in the

SPS ring which controls the spill-out. With the exception of the thin scintillators for the spill control, all intercepting material of the transfer-line monitors will normally be retracted from the external beams after setting up.

6.4 BEAMS TO THE EXPERIMENTAL AREAS

On their way to the experimental areas some of the lead ions will be absorbed in the steel septa of the splitter stations, whilst all ions must pass through beam windows and air in the target stations and the mobile dump regions of the secondary beams. A first assessment has been made of the effects to be expected because of nuclear and Coulomb dissociation ($\sim Z^2$) interactions of the lead ions [47]. This study indicates that at the end of the beam lines the contamination of the lead-ion beams by lighter nuclear fragments should not be larger than that which has been observed for oxygen and sulphur ions and which has proved not to be detrimental for the experiments [48]. However, because of the larger interaction cross-sections of lead ions, compared with lighter ions, a larger fraction (about 30%) of the beam flux would be lost in traversing the target stations and the mobile dump regions. It seems prudent to reduce these losses by a substantial factor, since the beam intensity expected from the proposed lead-ion source does not have much margin compared with the requirements of the experiments, as was already the case for the sulphur ions in 1987.

Given that the high intensity area ECN3, fed by the P0 beam uses at least 80% of the total intensity, it is most important to reduce the amount of material in this beam line. The losses can be reduced to less than 10% by reducing the amount of material in the beam path to the minimum that can realistically be achieved. The air in the parts of the beam path traversing the target station and mobile beam dump must be replaced by vacuum or helium gas contained between thin aluminium windows. All existing titanium or stainless-steel beam windows and the sensing foils of the target monitors will be replaced by foils made of a high-strength aluminium alloy of minimum thickness. In principle, the best solution would be to have a continuous vacuum system during operation with lead ions. However, this is not a realistic proposition because of the design constraints imposed by the existing installations and of the need to minimise the time of intervention when changing from proton to lead-ion operation and vice versa, because of the high level of radioactivity in the target stations. Under these conditions the solution described above is considered to be the best compromise.

In proton operation the profiles of the secondary beams are measured with wire chambers placed in air between beam windows. Since these measuring stations represent too much material in the beam path, they were replaced by a continuous vacuum pipe and the beams were operated 'blindly' during the previous light-ion runs. In this context it should be mentioned that the presence of material in the beam path downstream of the momentum-analysing sections cannot be tolerated since nuclear fragments produced at such places are not removed from the beam. For the operation with lead ions a number of wire chambers at critical locations in the different beams will be replaced by pairs (horizontal and vertical) of filament scintillation counters (FISCs), which are housed inside vacuum tanks and can be move by stepping motors to measure the position and profile of the lead-ion beams. An Italian contribution (University of Padua) will provide the mechanical parts of these FISCs as well as part of their electronics. A number of FISCs are already installed and the last pair in each beam line is equipped with a set of electronics for pulse-height analysis. For lead-ions, however, a higher resolution is required to allow the composition of the beam to be verified in terms of ion species. Such measurements have proved to be extremely useful in the previous light-ion runs [46].

It should be noted that four of the six locations available for lead-ion experiments are in open, i.e. unshielded, experimental areas. They are, therefore, designed to receive beams at intensities per SPS pulse of $\leq 5\times10^8$ elementary particles, which corresponds to $\leq 5\times10^5$ lead ions. Depending on the experiments approved, extensive shielding of the beam lines and associated modifications to the layout may be necessary.

7 FUTURE IMPROVEMENTS FOR ION PHYSICS IN THE LHC

The next major project at CERN will be the Large Hadron Collider [49] to be constructed in the LEP tunnel. It is designed to enable p-p collisions at 7.7 TeV per beam at luminosities of over 10^{34} cm^{-2} s^{-1}. An additional option calls for colliding highly relativistic lead ion beams at 3.06 TeV/u per beam.

7.1 LHC ION REQUIREMENTS

The LHC ion luminosity will be limited by the luminosity lifetime which depends on the emittance growth due to intra-beam scattering and on beam losses due to nuclear effects between colliding bunches [50]. For Pb ions this sets a limit to the luminosity per bunch (one interaction point) at 3.6 10^{24} cm^{-2} s^{-1}. Another limitation is dictated by the dynamic aperture at LHC injection (177 GeV/u) which restricts both transverse normalised r.m.s. emittances to $\varepsilon^* = 1.5$ μm. The LHC limit luminosity would then be reached with 9.4 10^7 ions per bunch, that is 2.0 10^{27} cm−2 s−1 for 560 bunches; more bunches would yield even higher limit luminosities.

7.2 THE LEAD ION FACILITY AS LHC INJECTOR

A straightforward approach to fill the LHC with Pb ions is to make use of the nominal beam of the Lead Ion Facility. In this scenario, no major hardware modifications, but some delicate beam manipulations with the RF systems in the synchrotrons of the injector chain are needed. Nine PS cycles of 16 bunches each (<4 ns length) fill the SPS with 144 bunches, and four SPS cycles provide either LHC ring with 560 bunches (~135 ns spacing) within a few minutes. Based on the intensities and efficiencies quoted earlier, one would achieve 3.4 10^6 ions/bunch, and a luminosity of about 2.6 10^{24} cm^{-2} s^{-1}. The intensity per bunch, and hence the luminosity, could be doubled by halving the number of bunches in the PS (8 instead of 16). However, the bunch spacing (265 ns) does not yield an integer bunch harmonic number in the LHC; to cope with this, the experimenters would have to rephase their detectors by 15 ns every 22 μs.

These (approximate) figures clearly prove that the Lead Ion Facility as conceived at present is unable to satisfy the LHC requirements: the achievable luminosity is down by three orders of magnitude and precludes useful physics in the LHC. The number of ions per bunch must be increased by a factor of ~30 so as to make up for this, either by increasing the linac current, or by applying storage and cooling techniques, or by a combination of both [51].

7.3 POTENTIAL IMPROVEMENTS OF LINAC 3

An apparantly straight forward way to gain the factor 30 in ion intensity is to upgrade the ECR ion source current from 80 μAe to 2.4 mAe Pb^{25+} ions (corresponding to 660 μAe instead of 22 μAe at PS Booster entry). A major change in technology (superconducting solenoid, pulsed magnet extraction) together with a sustained research effort in several places should ensure continuous improvements, but probably not by a factor 30. In any case major improvements to the low energy beam transport would also be required to handle the significantly greater space charge effects.

Ion sources tend to deliver much higher intensities at lower charge states, thus another way of gaining intensity would be replacing the LEBT and MEBT by a succession of acceleration and stripping sections (as in LBL and GSI) which transform the low charge states of the source to high charge states preferred by the linac.

Another avenue currently explored at CERN and some other laboratories is a laser-driven ion source where a hot plasma is formed by focussing a pulsed high-power laser onto a solid target. Indeed, very short (~ns) heavy ion pulses at charge state 25 have already been obtained with intensities - in terms of ions per pulse - competitive with ECR sources. The short pulses would enable single-turn injection (100% efficiency) instead of the lossy betatron stacking in the PSB; however, there is concern about space charge effects in the LEBT as well as about the survival of the C stripper foil at 4.2 MeV/u exposed to the high beam intensity.

7.4 COOLING AND STACKING SCHEMES

Even adopting an optimistic view on the possible intensity improvements in Linac 3, it is unlikely that the LHC specifications in terms of beam intensity and brightness can be met in this way. Therefore several scenarios for phase-space cooling are being contemplated, keeping in mind that the SPS has to be filled fast because of intra-beam scattering at injection (4.25 GeV/u), as has the LHC due to the tight dynamic aperture at injection.

Three possible schemes have been considered [51]. Of these, the most promising involves using the LEAR, or a ring similiar to it, to stack ions by means of electron cooling at 4.2 MeV/u. It was with this concept in mind that the heavy-ion facility was designed to operate at 10 Hz. The other schemes under scrutiny but with less chances of success are (i) ion stacking using stochastic cooling in the AAC, (ii) squeezing the ions into one single bunch by stochastic cooling on a flat-top in the PS. The intensity available with the heavy-ion facility, together with a cooling ring, should enable the LHC design luminosity to be attained.

COLLECTED REFERENCES

[1] R. Billinge, E. Boltezar, D. Boussard, E. Brouzet, R. Cappi, B. de Raad, N. Doble, P. Grafström, H. Haseroth (Ed.), C.E. Hill, K.H. Kissler, J. Knott, T. Linnecar, F. Nitsch, A. Poncet, U. Raich, N. Rasmussen, H. Schönauer, T.R. Sherwood, N. Siegel, U. Tallgren, P. Têtu, D. Warner and M. Weiss, 'Concept for a Lead-Ion Accelerating Facility at CERN', CERN 90–01, Feb. 1990.

[2] T. Sluyters, 'A Theoretical and Experimental Comparison of Proton and Deuteron Acceleration in the CERN Linear Accelerator', CERN 64–22 (1964).

[3] P. Asboe-Hansen, O. Barbalat, D. Boussard, M. Bouthéon, J. Gareyte, H. Haseroth, J. Jamsek, S. Myers, 'Acceleration and Stacking of Deuterons in the CERN PS and ISR', Proc. 7th US Particle Accel. Conf., Chicago, IEEE Trans. Nucl. Sci. NS-24 (1977) 1557.

[4] M. Bouthéon, R. Cappi, H. Haseroth, C.E. Hill, J.P. Koutchouk, 'Acceleration and Stacking of α-particles in the CERN Linac, PS and ISR', Proc. 9th US Particle Accel. Conf., Washington, IEEE Trans. Nucl. Sci. NS-28 (1981) p. 2049.

[5] K.H. Schindl, 'Light Ions Via the PS Booster', PS/BR/Note 81–10 (1981).

[6] H. Haseroth, 'Light Ions at CERN', Proceedings of the Bielefeld Workshop on Quark Matter Formation and Heavy Ion Collisions, May 1982, Eds. M. Jacob and H. Satz (1982) p. 557.

[7] R. Stock (Spokesman for the GSI-LBL Collaboration), 'Study of Particle Production and Target Fragmentation in Central ^{20}Ne on Pb Reactions, at 12 GeV/u Energy of the PS External Beam', Letter of Intent, CERN/PSCC/80–129, 1980.

[8] N. Angert, J. Klabunde, B. Langenbeck, K. Leible, P. Spädtke, J. Struckmeier, B.H. Wolf, S. Abbott, D. Brodzik, R. Gough, D. Howard, H. Lancaster, J. Staples, H. Haseroth, C. Hill, P. Têtu, M. Weiss, R. Geller, 'A Heavy Ion Injector for CERN Linac 1', Proc. of the 1984 Linear Accelerator Conf., Seeheim (Germany), Ed. N. Angert, report GSI-84-11, GSI-Darmstadt, 1984, p. 374.

[9] B.H. Wolf, K. Leible, P. Spädtke, J. Klabunde, B. Langenbeck, N. Angert, R.A. Gough, J. Staples, R. Caylor, D. Howard, R. MacGill, J. Tanabe, H. Haseroth, C. Hill, P. Têtu, M. Weiss, R. Geller, 'Heavy Ion Injector for the CERN Linac 1', NIM A258 (1987) 1.

[10] H. Haseroth, C. Hill, P. Têtu, M. Weiss, B.H. Wolf, K. Leible, P. Spädtke, J. Klabunde, B. Langenbeck, N. Angert, R.A. Gough, J. Staples, R. Caylor, D. Howard, R. MacGill, J. Tanabe, 'Ion Acceleration in the CERN Linac 1', 1986 Linear Accelerator Conf., Stanford, California, USA, SLAC–303 (1986) p. 355.

[11] B.H. Wolf, K. Leible, P. Spädtke, N. Angert, J. Klabunde, B. Langenbeck, R.A. Gough, J. Staples, R. Caylor, D. Howard, R. MacGill, J. Tanabe, 'Performance of the Oxygen Injector for the CERN Linac 1', Report GSI-86-2, 1986.

[12] N. Angert, E. Brouzet, R. Garoby, S. Hancock, H. Haseroth, C.E. Hill, K. Schindl, P. Têtu, 'Accelerating and Separating Mixed Beams of Ions with Similar Charge to Mass Ratio in the CERN PS Complex', Proc. EPAC, Rome, 1988, p. 1367.

[13] H. Haseroth, A. Lombardi, M. Weiss, 'Feasibility Study Concerning a Possible Layout for a Lead-Ion Injection for the CERN Accelerator Complex', Proc. 1987, IEEE Part. Acc. Conf., Washington, IEEE Catalogue No. 87CH2387-9, p. 295.

[14] P. Lapostolle, 'New Heavy Ion Accelerators', IEEE Trans. Nucl. Sci. NS-30, No. 4, August (1983) p. 1957, and references quoted therein.

[15] B. Franzke, 'Vacuum Requirements for Heavy Ion Synchrotrons', IEEE Trans. Nucl. Sci. NS-28 (1981) 2116.

[16] H. Gould and B. Feinberg (LBL), private communication, 1988.

[17] W.G. Graham, K.H. Berkner, R.V. Pyle, A.S. Schlachter, J.W. Stearns, J.A. Tanis, 'Charge-Transfer Cross-Sections for multiply Charged Ions Colliding with Gaseons Targets at Energies from 310 keV/u to 8.5 MeV/u', Phys. Rev. A30 (1984) 722.

[18] Minutes of the 5th Lead Linac Meeting, CERN Int. Rept. PS/DI/DS/Min 88-5 (1988), Figs. 1 and 2.

[19] R. Geller, B. Jacquet, 'Mini Mafios, Source d'Ions Pulsée Fournissant des Faisceaux d'Ions Complement Epluchés', Nucl. Instr. and Meth., Vol. 202 (1982) p. 399.

[20] B. Jacquot, R.Geller, 'Caprice 10 GHz-New $2\omega_{ce}$ Radial B Field', Int. Conf. on ECR Ion Sources and Their Applications, MSU, Nov. 1987, NSCL Report MS UCP-47, Dec 1987, p. 254.

[21] P. Sortais, P. Attal, M. Bisch, M.P. Bourgarel, R. Lehérissier, J.Y. Pacquet; 'ECRIS Development at GANIL', Int. Conf. Ion Sources, Berkeley, 1989, Ed. I.G. Brown, Rev. Sci. Instr. 61, No. 1, Part. II (1990) p. 288.

[22] M.P. Bourgarel, P. Sortais, P. Attal, M. Bisch, P. Lehérissier, J.Y. Pacquet, J.R. Rataud, G. Schmiechen, 'First Results of the 14.5 GHz GANIL ECR Ion Source with the CW and the Pulsed Operation Mode', 2nd EPAC, Nice, Vol. 1 (1990) p. 645.

[23] M.P. Bourgarel, 'Space Charge Effects and Total Emittance Measurements of the Afterglow Beam on the Test Bench', Private Communication to C. Hill on 20 July 1992.

[24] N. Angert, L. Dahl, J. Glatz, J. Klabunde, M. Müller, U. Ratzinger, B. Wolf, H. Deitinghof, J. Friedrich, H. Klein, A. Schempp, 'A New 1.4 MeV/u Injector Linac for UNILAC', Proc. 1990 Linear Acc. Conf., p. 749.

[25] E.D. Courant and H.S. Snyder, 'Theory of the Alternating-Gradient Synchrotron', Annals of Physics, Vol. 3, (1958) p. 1-48 see particularly equations 4.8 and 3.22.

[26] K.R. Crandall, 'TRACE-3D Documentation', LA-UR-90-4146, (1987).

[27] I.M. Kapchinskij, V.A. Tepliakov, 'Linear Ion Accelerator with Spatially Homogeneous Strong Focusing', Prib. Tekh. Eksp. 2 (1970) 19.

[28] S. Yamada, 'Buncher Section Optimization of Heavy Ion RFQ Linacs', Proc. 1981 Linear Acc. Conf., Santa Fe, LA-9234-C (1982) p. 316.

[29] G. Amendola, A. Pisent, J. Quesada, M. Weiss, 'Beam Dynamics Studies for the CERN Lead-Ion RFQ', Proc. 1992 European Particle Acc. Conf., Berlin, March 1992, p. 973.

[30] K.R. Crandall, 'Proposal for a New RMS for RFQ Linacs', LANL Internal Report, January 1983.

[31] I.M. Kapchinskij, 'Choice of the Method of Adiabatic Bunching in the Linear Accelerator with Spatially Uniform Quadrupolar Focusing', ITEP 64-90, Moscow, 1990 (in Russian).

[32] A. Schempp, H. Deitinghoff, M. Ferch, P. Junior, H. Klein, 'Four-Rod-l/2-RFQ for Light Ion Acceleration', Nucl. Instr. and Meth. Phys. Res. B10/11 (1985) 831.

[33] A. Fabris, A. Massarotti, M. Vretenar, 'A Model of Four-Rods RFQ', Seminar on New Techniques for Future Accelerators Erice, 1986, (New York, Plenum 1986) 265.

[34] A. Lombardi, G. Parisi, M. Vretenar, 'Comparison study of RFQ Structures for the Lead Ion Linac at CERN', Proc. 1992 European Particle Acc. Conf., Berlin, March 1992, p. 557.

[35] U. Ratzinger, 'The IH-Structure and its Capability to Accelerate High Current Beams', Conf. Record of the 1991 IEEE PAC, San Francisco, 91CH3038-7, p. 567.

[36] Y. Bylinsky, H. Kugler, P. Lapostolle, U. Ratzinger, E. Tanke, S. Valero, D. Warner, 'Dynamics and Tolerances for the CERN Interdigital H Linac', Proc. 1992 Linear Accelerator Conf., AECL-10728, Vol. 1, p. 220.

[37] K.R. Crandall and T.P. Wangler. 'PARMTEQ-A Beam-Dynamics Code for the RFQ Linear Accelerator', Linear Accelerator and Beam Optics Codes, AIP Conference Proceedings, Vol. 177 (1988) 22.

[38] A. Sullivan, 'Radiation Expected from the Lead Linac to Be Constructed at CERN', TIS-RP/IR/92–15, PS/HI Note 92–06.

[39] H. Schönauer, N. Rasmussen, 'PSB ME-News: Injection and Capture at Large Bdot', PS/HI/ME 92–01 and 92–02.

[40] N. Rasmussen, 'Influence of Voltage Function on RF Trapping', PS/HI/Note 92–09.

[41] F. Völker, 'Vertical Pb-Ion Beam Distribution in the Injection Line of the PS-Booster', PS/PO Note 92–05;

[42] K.D. Metzmacher, 'PS/RF Kickers: Present and Future Projects', PS/RF/Note 92–11 Rev.

[43] K.D. Metzmacher, Technical Specification IT-2085/PS, PS/RF/Spec. 92–3 (Rev.1).

[44] E. Sigaud, 'Système MTV du PSB: Projet Séquentiel en PPM', PS/HI Note 91–04.

[45] E. Brouzet, W.C. Middelkoop, 'Performance of the PS and SPS Accelerator Complex with Oxygen Ions' Proc. 1987, IEEE Part. Acc. Conf., Washington, USA, IEE Catalogue No. 87CH2387–9, p. 50.

[46] D Boussard, J.M. Brennan, T.P.R. Linnekar, 'Fixed Frequency Acceleration in the SPS', CERN SPS/89–49 (1989).

[47] P. Grafström, 'Note on the Possibility to Transport Lead Ions in the SPS Secondary Beams', Report to the SPSC by the Heavy Ion Discussion Group, CERN/SPSC 87–52, SPSC/T27 (1987), p. 43.

[48] H.W. Atherton, N. Doble, G.P. Ferri, M. Glaser, P. Grafström, J.B. Jeanneret, F. Lemeilleur and M. Reinharz, 'Contamination of Nuclear Fragments in a 200 GeV per Nucleon Oxygen Ion Beam at CERN', CERN/SPS/87–11 (EBS) and Proc. Washington Conf. in Ref. 12, Vol. 3, p. 1752.

[49] 'Design Study of the Large Hadron Collider (LHC)', CERN 91–03, May 1991.

[50] D. Brandt. E. Brouzet and J. Gareyte, 'Heavy Ions in the SPS – LHC Complex', SL/Note (92–47 (AP), (LHC Note 208).

[51] D. Brandt, E. Brouzet, R. Cappi, J. Gareyte, R. Garoby, H. Haseroth, P. Lefèvre, S. Maury, D. Möhl, F. Pedersen, K. Schindl, T.R. Sherwood, L. Thorndahl, D. Warner, 'High Intensity Options for the CERN Heavy Ion Programme', Proc. European Part. Acc. Conf., Nice, (1990), Vol. 1, p. 49, and CERN/PS 90–20 (DI). An extended and updated version of this report is in preparation.

APPENDIX: DETAILED PARAMETER LISTS

INTRODUCTION

Table A1.3.1: Nominal intensities and efficiencies

Accelerator (or element)	Output β	Output T	Effic. η	Pb ions per PS cycle[1]	Pb ions per SPS cycle[1]	Comments
ECR Source	0.0023	2.5 keV/u		7.13 10^9	2.85 10^{10}	80μAe, 400μs Pb^{28+}
RFQ	0.023	250 keV/u	0.9			
IH Linac	0.094	4.2 MeV/u	0.9	5.78 10^9	2.31 10^{10}	65μAe Pb^{28+}
Stripper foil			0.16	9.25 10^8	3.70 10^9	Pb^{28+} => Pb^{53+} (20μAe) stripping loss
PSB injection			0.4			Multiturn injection, 4 * 18 turns
Acceler. (h=10)	0.421	95.4 MeV/u	0.6	2.22 10^8	8.88 10^8	RF capture, vacuum
PS injection			0.95			Including PSB-PS transfer (2 bunches => 1 bucket)
Acceler.(h=20)	0.984	4.25 GeV/u	0.7	1.48 10^8	5.91 10^8	Vacuum
Stripping			1.0			Pb^{53+}=> Pb^{82+}
SPS injection			0.95			Including PS-SPS transfer
Acceleration	~1	177 GeV/u	0.7		3.93 10^8	

[1]Source, RFQ, IH Linac, PSB: all one cycle per PS cycle. Four PS cycles per SPS cycle.

Overall ion acceleration efficiency between ion source and SPS extraction: $\eta = 0.014$

ECR ION SOURCE

Table: A.2.2.1: Main source parameters

Magnetic field

Peak Axial Field	1.1	T
Solenoid Magnet Power	60	kW
Maximum Solenoid Current	1250	A
Typical Solenoid Current	1100	A
Mirror Ratio	2.2	
Mirror Ratio Range	90	mm
Length of 2nd Stage Mirror	180	mm
Sextupole Magnet Material	Fe-Nd-B	
Coercive Field	1400	kA/m
Pole Tip Field	1.2	T

RF system

Frequency	14.5	GHz
RF Power Input	2	kW

Dimensions

Solenoid Inner Diameter	180	mm
Solenoid Outer Diameter	330	mm
Sextupole Inner Diameter	200	mm
Sextupole Length	200	mm
Plasma Chamber Bore Diameter	66	mm
Anode Aperture	16	mm
Extraction Aperture	13	mm
Total Length	600	mm
Total Outer Diameter	400	cm
Total Weight	≈500	kg

Coils

Number of Coils	2	
Number of Pancakes/Coil	5	
Nominal Resistance/Coil	27	mΩ
Nominal Voltage/Coil	30	V
Nominal Current	1100	A
Maximum Current	1250	A
Inductance/Coil	≈3	mH
Time Constant	≈70	ms
Parallel Cooling Channels/Coil	5	
Water Flow	35	l/min
Input Temperature	20	°C
Temperature Rise (approx.)	20	°C
Water Pressure Input	15	bar
Output	2	bar

Power supplies

Number of Power Supplies	2	
Nominal Current	1100	A
Maximum Current	1300	A
Maximum Voltage	35	V
Security Current Level	850	A
Voltage Stability (drift + ripple)	<50	mV
Current Stability at 1100A	$\pm 10^{-4}$	

RF transmitter

Frequency (fixed)	14.5	GHz
Power Modulation	External	
Output Power Range	0-2.2	kW
Power Slew Rate	<1	ms
Power Stability	$\pm 10^{-3}$	
Waveguide	WR62	
Duty Cycle	0-100	%
Repetition Rate	<1	kHz
Rise/Fall time	1	µs

Table A2.3.1: Bending magnets

Type	'H'
Bending angle	67.5°
Bending radius	0.4 m
Focussing angle in	25°
Focussing angle out	25°
B max	0.17 T
Gap height	90 mm
Pole width	480 mm
Radial homogeneity	$2 \times 10\text{–}4$ in ± 190 mm

Table A2.3.2: Quadrupoles

Pole length	150 mm
Effective length	204 mm
Aperture	120 mm
Max gradient	2.7 T/m

Table A2.3.3: Solenoids

Max axial field	0.625 T
Max integral $[\int B^2\, dz]$	0.092 T^2m
Effective length	0.300 m
Overall length	0.320 m
Aperture	120 mm

Table A2.3.4: Nominal fields and gradients of LEBT magnets

BHZ01	+0.15 T
BHZ02	+0.15 T
QDN01	–0.76 T/m
QFN03	+1.50 T/m
QDN04	–1.16 T/m
QFN05	+0.30 T/m
SOL01	+0.41 T
SOL02	+0.43 T

RADIO FREQUENCY QUADRUPOLE

Table A2.4.1: Specifications

Particles	Pb^{25+}
Input energy	2.5 keV/u
Ouput energy	250 keV/u
RF frequency	101.28 MHz
Max. surface field	< 23 MV/m
Acceptance	≥ 0.8π mm mrad
Longitudinal emittance	< 1.08π keV ns/u (40π deg. keV/u)*
Transmission	> 90%
Output energy spread	< ±2%
Output phase spread	< ± 12°
Repetition rate	10 Hz
Duty cycle	0.4%

* 'Practical' units used in computer program (deg. at 101.28 MHz)

Table A2.4.2: Dynamics parameters

Vane length	2500 mm
Vane voltage	70 kV
Average aperture radius r_0	4.5 mm
Transverse vane tip radius ρ	4.28 mm
Transmission	93%
Transverse emittance increase	–
Longitudinal emittance (5×rms)	0.94π keV ns/u*

* Equivalent to 34 π deg keV/u from computer program.

Table A2.4.3: Dimensions

Overall tank length	2660 mm
Int. tank dimensions	590 × 440 mm
Ext. tank dimensions	610 × 480 mm
Number of supports	14
Cell length	179 mm

Table A2.5.1: Beam parameters in LEBT, RFQ and MEBT

	LEBT (ITL)	RFQ (IAQ)	MEBT (ITM)		
Length	7.05	2.50	1.60		m
Acceptance	0.46	0.80	1.00		mm mrad
Energy	2.5	2.5	250	250	keV/u
$\varepsilon_{x,y}/\pi$	0.35	0.50	0.50	0.50	mm mrad
α_x	0.0	0.8	-1.5	1.7	-
α_y	0.0	0.8	1.2	0.5	-
β_x	0.025	0.024	0.23	0.96	m
β_y	0.025	0.024	0.24	0.55	m
ε_l/π	-	-	0.94	1.08	keV ns/u
ε_l/π	-	-	35	40	°keV/u
β_l	-	-	3.3	4.77	°/(keV/u)
$\Delta\varphi$	-	-	10	13.8	°
α_l	-	-	0	-1.28	-

Table A2.5.2: Parameters of the MEBT quadrupoles and steering dipoles

Name	Pole length (mm)	Eff. length (mm)	Aperture (mm)	Max grad. (T/m)	Nom grad. (T/m)
QFN01	135	150	40	30	+26
QDN02	135	150	40	30	-24
QFN03	105	120	32	37	+28
QDN04	105	120	32	37	-21
DHZ01	*	*	*	-	-
DVT01	*	*	*	-	-
DHZ02	*	*	*	-	-
DVT02	*	*	*	-	-

*Steering dipole parameters not yet determined

INTERDIGITAL-H LINAC

Table A.2.6.1: Parameters of the IH Linac

Design ion	$^{208}Pb^{25+}$
Energy range	250 keV/u - 4.2 MeV/u
Eff. voltage gain (MV)	32.9
Total length (mm)	8129
No. of 0° synchr. particle sections	5
No. of cavities	3
No. of quadrupole triplets	4
No. of segmented capacitive pick-up probes	2
No. of xy steering units	2
No. of accelerating gaps	99
Inner drift tube diameter (mm)	18 (section 1) 20 (section 2) 22 (sections 3, 4, 5)

TANK 1 (IA1)

RF frequency (MHz)	101.28
Length between end flanges (mm)	3567
No. of synchr. part. sections	3
Eff. shunt impedance (MΩ/m)	270
RF power (kW)	205

Section 1

No. of gaps	13
Synchr. particle phase (°)	0
Eff. voltage gain (MV)	3.64

Quadrupole Triplet 1 (QFN01, QDN02 and QFN03S)

Length of the housing (mm)	429
Eff. pole length (mm)	92/162/92
Field gradients (T/m)	62.5/56.5/62.5

Section 2

No. of gaps	14
Synchr. particle phase	3x -30°, 11 x 0°
Eff. voltage gain(MV)	5.21

Quadrupole Triplet 2 (QDN04, QFN05 and QDN06S)

Length of the housing (mm)	437
Eff. pole length (mm)	92/162/92
Field gradients (T/m)	66.5/65/66.5

Section 3

No. of gaps	14
Synchr. particle phase	4 x -30°, 10 x 0°
Eff. voltage gain (MV)	4.65

Intertank Quadrupole Triplet 1 (QFN07, QDN08 and QFN09)

Length between flanges (mm)	484
Eff. pole length (mm)	92/162/92
Field gradients (T/m)	68.5/68.5/68.5
Steering dipole windings on QDN08	IA1.DHS, IA1.DVS

Table A.2.6.1 (continued)

TANK 2 (IA2)

RF frequency (MHz)	202.56
Length between end flanges (mm)	1549
No. of gaps	28
Synchr. particle phase	5 x -30°, 23 x 0°
Eff. voltage gain (MV)	9.88
Eff. shunt impedance (MΩ/m)	265
RF power (kW)	250

Intertank Quadrupole Triplet 2 (QFN01, QDN02 and QFN03)

Length between flanges (mm)	510
Eff. pole lengths (mm)	99/184/99
Field gradients (T/m)	69/67/69
Steering dipole windings on QDN02	IA2.DHS, IA2.DVS

TANK 3 (IA3)

RF frequency(MHz)	202.56
Length between end flanges (mm)	2019
Eff. no. of gaps	30
Synchr. particle phase	7 x -30°, 23 x 0°
Eff. voltage gain (MV)	9.79
Eff. shunt impedance (MΩ/m)	200
RF power (kW)	285

BEAM TRANSPORT AND MONITORING IN THE FILTER REGION

Table A2.8.1: Parameters for ITF line

Beam Parameters at Entrance of the ITF Line

	Before stripper	After stripper
Type of particle	Pb^{28+}	Pb^{53+}
Energy (MeV/u)	4.20	<4.20
Current (μAe)	65	20

Transverse phase planes

	Horizontal	Vertical
Emittance (Π mm mrad)	8.5	8.4
Normalised emit.(Π mm mrad)	0.81	0.80
Alpha	–2.3	–2.6
Beta (mm/mrad)	4.3	4.6

Longitudinal phase plane

	Before stripper	After stripper	After Debuncher
Emittance (π keV ns/u)	1.82	>1.82	>1.82
dW(MeV); dW/W (%)	23;0.5	>23;>0. 5	<2.1;<0.05
dt(ns); dϕ(deg.)	0.08;6.0 (at 200 MHz)	0.1;7.2 (at 200 MHz)	1.07;39 (at 100 MHz)

The length of beam pulse will be 400 μs (max. 600 μs) with a repetition time 1.2s.

Bending magnets

Name	Magnetic Length (m)	Deflection Angle (mrad)	Vertical Aperture (mm)	B Nominal (T)	Current (A)	Angle (mrad) Entrance	Exit
BHZ11	1.2	500	70	1.25	710	0	7
BHZ12	0.6	500	70	1.02	780	7	7
BHZ13	0.6	500	70	1.02	780	7	7
BHZ14	0.6	500	70	1.02	780	0	0

Quadrupole triplet at IA3 output

Name	Magnetic Length (mm)	Aperture (mm)	Gradient (T/m)	Q Spacing (mm)
QFN01	135	35	40	32
QDN02	270	35	40	32
QFN03	135	35	40	32

Matching quadrupoles

Name	Magnetic Length (mm)	Aperture (mm)	Gradient (T/m)
QFN04*			
QDN05	150	70.5	11
QFN06			

*These three laminated quadrupoles are Linac 2 Type 9 (pulsed)

Steering magnets

Name	Length (mm)	Aperture (mm)	Max Deflection (mrad)
DHV01;02;03;04*	250	100	3

*These small laminated steering dipoles have a double winding allowing slight trajectory corrections in the horizontal and vertical planes.

Debuncher parameters

Name	Frequency MHz	Aperture Diameter mm	δW/W (%) entry	exit
CDB01	101.28	60	0.5	0.05 to 0.25

SEMgrids and SEMfils parameters

Name	Type	Steps (mm)	No of Channels	Sensitivity uA(beam)
MSGHV01	SEMgrids	2.0	16	<0.1
MSGHV02	SEMfils	2.5	24	<1.0
MSGHV03	SEMfils(H)	<2.5	24	<1.0
	SEMgrids(V)	3.5	16	<0.1
MSGHV04	SEMgrids	3.5	16	<0.1
MSGHV05	SEMgrids	3.5	16	<0.1
MSGHV10	SEMfils(H)	1.0 to 2.5	24	<1.0
	SEMgrids(V)	3.5	16	<0.1

Table A2.9.1: Beam characteristics throughout LINAC 3

Beam characteristics for a pulse-length of 400 μsec at 2 Hz repetition rate	position 1	2	3	4	5	6	7	8	9	10	11	12
	ECR = LEBT out in	LEBT = RFQ out in	RFQ = MEBT out in	BUNCHER in	BUNCHER out	MEBT out	IH in	IH = ITF out in	STRIPPER in	STRIPPER out	BUNCHER in	BUNCHER out
Particle	208 Pb 25+									208 Pb 53+		
Energy [MeV/u]	.0025		.25					4.2				
Relativistic beta	2.31 E-3		2.31 E-2					9.43 E-2				
Pulse current [μAe]	80		72					65		20		
Accelerating frequency [MHz]		101.28	101.28	101.28	101.28		101.28	202.56			101.28	101.28
Horizontal acceptance /π [mm mrad]	200	350	45	45			44					
Horizontal emittance /π [mm mrad]	120	150	17.3	17.3	17.3	17.3	32	8.5	8.5	10	10	10
Normalized hor. emitt. /π [mm mrad]	.28	.35	.40	.40	.40	.40	.74	.81	.81	.95	.95	.95
Horizontal alpha	0	.8	- 1.37	- 2.09	- 3.84	1.70	1.69	- 2.29	0	0	.46	
Horizontal beta [mm/mrad]	.025	.024	.225	.777	1.337	.960	.94	4.26	1.02	.87	15.0	
Vertical acceptance /π [mm mrad]	200	350	45	45			44					
Vertical emittance /π [mm mrad]	120	150	17.3	17.3	17.3	17.3	32	8.4	8.43	10	10	10
Normalized vert. emitt. /π [mm mrad]	.28	.35	.40	.40	.40	.40	.74	.80	.80	.95	.95	.95
Vertical alpha	0	.8	1.75	4.17	2.26	.510	.47	- 2.64	0	0	.151	
Vertical beta [mm/mrad]	.025	.024	.256	1.757	1.081	.550	.55	4.55	1.03	.88	3.65	
Longitudinal accept. /π [deg MeV/u]							.105					
Longitudinal emittance /π [deg MeV/u]			.028	.028	.032	.032	.053	.135	.135	> .135	> .068	> .068
Longitudinal emittance /π [keV ns /u]			.76	.76	.86	.86	1.43	1.82	1.82	> 1.82	> 1.82	>1.82
Energy spread [MeV/u]			.0028	.0028	.0042	.0042	.0054	.0224	.0224	> .0224	> .0224	< .0021
Phase spread [deg]			10	32	33	12.4	15.9	6.2	17		39	> 39
Tilt [deg]			0	- 30	32	9.8	12.6	- 1.2	- 16		- 39	0

In this table the horizontal plane = x - plane
Longitudinal emittances and phase spreads are given w.r.t. the frequency of the (in some cases preceding) accelerating device
Longitudinal emittances are also given in MKS units
Tilt = phase spread for the maximum of E - Emean

Table A3.3.1: RF amplifiers

	BUNCHERS (ITM.CRF & ITF.CRF)	RFQ & IH1 (IAQ & IA1)	IH2 & IH3 (IA2 & IA3)
Centre frequency (MHz)	101.28	101.28	202.56
Bandwidth (1 dB) (MHz)	2.0	2.0	4.0
Pulse power (kW)	2.5	350	400
Pulse duration (ms)	1.0	1.0	1.0
Rise-time from zero to flat-top (with rectangular input pulse) (ms)	0.1	0.1	0.1
Pulse repetition frequency (Hz)	10	10	2
Max. average output power W	25	3500	800
Peak input power (W)	1	1	1
Amplification (dB)	34	–	–
Max. harmonic level matched load (dBm) (dBc)	< 30 <–30	– <–30	– <–30
Max. output at any non-harmonic freq. (all power levels/matched load (dBc))	<–60	<–60	<–60
Input connector	N female	N female	N female
Output connector	N female	42/98 mm GSI	42/98 mm GSI
Input impedance (Ω)	50	50	50
VSWR	1.2	1.2	1.2
Output impedance (Ω)	50	50	50
Output VSWR	2.0	2.0	2.0
Pre-driver (W)	–	600 (solid state)	1500 (tetrode)
Driver (air-cooled tetrode) (kW)	–	20	25
Final stage	Solid state	water-cooled tetrode	water-cooled triode
Power Output	2.5	350	400
Linearity of amplification between 10% & 90% output power (dB)	1.5	3	3
Mains Supply (V)	230	3x398, +6/-10%	3x398, +6/-10%
Cooling		Force Air-cooling	
Environmental temperature	+10 to +40°C	+10 to +40°C	+10 to +40°C
Variation of power, pulses asynch to mains power pulses		10%	10%

Table A3.4.1: Vacuum components

Getter Ion pump of 230 l/s for larger volumes	9
Getter ion pump of 60 l/s for small diameter beam pipes	7
Roughing station with turbo molecular pump and dry N2 inlet	5
Roughing stations on source and air-lock	2
Turbomolecular pumps with magnetic bearings on source	2
Sector valves between 60 and 160 mm	5
Pirani Penning vacuum gauge pair, also for controls interlocks	10
Penning gauge for specific element surveillance	5
Pressure read-out equipment	7

Table A4.2.1: PSB parameters relevant for acceleration of Pb^{53+} and protons

Parameter	Pb^{53+} Ions	Protons	Unit	Comments
Charge State	53	1		
Atomic Mass	207.948	1.007	u	53 e^- masses subtracted from Pb atomic mass
Injection:				
Kinetic Energy	4.2	49.6	MeV/u	i.e. 50 MeV protons
$\beta = v/c$	0.0946	0.314		
$(B\rho)$	1.159	1.0353	T m	
Bending Field B	0.141	0.1255	T	
Main P.C.: Initial dV/dt	150	45	V/ms	
Revolution Period	5.536	1.668	μs	
Number of Turns Injected	< 25	< 18	/Ring	
Injection Efficiency	0.4	0.55		
Length of Linac Pulse / Ring	< 138	< 30	μs	
RF Frequency	3.61	3.0	MHz	
1st Acceleration:				
Harmonic Number	20	5		
Max. dB/dt	3.4	2	T/s	
Max. Stable Phase	21	11	deg	
Duration	59.3	390	ms	
Transmission due to Charge Exchange Loss (1st accel.)	0.74	1		Eff. non-hydrogen pressure 9 10^{-10} Torr
Intermediate Flat Top				
Kinetic Energy	17.1		MeV/u	
Bending Field B	0.285		T	
RF Harmonic Number	20/10			Harmonic nr. change
RF Frequency	7.23/3.61		MHz	by de- & rebunching
Duration	20		ms	
Transmission due to Charge Exchange Loss (Int. flat top)	0.97			Eff. non-hydrogen pressure 9 10^{-10} Torr
2nd Acceleration				
Duration	153.3		ms	
Transmission due to Charge Exchange Loss (2nd accel.)	0.89			Eff. non-hydrogen pressure 9 10^{-10} Torr
Ejection Flat Top				
Kinetic Energy	95.40	993	MeV/u	i.e. 1000 MeV protons
$(B\rho)$	5.66	5.66	Tm	
Bending Field	0.689	0.689	T	
β	0.421	0.875		
Revolution Period	1245	599	ns	
RF Frequency	8.05	8.35	MHz	
Duration	25	25	ms	
Total Duration of Acceleration Cycle	257.6 (computed)	415 (measured)	ms	
Global Transmission due to Charge Exchange Loss	0.62	1		Eff. non-hydrogen pressure 9 10^{-10} Torr

Table A4.3.1: Ion distributor parameters

Number of Modules	4
Module Type	Window-frame, single-turn, vertical deflection magnet
Module Dimensions	Aperture (V x H) 75 x 140 mm, Length 260 mm
Yoke	Ferrite (high-μ, slow) slabs
Coil	brass, air-cooled
Load Impedance	0.5 μH, 0.3 mohms
Max. Field in Gap/Ferrite	0.025 / 0.118 T
Deflection Angle	3.0 mrad / kA, max. 5 mrad (Pb^{53+} at 4.2 MeV/u)
∫B.dl	0.006 T m
Ceramic Chamber	Racetrack cross-section, 60 x 110 mm int.diameter Length <1.2 m
Pulse Generator:	a) fast-rise generator in short-circuited PFN mode or: b) fast-fall generator with slow-rising PFN's Max. Current: 1700 A Pulse length (total): 550 μs
Comp. Control Interface	CERN ECA standard, G64 bus

Table A4.3.2: Cables required for PSB kickers

Type	Destination	Nbr	Length[m]	Total [m]
A	Feeder BE.KFA	32	17	544
B	Feeder BT.KFA10	16	33	528
C	Feeder BT.KFA20	8	21	168
D	PFN BE.KFA, BT.KFA10	24	155	3720
E	PFN BT.KFA20	8	283	2264
	Spare	1	276	276
	Total	89		7500

Table A4.3.3: Specifications of PSB kicker cables

Insulation	SF_6 pressurised	
Operating Voltage	40 (max. 60)	kV
Impedance	25 ± 0.5	ohms
Velocity of Propagation	4.95	ns/m
Attenuation at 10 MHz	< 0.8	dB/100 m
Diameter of dielectric	28.3	mm
Total Length incl. spare	7500	m
Manufacturer	Brugg Kabel AG (CH)	

Table A4.3.4: Ion beam-control system

Analog Part	Pure RF signals: Pick-ups, AVC, Superheterodyne, Phase discriminator at fixed IF of 10.7 MHz
Digital Part	Revolution frequency programme, derived from B-Train Control of harmonic number Type of particle control RF direct synthesis (no frequency multiplication) B-Train error correction Common 10 MHz atomic clock for all machines
Mechanical Standards	NIM standard Only front panel connectors RF Connectors: LEMO 00

Table A5.2.1: Acceleration of Pb^{53+} with comparison for protons

Parameter	Pb^{53+} Ions	Protons	Unit
Charge State	53	1	
Atomic Mass	207.948	1.007	u
Injection:			
Kinetic Energy,T	95.4	993 1000	MeV/u MeV
$\beta = v/c$	0.421	0.875	
$\gamma = E/E_0$	1.102	2.066	
Bending Field, B	0.08073	0.08073	T
Magnetic Rigidity, Bρ	5.657	5.657	Tm
dB/dt	0	0	T/s
Total Energy, E	1.027	1.924	GeV/u
Momentum, p	0.432	1.684	GeV/c/u
$\eta = \gamma_t^{-2} - \gamma^{-2}$	-0.796	-0.207	
Revolution Frequency, f_0	200.8	417.5	kHz
Revolution Period, T_0	4.98	2.39	μs
Horizontal Tune, Q_x	6.25	6.25	
Vertical Tune, Q_y	6.25	6.25	
Two bunches into one bucket RF capture			
Bunches from PSB:			
Bunch Length, τ_b	45	50	ns
Longit. Emittance, ε_l	$8.0\ 10^{-3}$	0.157	eVs/u
Half Mom. Spread, dp/p	0.6210^{-3}	1.3510^{-3}	
PS Capture			
RF Voltage, V_{RF}	50	50	kV
Harmonic Number, h	20	20	
RF Frequency, f_{RF}	4.02	8.35	MHz
Synchrotron Frequency, f_{s0}	2.68	1.97	kHz
Longit. Acceptance, A_l	$96\ 10^{-3}$	0.51	eVs/u
Half Bucket Height, Δp/p	$1.67\ 10^{-3}$	$2.27\ 10^{-3}$	
Bunches after filamentation			
Bunch Length, τ_b	170		ns
Longit. Emittance, ε_l	$66\ 10^{-3}$		eVs/u
Half Mom. Spread, dp/p	$1.37\ 10^{-3}$		
Hor. Transv. Emitt., ε_x (2σ)	26		π mm mrad
Vert. Transv. Emitt., ε_y (2σ)	13		π mm mrad

Table A.5.2.1 (continued)

Parameter	Pb^{53+} Ions	Protons	Unit
Acceleration			
Max. dB/dt	2.2	2.2	T/s
RF Voltage, V_{RF}	200	200	kV
RF Harmonic Number	20	20	
Duration	0.7	0.7	s
Extraction			
Kinetic Energy, T	4.25	19.07	GeV/u
$\beta = v/c$	0.984	0.999	
$\gamma = E/E_0$	5.558	21.33	
Bending Field, B	0.9512	0.9512	T
Magnetic Rigidity, $B\rho$	66.66	66.66	Tm
dB/dt	0	0	T/s
Total Energy, E	4.25	20.0	GeV/u
Momentum, p	5.09	20.0	GeV/c/u
$\eta = \gamma_t^{-2} - \gamma^{-2}$	-0.0054	0.025	
Revolution Frequency, f_0	469.3	476.6	kHz
Revolution Period, T_0	2.13	2.1	μs
Horizontal tune, Q_x	6.25	6.25	
Vertical tune, Q_y	6.25	6.25	
RF Voltage, V_{RF}	200	200	kV
Harmonic Number	20	20	
RF Frequency, f_{RF}	9.39	9.53	MHz
Synchrotron Frequency, f_{s0}	195	423.9	Hz
Longit. Acceptance, A_l	5.3	9.6	eVs/u
Half Bucket Height, $\Delta p/p$	$7.8\ 10^{-3}$	$3.58\ 10^{-3}$	
Bunch Length, τ_b	9	18	ns
Longit. Emittance, ε_l	0.072	0.53	eVs/u
Half Mom. Spread, dp/p	$1.02\ 10^{-3}$	$0.94\ 10^{-3}$	
Hor. Transv. Emitt., ε_x (2σ)	3	3	π mm mrad
Vert. Transv. Emitt., ε_y (2σ)	2	2	π mm mrad

Table A6.1.1: Nominal SPS parameters with Pb ions

Mode of SPS operation:	with ions	with protons
	interleaved with lepton beams for LEP	
Cycles in SPS supercycle:	Pb ions e^+ e^+ e^- e^-	(Protons e^+ e^+ e^- e^-)
Nominal length of SPS supercycle:	19.2 s	(14.4 s)
Nominal length of one e-cycle:	1.2 s	(1.2 s)
Nominal length of the ion cycle:	14.4 s	(9.6 s)
Nominal ion energy:	up to 177 GeV/u	(450 GeV)
Injection energy E:	4.25 GeV/u	(14 GeV)
β at injection:	0.984	(0.998)
Horizontal tune:	26.6	(26.6)
Vertical tune:	26.6	(26.6)
Transverse normalized emittances (at 2 σ):	15 π mm mrad	(40)
Foreseen intensity:	3.93 10^8 Pb ions 3.2 10^{10} charges	(3 10^{13}p)
Debunched beam with slow extraction:		
Slow extraction duration	2.5 s at top energy	
$\Delta p/p$ at extraction	10^{-3}	